CHARACTERISATION OF PARTICULATES PRODUCED FROM CHAIN GRATE AND PULVERISED COAL COMBUSTION PROCESSES

Student Name: Tsebo Molapo

A Research Report submitted to Faculty of Engineering and the Built Environment, University of the Witwatersrand, Johannesburg in partial fulfillment of the requirements for the Degree of Master of Science in Engineering.

4th May 2011

Declaration

I, Tsebo Molapo declare that this research report is my own unaided work. It is being submitted for the degree of Master of Science in Engineering to the University of the Witwatersrand, Johannesburg. It has not been submitted before for any degree or examination to any other University.

.....
(Signature of Candidate)

.....day of.....year….....

Abstract

Most of the electrical power produced in South Africa arises from the combustion of coal. The combustion of coal produces by-products in the form of fine particulates that are released to the atmosphere and these may cause respiratory infections in humans. The current literature studies have divided such particulates into three modes based upon particle size. For example, pyrolysis, i.e. that part of combustion of coal that leads to the emissions of gaseous and heavy hydrocarbon products, characteristically produces ultrafine fly ash particles smaller than 1 micron. The burning of porous char particles or particles that fragment lead to particle size ranges mainly between 1 and 3 microns; while dense chars and mineral forms that melt and coalesce with each other produce larger fly ash particles generally larger than 3 microns.

The original aim of this study was to characterise the three modes of coal fly ash formed by South African coals when combusted in a pulverised fuel (Pf) boiler and a chain grate stoker boiler. This, however, was not possible due to the lack of appropriate equipment for the capture of fly ash material in the three different sizes. For this reason, an alternate approach was taken. Namely, bulk samples of fly ash were taken from an electrostatic precipitator (ESP) of Pf boilers, chain grate boiler, from the out-going stack of a Pf boiler, and from the exit stack of a chain grate stoker. Particle size distribution analyses were undertaken on these samples and the <10 micron material was send out for further analyses using XRD, SEM EDS and XRF. The samples taken from the stack of the Pf boiler were iso-kinetically sampled and the fly ash was captured in the filter fibres of thimbles. Due to the small quantity of sample and the fact that the fly ash was effectively trapped within the fibers, no particle sizing analysis could be undertaken on these samples, only SEM EDS was used to analyse the fly ash particles trapped within the fibers. The feed coals were analysed using similar techniques to those used on fly ash particles.

The purpose of the amended investigation was to compare; (1) the size distributions and qualities of the <10 micron fly ashes from a Pf boiler ESP and the chain grate stoker relative to one another and to their feed coals, and (2) the Pf boiler ESP fly ash sample and the out-going stack sample from the same boiler.

The research has shown that the fly ash compositions reflect the feed coal mineral content, and that the ESP at the back end of the Pf boiler has efficiently captured most of 5-10 micron particles and less than 5 micron material through, as seen in the stack samples. The chain grate

Abstract

stoker fly ash samples have not passed through an efficient pre-screening process, thereby allowing both ultra fine <5 micron and 5 to10 micron material into the atmosphere.

Acknowledgements

The author would like to thank Lets'eng Diamonds and Lesotho Government for the financial support of the project and Professor Rosemary Falcon and Professor Nicola Wagner for their superb supervision and patience. I would also like to thank my Coal and Carbon Research Group colleagues for their assistance with proof reading and Universal Measurements for assisting me with iso-kinetic sampling. I am grateful to Mr. D. Vetter for assisting with proof reading.

Table of Contents

Contents

Introduction

Literature Review

Experimental Program

Table of Contents

Results & Discussion

Table of Contents

Conclusions & Recommendations

List of References

Appendix

List of Figures

List of Figures

List of Tables

List of Tables

Glossary

List of Abbreviations

EPA	Environmental Protection Agency
CG	Chain Grate
EDS	Energy Dispersive X-ray Spectroscopy
ESP	Electrostatic Precipitator
Pf	Pulverised Fuel
PM	Particulate Matter
$PM_{2.5}$	PM Particle with aerodynamic diameter of 2.5 microns
PM_{10}	PM Particles with aerodynamic diameter of 10 microns
PSD	Particle Size Distribution
SEM	Scanning Electron Microscope
XRD	X-Ray Diffraction
XRF	X-Ray Fluorescence
IA14	ESP outlet dust
JL10	FFP outlet dust
HY23	ESP outlet dust
JV13	ESP outlet dust

1.1 Introduction

Particulates are comprised of tiny particles of solid or liquid suspended in a gas (Douglas *et al.*, 1993, World Health Organization, 2005; Amann *et al.*, 2006). Sources of particulates are both anthropogenic and natural. Some examples of natural sources of particulates are volcanoes, dust and material released by living vegetation. Anthropogenic activities such as the combustion of fossil fuels and various industrial processes also produce large amounts of particulates.

Anthropogenically produced particulates are comprised mostly of acids, inorganic matter, organic matter metals and gases (Linak *et al.*, 2000) along with other hazardous airborne material that may be inhaled into human and animal respiratory systems.

Particulates from combustion of oil, biomass and coal contain elemental carbon that exists in both organic and inorganic form from fuel carbon. The sulphate formed from sulphur dioxide emissions that emanate from coal combustion and other processes in the presence of sulphur containing material also exists in both forms. Alumino-silicates and alkaline earth metals are also present in numerous forms. Nitrates produced from atmospheric nitrogen reactions (Myaliwiec and Kleeman, 2002) and the transformation of mineral bound nitrogen from coal combustion (Amann *et al.*, 2006) results in several forms of nitrates; however nitrates do not occur in significant amounts.

In respect to the size range of particulates produced during coal combustion, some particles are large enough to be seen as soot or smoke while some particles are only visible under an electron microscope. The particulates produced from coal power stations below 1 micron are normally referred to as ultrafine particles while the range between 1 micron and 3microns are central mode particles that make up a family of particulates with an aerodynamic diameter of 2.5 microns ($PM_{2.5}$). Particles bigger than 3 micron are part of coarse mode particles that form a family of particulates with aerodynamic diameter of 10 microns (PM_{10}).

Fine particles that make up a family of $PM_{2.5}$ can travel many thousands of kilometres in the atmosphere after being emitted from industrial stacks, while PM_{10} may only travel a few hundred kilometres or less depending on atmospheric conditions (Amann *et al.*, 2006). PM_{10} particles settle down to ground faster than the $PM_{2.5}$.

The particulates formed as a result of intermediary reactions of gases and some solid particles in the atmosphere are termed secondary particulates. Secondary particulates are mostly an end product of sulphur and nitrogen oxidation (Hetland *et al*., 2001; Myaliwiec and Kleeman, 2002 Amann *et al.*, 2006). The precursor materials are initially released as part of the flue gases from power stations, vehicle exhausts and other sources.

With regard to human health, the potential hazards of particulates are determined by particulates chemistry and particle size. Particulates may rupture, block and/or pass through alveoli. This can lead to cancer, atherosclerosis and a permanent decline in lung capacity in the human respiratory system (Soukup and Becker, 2001).

1.2 Particulates Toxicology as Function of Particle Size

Some inhaled particulates accumulate in the human respiratory system reducing lung permeability and this result in reduced lung function. Decreased lung function results in different diseases due to decreased oxygen concentration in human blood. The elderly and children appear to be the most prone to the negative impact of hazardous particulates. The increasing levels of anthropogenic particulates in the atmosphere are increasing health hazards such as heart disease, altered lung function and lung cancer (Soukup and Becker, 2001).

Toxicological experimental studies have been carried out on animals using ambient atmospheric ultrafine particulates (Amann, *et al.*, 2006, Yinon, 2010), central mode particulates and coarse particulates. The studies found that on a mass basis, the concentration of ultra fine particles are more inflammatory to tissues than coarse particles (Amann *et al*, 2006). This is due to the larger surface area that induces more reactivity with human tissue, as well as the possibility of increased penetration into the blood system (National Environment Protection Council (1), 2003, Amann *et al*, 2006). Coarse particulates have to break up before they can be absorbed on or penetrate into human tissue and blood.

Coarse particles (size range ±10 microns) have a greater potential of being exhaled before causing any damage to human tissues. The coarse portion of ambient particulates is however likely to be more toxic due to the wider range of its chemical composition (Harrison and Jianx,

2000)

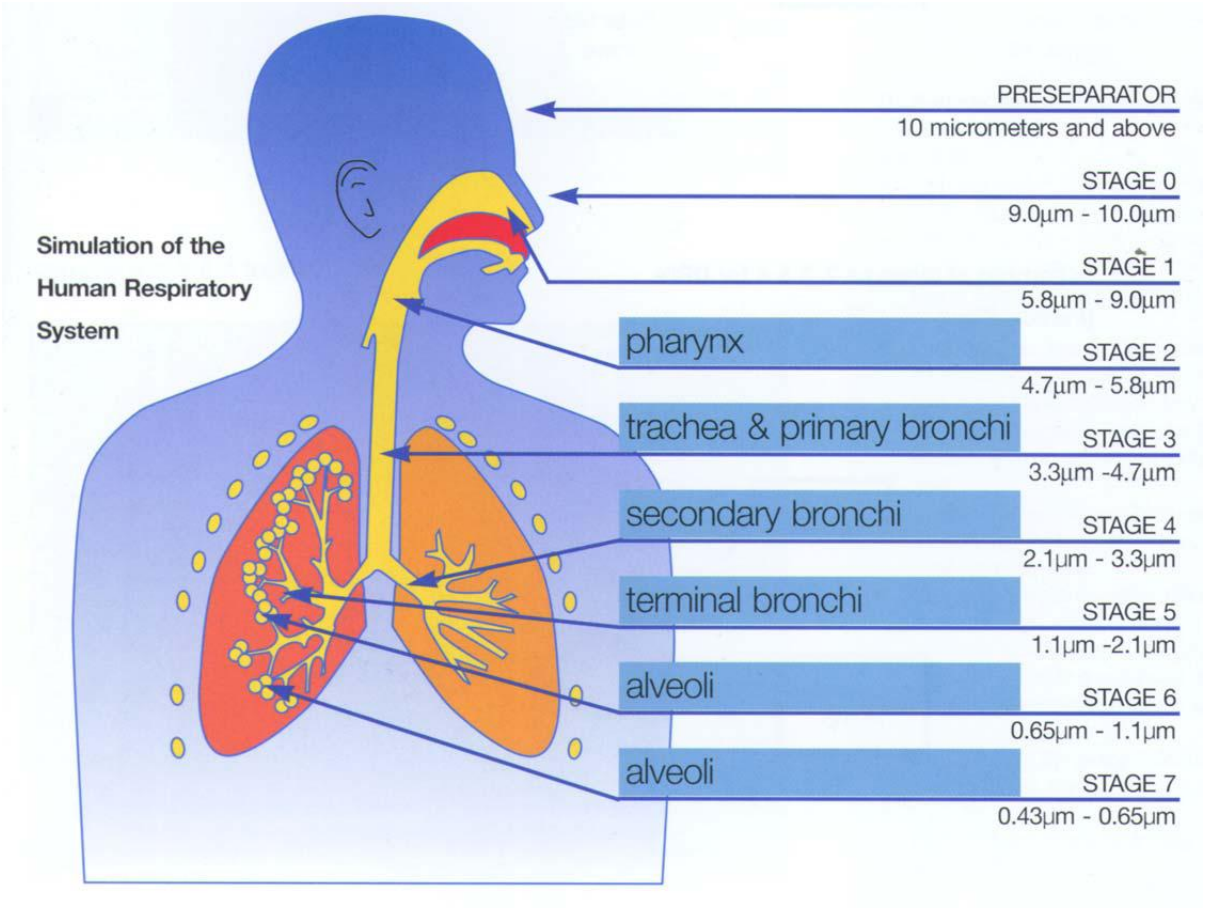

Figure 1.1: Penetration of particulates in human respiratory system (Dunbar, 2005).

Secondary fragmentation of coarse particles in human respiratory systems increases the concentration of ultra fine particulates that is absorbed in human lung alveoli as indicated in Figure 1.1. Most of the coarse particulates that do not fragment can be easily exhaled before infiltrating deeper into the respiratory system. Figure 1.1 shows that particulates smaller than 5 microns are more penetrative and hazardous it is. To limit the potential hazards of particulates the concentration of ultra fine particulates in the atmosphere must be reduced greatly, since the respiratory system is more resistant towards coarse particulates than to ultra fine particles.

1.3 Legislation

The outcome of research studies conducted on the impact of particulates on human health has led to various governments establishing and revising environmental regulations pertaining to particulates emissions. Stringent emission standards and laws have been launched to minimise ambient concentrations of fine particulates. The United States of America (USA) introduced the National Ambient Air Quality Standard (NAAQS) for both PM_{10} and $PM_{2.5}$ (Lee, 2010). The National Environment Protection Measure (NEPM) of Australia has been revised to integrate advisory reporting standards for $PM_{2.5}$ in January 2004 (National Environment Protection Council (2), 2003; Buhre *et al.*, 2006; Lee, 2010). Australia's NEPM Ambient Air Quality measures accounted for PM_{10} since 1998 (Buhre *et al.*, 2006; Lee, 2010). Before the potential hazards of $PM_{2.5}$ were understood, the legislation accounted for emissions and control of PM_{10} only. Coal fired power stations are increasingly being required to control and characterise their particulates emissions in Australia and USA (World Health Organization, 2005).

South Africa introduced new legislation in the form of the National Environmental Management Air Quality Act (AQA) 2004 (No. 39 of 2004). This accounts for the control of particulates emissions and pollutants from pulverised coal fired power stations and various other sources. The introduction of AQA by South Africa acted as a transition from source-based emission command-and-control to ambient air quality management (South African No.31987 Government Gazette, 2009).

The current set of ambient levels standards in AQA incorporates particulates (specifically PM_{10}), sulphur dioxide (SO_2), oxides of nitrogen (NO_x), ozone (O_3), lead, carbon monoxide (CO) and benzene (South African No.31987 Government Gazette, 2009). The national ambient air quality standards for PM_{10} in South Africa are recorded in Table 1.1. The Vaal Triangle area has been declared as a priority area as published in the Government Gazette in terms of Section 18(1) of the National Environmental Management Act because of high ambient particulates concentrations (South African No.31987 Government Gazette, 2009, Singleton, 2008). The Highveld area in Mpumalanga has also been declared a priority area because of the high concentrations of particulates in the atmosphere (South African No.31987 Government Gazette, 2009). The current AQA does not account separately for $PM_{2.5}$, even though $PM_{2.5}$ is considered to be more deadly than PM_{10} by medical research records (Douglas *et al.*, 1993; Amann *et al.*,

2006). The exposure amounts of $PM_{2.5}$ permitted by legislation of other countries are lower than PM_{10} exposure amounts as recorded in Tables 1.2 and 1.3.

Table 1.1: National Ambient Air Quality Standards for PM_{10} in South Africa (South Africa No.31987 Government Gazette, 2009).

Averaging Period	Limit value(LV)	Frequency of Exceedence	Compliance Date
24 hours	75µg/m^3	4	Immediate
1 year	40µg/m^3	0	Immediate

Table 1.2: Ambient Air Quality Standards for Different Countries for PM_{10} (Lee, 2010).

Country	Limiting value(µg/m^3)	Averaging Period
USA	150	24 hours
EU	20-30	24 hours
Australia	50	24 hours

Table 1.3: Ambient Air Quality Standards for Different Countries for PM2.5 (Lee, 2010).

Country	Limiting value(µg/m^3)	Averaging Period
USA	35	24 hours
EU	20-30	24 hours
USA	15	Annual
EU	7-10	Annual

1.4 Problem Statement

Energy in South Africa is mostly produced from coal combustion. The coal combustion technology utilizes coal that produces very fine fly ash particles. The fly ash that escapes emission control equipment makes a significant contribution to ambient airborne particulates and especially $PM_{2.5}$ (Yuanzhi *et al*, 2004). There has been little or no research to establish whether South African coals produce ultra fine particulates when combusted in both pulverised fuel (Pf) boilers and chain grate stokers and no investigations in terms of particle size distribution, nature, morphology and chemical composition. Nor has the impact of the particulates specifically from coal combustion on human health been studied even though the National Ambient Air Quality

Standards for control of fly ash particles of aerodynamic diameter of 10 microns has been developed in South Africa. The analysis of individual fly ash particles and bulk fly ash will provide important knowledge and understanding into the processes of formation, characteristics and potential effects of coal produced particulates on human health (Yuanzhi *et al*., 2004). It may also grant a better understanding required for environmental legislation development and revision since coal combustion is one of the chief sources of particulates.

1.5 Research Questions

Do Pf boilers and chain grate stokers combustion processes of South African coals produce particulates less than 10 microns? If so, how do the morphologies and chemical compositions of different particle size modes differ, and can they be related to their original coal feedstock?

1.6 Scope of the Project

The scope of the project covers the characterisation of the feed coal mineral matter constituents and the produced fly ash mineralogy for both Pf fired boilers and chain grate stokers. The study includes the characterisation of parent coal and the fly ash particles morphology, PSD, chemical composition and mineralogy. The fly ash particles PSD cover the particle size range from -1 micron to 10 microns. The project does not include the study of organic particles in fly ash (i.e. un-burnt carbon).

1.7 Aim and objectives

The initial aim of the project was to determine and characterize the quantity and quality of the three particulates size classes namely: ultrafine (-1 micron), central mode (1-3 micron) and coarse mode (+3 microns) that may be expected to arise when burning South African coal in Pf boilers and chain grate stokers. Due to the lack of proper sampling equipment, it was not possible to carry out the initial aim.

The research objective was then adapted to determine and characterize the quantity and quality of the fly ashes in bulk without separating them physically into three particulates size classes below 10 microns. Where possible, the characteristics of the three different size modes were observed using chemical and optical procedures.

The objectives will be achieved by:

- Establishing the PSD of the fly ash by using a sieve screen stack and Malvern particle size analyzer to determine the quantity of each size class arising from a Pf coal boiler and a chain grate stoker.

- Characterising the feed coals and fly ash mineral matter constituents using XRD in order to establish the relationship between coal mineral matter to particulates mineral matter following combustion.

- Characterising the feed coal and fly ash particulates elemental chemistry using XRF and SEM EDS to establish a relationship between coal chemistry and the resultant fly ash particulates.

- Investigating the modality and morphology of the fly ash particulates using SEM in order to establish the impact of the different combustion processes on ash formation.

- Estimating the importance and relevance of the fly ash particulates produced by the two combustion processes from the perspective of exposure humans and animals and the risk to their health.

2.0 Introduction

This chapter reviews previous work conducted on the properties of coal combustion fly ash below 10 microns in terms of morphology, chemical composition and the PSD. The PSD of the fly ash particles from coal combustion is considered to be trimodal (Linak *et al*., 2002, Seams, 2003). The three regions are ultra fine particles size, central mode size and coarse mode size particles. The PSD regions of coal combustion fly ash particles size ranges are recorded in Table 2.1 for a number of articles. The chemical composition, particle morphology and PSD inflexion points are parameters and indicators that have been used to determine the particle size ranges of the ultrafine particles, central mode particles and coarse particles. In some cases the central mode is referred to as the fine fragmentation region and the coarse mode particles as the super micron region (Seams, 2003).

Current publications normally classify particulates into three size class ranges (Kanf *et al*., 1992, Seams, 2003). Particulates with aerodynamic diameter $\leq$ 2.5 microns are referred to as $PM_{2.5.}$ Particulates with aerodynamic diameter $\leq$ 10 microns are referred to as PM_{10} (Wang *et al*., 2007, Wang *et al*., 2008).

Some of the fly ash produced from coal combustion escapes the emission control equipment and is emitted to the atmosphere via a stack. The emitted fly ash particles sizes range from +10 microns to -0.1 microns, and are normally referred to as particulates. Particulates are also normally referred to as PM_{10} or $PM_{2.5}$ even though the coal combustion fly ash PSD is considered to have three modes. PM_{10} accounts mostly for the coarse particles while $PM_{2.5}$ mostly accounts for both central mode and ultrafine particles. PM_{10} and $PM_{2.5}$ are used to refer to particulates produced from both natural and anthropogenic sources while the three particle size modes are used to define coal combustion fly ash particles based on fly ash particles PSD.

2.1 Fly Ash Formation

The initial mechanisms of fly ash formation are comprised of vaporization and recondensation of volatile components of coal mineral matter or ash that evolve during coal pyrolysis and devolatilization (Baxter, 1992). The initial steps are responsible for the formation of ultrafine fly ash particles from 0.08 micron to 1 micron (Baxter, 1992). The succeeding mechanisms consist of coal char fragmentations that are comprised of structural bulk breakup and shedding of ash particles from the surface of chars during combustion depending on char temperature and char porosity (Baxter, 1992). The char fragmentation contributes to the formation of central mode particles and coarse mode particles depending on the extent of char fragmentation. The coalescence of mineral matter on char particles results in the formation of coarse mode particles. The particulates in the atmosphere originate from fly ash particles that escape the emission control equipment that captures the majority of fly ash particles. PM_{10} is formed from coarse mode particles and the agglomerations of ultrafine and central mode particles. $PM_{2.5}$ is formed from ultra fine and central mode particles. The mechanisms of fly ash formation during coal formation are shown in Figure 2.1

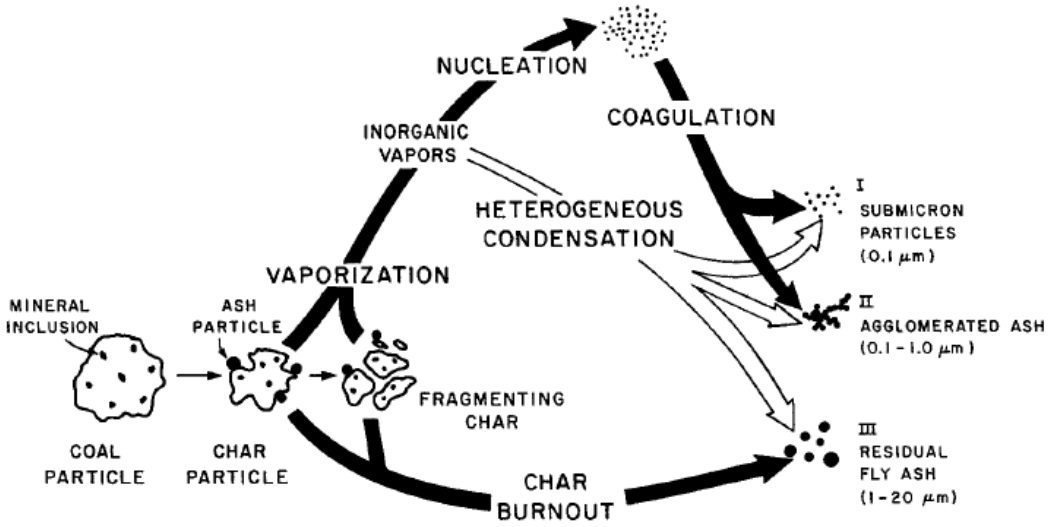

Figure 2.1: Coal fly ash formation processes (Seams, 2003).

2.1.1 Ultra Fine Mode

The initial step in coal combustion is pyrolysis, which occurs at a lower temperature of 330^{o}C-500^{o}C (Shao *et al.,* 1994, Kok *et al.,* 1998) relative to the coal char combustion temperature that is above 600^{o}C. During pyrolysis, volatile matter in raw coal and organically bound metals are released from the carbonaceous matrix (Zhang *et al.,* 2006). Released volatile matter reacts with oxygen and burns; as a result of volatile matter combustion, organically bound metals are oxidized. After oxidation they nucleate and form ultra fine particles (Zhang *et al.*, 2006).

Inorganic metals released during char combustion also contribute to the formation of ultra fine particulates. It is evident from Figure 2.2 (a) and (b) that char combustion contributes to the formation of ultra fine particles since ultra fine particles have been identified by Zhang *et al.* (2006) from char combustion even though the quantities were not very significant. According to Buhre *et al.* (2006) vaporization of inorganic metals from char surfaces during char combustion is strongly influenced by the following characteristics and parameters:

- Char combustion temperature
- Amounts of readily vaporized substances such as alkalis, sulphur and phosphorous, and
- PSD of minerals included in the carbon matrix containing refractory metals.

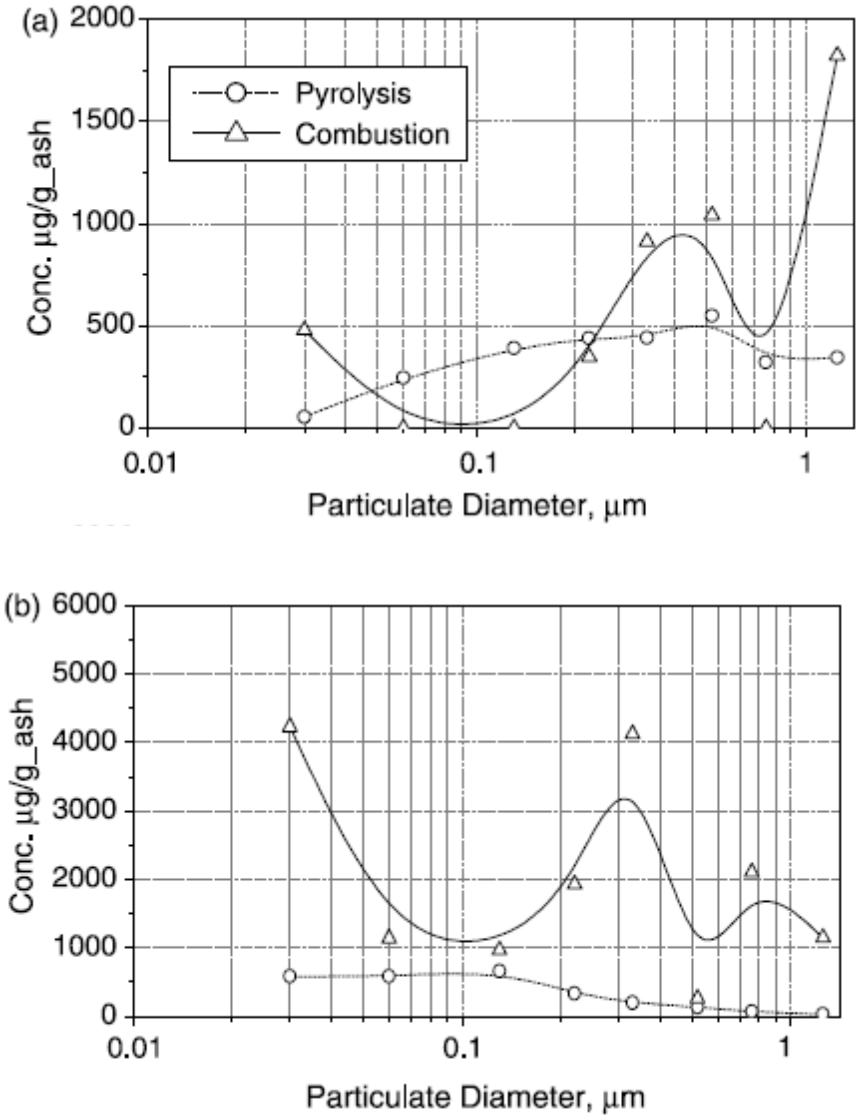

Figure 2.2: PSD of smaller than 1 micron formed from coal pyrolysis and combustion (a) for 1473K and (b) for 1723K (Zhang *et al*., 2006).

2.1.2 Central Mode

Central mode particulates (-1 micron to 3 microns) are mostly formed from heterogeneous condensation and adsorption of vaporized species on fine rather than ultrafine residual ash particles (McElroy *et al.*, 1982). Some authors find central mode particulates chemical composition to have some similarities to the coarse mode (+3micron) chemical composition (Dunxi *et al.*, 2007). Linak *et al* (2002) proposed that central mode particulates and coarse mode have similar formation mechanisms. Linak *et al* (2002) attributed the formation of central mode to char fragmentation processes and mechanisms. Studying the morphologies of central mode particulates of coal combustion indicate that most particle shapes are irregular with very few round and spherical particulates.

Xu *et al* (2009) studied three possible origins of central mode particles, namely char fragmentation, transformation of fine particles from raw coal feed and excluded minerals directly into particulates.

2.1.2.1 Formation of Central Mode Particles by Coal Char Fragmentation

Baxter (1992) and Helble and Sarofim (1989) cited that char thermal fragmentation plays an important role in the formation of central mode particulates. How char fragmentation contributes to central mode particulates PSD formation was not however explained.

Helble and Sarofim (1989) used synthetic chars to study the impact of char fragmentation on ash PSD. Synthetic chars offered the opportunity to vary the macro porosity of the chars. This is important since char porosity is a parameter considered to be important in controlling the fragmentation of burning char. All synthetic chars were prepared with a single mineral additive.

The Helble and Sarofim (1989) experiments were carried out with uniform-porosity synthetic chars in order to eliminate or minimize the complexity brought by varying mineral sizes and pore size distributions. These would make it difficult to identify parameters that play an important role in char fragmentation during coal combustion (Helble and Sarofim, 1989). Helble and Sarofim (1989) found no residual ash in the 1-5 microns size class range produced by the microporous synthetic char doped with sodium silicate.

However, a residual ash in the 1-5 microns size class range was produced when using a macroporous spherocarb synthetic char, also containing sodium silicate of equal mass to the previous char, under the same combustion conditions and behaviour. Helble and Sarofim (1989) have defined micro-porosity to be pores less than 0.05 microns while macro-porosity was defined to be pores greater than 0.05 microns in diameter. Helble and Sarofim (1989) did not however consider a third synthetic char that had meso-pores defined within it.

2.1.2.2 Impact of Oxygen and Combustion Temperature on Char Fragmentation

The influence of combustion temperature on char fragmentation is greatly dependent on the oxygen concentration, presence of macropores (>50nm) (Kanf *et al.,* 1989) and char particle size (Baxter 1992). Pores are normally grouped into three classes: micropores, macropores and mesopores (Bar-Ziv and Kantorovich, 2001). Particle size and porosity are the most influential parameters on char fragmentation since they control the effect of oxygen concentration and particle temperature. Char particle porosity is dependent on pyrolysis temperature since the swelling ratio is dependent on temperature during the initial stages of devolatilisation. The volatile matter vented rapidly under high pressure and temperature has limited time to break away from the coal particle through small pores in the particle surface, resulting in a huge pressure build up and intensive bubbling phenomena within the particle that enhance swelling (Dunxi *et al.,* 2005)

When the oxygen concentration is low, char particles are probably oxidized mainly on the external surface (Xu *et al.,* 2007). High concentrations of oxygen lead to more internal oxidation depending on char particle size and the pore volume. Increasing oxygen concentration leads to a higher particle heating rate and as a result, the particle temperature increases rapidly.

The extent of char fragmentation depends on the char swelling behavior during combustion (Liu *et al*., 2000). Xu *et al* (2007) studied the char particles characteristics namely: PSD, surface area, pore size distribution, swelling behavior and morphology. Xu *et al* (2007) found that swelling ratios of char samples increased with increasing temperature from 1373 to 1523 K, and then decreased when the temperature was further increased to 1623 K. This led to a conclusion that swelling ratio increases with increase in temperature over limited temperature range.

The work by Baxter (1992) was confirmed by Wu *et al* (1999) in which Baxter (1992) maintained that char particles with various structural and morphological characteristics show evidence of diverse char fragmentation patterns. Very porous char particles fragment extensively and produce more ultra-fine and central mode particulates. Coal char particles with low porosity especially from high rank coals demonstrate poor degrees of fragmentation which results in the formation of coarser mode particulates. Low rank bituminous coals normally undergo high swelling upon heating relative to high rank coals and, as a result of extensive swelling, huge portions of char particles with highly porous structures with ceno-spherical profiles are produced. These highly porous chars have a tendency to go through extensive fragmentation during combustion which reduces the degree of coalescence of included mineral matter (Dunxi *et al.*, 2005).

2.1.2.3 Impact of Fine Particles in the Feed Coal

Most researchers (Ninomiya *et al.*, 2004, Xu *et al.*, 2007) studied the impact of coal feed PSD on overall particulates production while Xu *et al* (2009) studied the role that fine particles play both when attached to big coal feed particles surfaces and when free. Holve (1986) attributed the lack of information on fines in coal feed both in the form of free fines and fines attached to the feed coal surface as most probably due to the unavailability of a quantitative measurement technique (Holve, 1986) or to the narrowly size-classified coal feed samples used (Helble and Sarofim, 1989). Recent research has been conducted on mono-sized coal samples on laboratory scale (Ninomiya *et al.*, 2004, Xu *et al.*, 2007). Xu *et al*. (2009) pulverised bituminous coal into two size classes. One size class was <63 microns (named fine feed) while the other size was 100–200 microns (coarse feed). Xu *et al* (2009) used these two size classes to study the impact of coal feed PSD on the formation of central mode particles. More central mode particles were produced from fine coal feed as shown in Figure 2.3 thereby indicating that coal particle size plays an important role in the formation of particulates of specific modes.

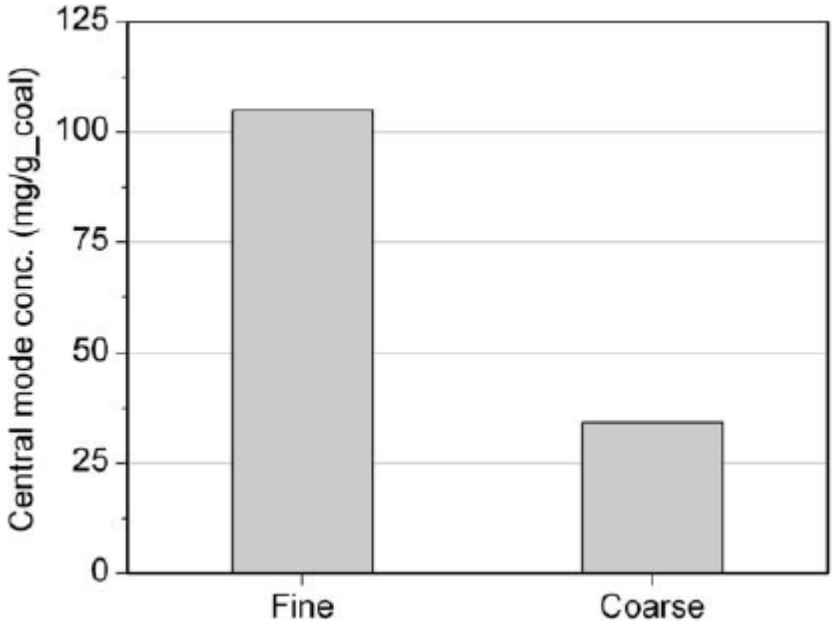

Figure 2.3: Central concentrations for sized coal fractions at 1673K (Xu *et al*., 2009).

2.1.2.4 Contribution of Excluded Minerals and Included Minerals

Mineral grains associated with the coal carbon matrix are classified as included or excluded. Minerals included in the carbon matrix refer to isolated mineral grains that are associated with organic matter. Excluded minerals are free and liberated and have little or negligible interaction with coal organic matter.

Mineral grains included within the carbon matrix transform differently from excluded mineral grains due to variations in particle temperature, local atmosphere, and proximity to other included mineral grains (Yinghui *et al.*, 2007). Work done by Kramlich and Newton (1994) showed no contribution of excluded minerals to formation of central mode particulates while included minerals did show some contribution to formation of central mode particulates, however, Xu *et al.* (2009) records that excluded minerals contributed significantly to the formation of central mode particulates.

Ninomiya *et al.* (2004) studied the distribution of both included and excluded minerals within raw coal feed PSD. The concentration of included minerals increased with increasing coal feed size and decreased with decreasing coal feed particle size.

The two Figures 2.4 (a) and 2.4 (b) by Ninomiya *et al.* (2004) show the relationship of both excluded and included minerals with particulates production in two different size ranges. Excluded mineral particles less than 10.0 microns are readily transformed into particulates during coal combustion (Ninomiya *et al.,* 2004). Some of these excluded minerals undergo different transformations, some become unconverted particulates (ie quartz), while some fragment, and some contribute to the production of central mode and ultra-fine particulates production. Ninomiya *et a.l* (2004) recorded an increase in the concentration of emitted particulates with the increasing ratio by mass of excluded to included minerals (< 10 microns) in the raw coal.

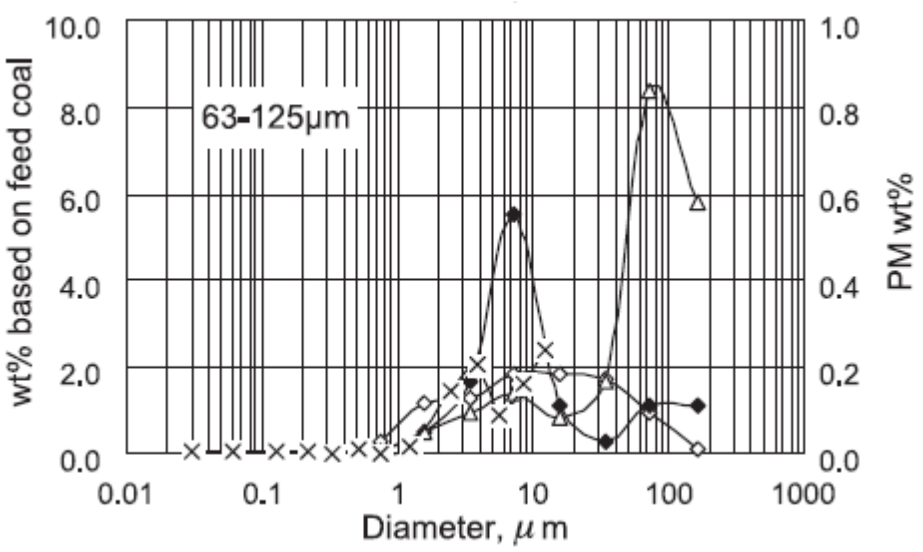

Figure 2.4(a): Relationship between excluded mineral and included mineral and PM in 63-125 micron size range (Ninomiya *et al*., 2004).

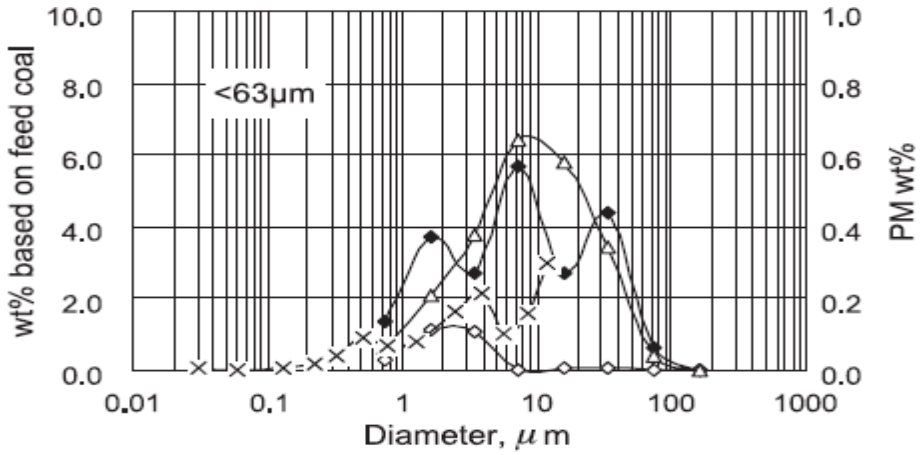

Figure 2.4(b): Relationship between excluded mineral and included and PM in 63-125 micron size range (Ninomiya *et al.*, 2004)

2.1.3 Coarse Mode

Fragmentation mechanisms have been thought to be responsible for the formation of coarse mode particulates. The mechanism of fragmentation involves particle inflation, cracking and material shedding as a result of expanding gases within coal particles during char combustion (Dunxi *et al.*, 2007). The formation of coarse particles is governed by swelling in chars. In cases of chars that possess more mineral matter, the mineral matter coalesces and forms large particles sometimes gluing together fragmented particles (Buhre *et al.*, 2006). Extensive char swelling produces both small fragments and moderately large fragments forming part of the coarse mode particulates. Char particles characterised by poor porosity fragment less, and naturally form coarse particles (Xu *et al.*, 2007). Highly porous chars produced from high swelling bituminous coals undergo extensive fragmentation during char combustion. Extensive char fragmentation reduces the degree of coalescence of included minerals (Xu *et al.*, 2007). Non-fragmenting char particles with included minerals may result in ash coalescence within the particles. This is controlled by the type, size and distribution of the included minerals (Buhre et al., 2006). This indicates that included minerals become viscous and coalesce under high char combustion temperatures (Buhre *et al.*, 2006). Ninomiya *et al* (2004) and Buhre *et al.* (2006) confirm this finding. Some of the inorganic matter vaporized during coal combustion is found agglomerated on the surfaces of central mode and coarse particulates.

2.2 Fly Ash PSD

Fly ash produced from coal combustion is produced within the following aerodynamic diameter range: 0.03 microns to 100 microns. The fly ash resultant PSD has several peaks within it and some inflexion points (Zhang *et al.*, 2006). The inflexion points and highest peaks are normally used to identify PSD mode boundaries.

Particle mode units that are often used to characterise particulates PSD are mass, particle number, volume and surface area (Dunxi *et al.*, 2008). Parameters used for characterising combustible particulates generally have one shortcoming in common, namely they are highly reliant on the precision and sensitivity of the instrumentation used to quantify them (Dunxi *et al.*, 2008). Boundaries that exist within particulates PSD modes have not been clearly defined. Authors have assigned different particle size ranges to ultra fine, central mode and coarse mode depending on the inflexion points of the PSD as indicated in Table 2.1. For instance, Xu *et al* (2008) did not show exact boundaries of ultra fine, central mode and coarse mode by means of particles size because particulates produced from three different coals produced PSDs with different boundary particle size ranges for all three mention modes. The boundary values have been chosen from PSD inflexion points and PSD peaks.

Due to different inflexion points and peaks from different PSDs as reported by different authors, there is no exact boundary value. Instead the boundary is possibly identified by the range that is used. Dunxi *et al.* (2007) used a new approach for characterising particulates PSD by means of elemental mass fraction found in the ultrafine and coarse modes in the size ranges of 0.0281–0.258 microns and 2.36–9.8 microns, respectively, while the central mode is taken to be between 0.377 and 1.58 microns.

Table 2.1 Comparison of modes size ranges from various publications

Publication Authors	Ultra Fine	Central Mode	Coal Type	Combustion Unit
	Particle Size Range			
Linak *et al*.(2002)	0.1 micron	0.7≤x≤3 micron	Bituminous	Boiler
Seams (2003)	0.1 micron	1≤x≤2 micron	Bituminous	DTF
Dunxi *et al* (2007)	x≤0.3 micron	0.3≤x≤3 micron	Bituminous	DTF
Xu *et al* (2009)	x≤0.3 micron	0.3≤x≤5 micron	Bituminous	DTF

According to Wang *et al.* (2008) the most important factors influencing the formation and modal size class ranges of particulates are:

- Coal rank
- Coal type
- Coal particle size
- Oxygen content
- Coal mineral content
- Combustion process conditions, and
- Particle residence time

Initial studies (Flagan *et al.*, 1977, Sarofim *et al.*, 1977, Desrosiers *et al.*, 1979) of coal combustion had stated that the fly ash PSD is bimodal. Particulates or fly ash PSD obtained by Sarofim *et al.* (1977), Helble *et al.* (1986) and McElroy *et al* (1982) are shown in Figure 2.5(a) and 2.5(b). This led to the conclusion that particulates produced from coal combustion are best characterised as a bimodal PSD.

However recent studies by Seams (2003), Dunxi et al (2007) and Linak et al (2002) contradict initial studies by Sarofim *et al.* (1977), Flagan *et al.* (1977) and McElroy *et al.* (1982), concluding that the PSD for particulates arising from coal combustion is trimodal. The discovery of a third mode in PSD resulted from the use of high resolution instruments used to characterize the PM (Dunxi *et al.*, 2007; Linak *et al.*, 2002). Most authors that have found particulates PSD from coal combustion to be trimodal used cascade impactor and image analysis instruments to quantify particulates PSD.

These results suggest that the conclusions reported in previous studies by Sarofim et al (1977) and Flagan *et al.* (1977) might have been limited by instrument precision and resolution as recorded by Dunxi *et al.* (2007), Linak *et al.* (2002) and Seams (2003).

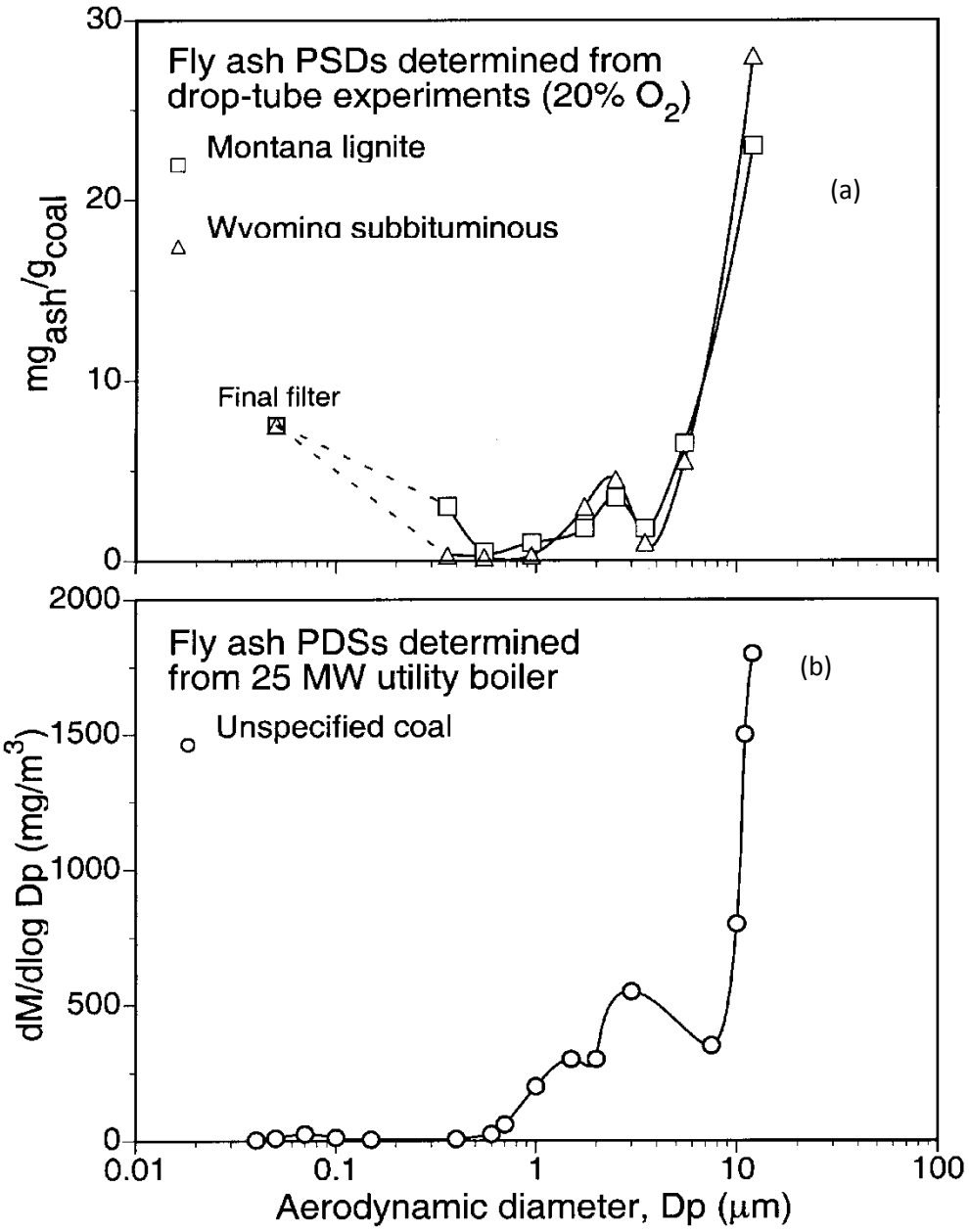

Figure 2.5 (a): Fine fly ash PSD from pulverised coal combustion (Linak *et al.*, 2002)

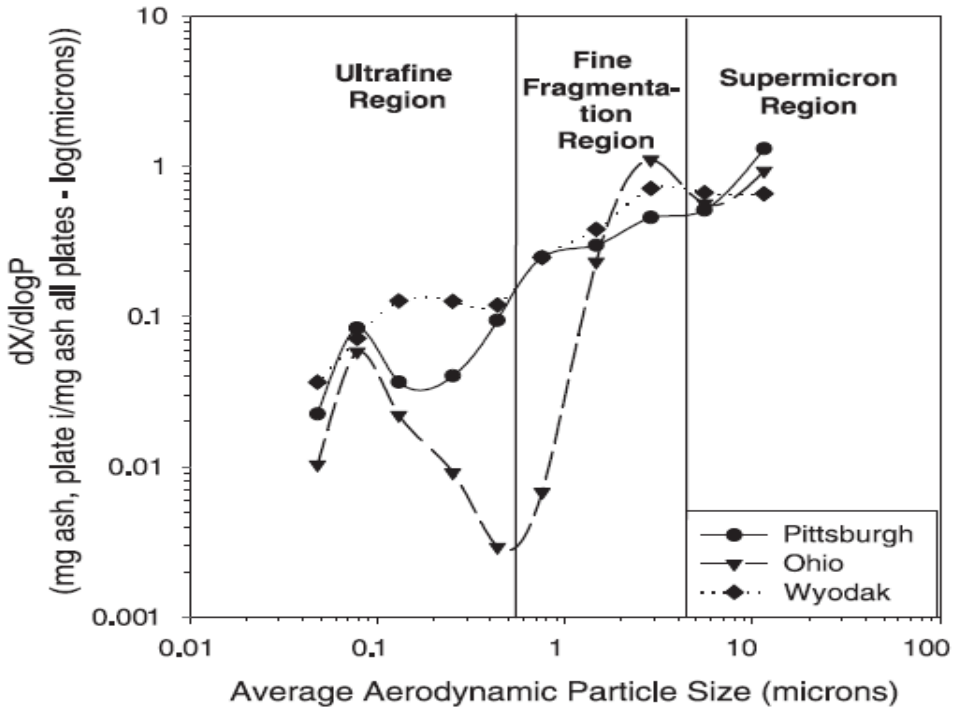

Figure 2.6: Trimodal fly ash distributions from three coals by Seams (2003).

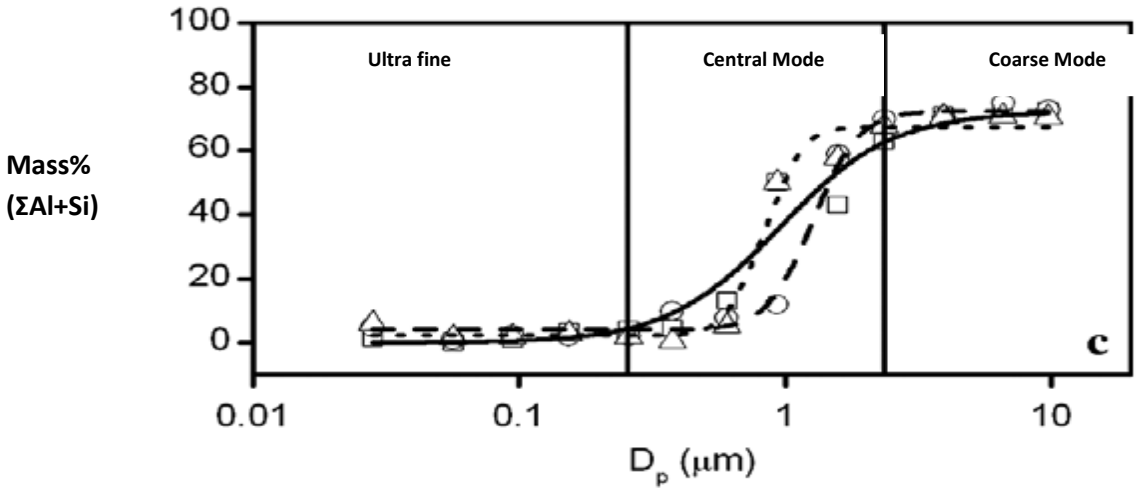

Figure 2.7: Trimodal PSD showing mass fraction of Aluminum and Silicon (Dunxi *et al.*, 2007)

△ Coal A, O Coal B, ▢Coal C

Figure 2.6 and Figure 2.7 by Seams (2003) and Dunxi *et al.* (2007) respectively show trimodal PSD obtained in recent years even though both Figure 2.6 and 2.7 do not show exact boundaries. Figure 2.8 (a) and (b) also show trimodal PSD. Each particle size mode range of particulates PSD is believed to arise from specific chemical processes and mechanisms. Morphologies and elemental composition of the PSD modes boundaries have also been examined and studied further in literature (Dunxi *et al.*, 2007; Dunxi *et al.*, 2008) in order to advance the understanding of the processes believed to govern the formation of particulates.

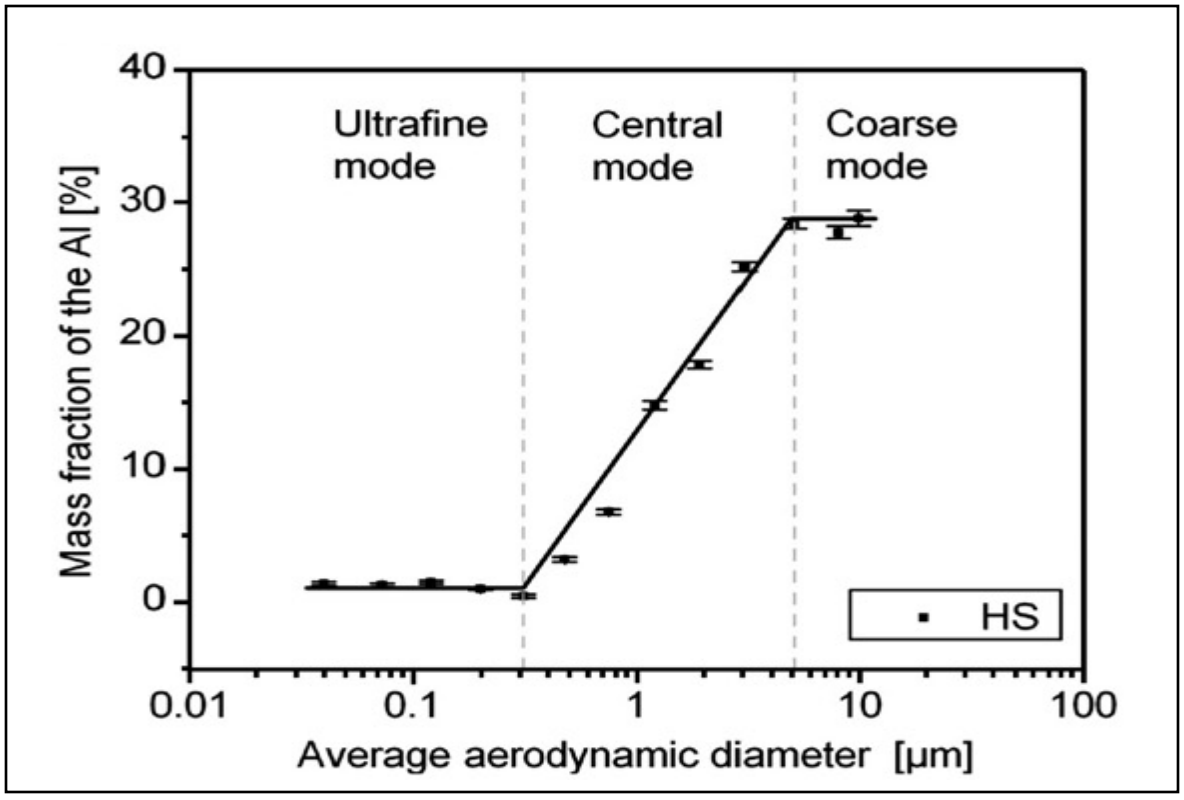

Figure 2.8(a): Fly ash PSD elemental mass fraction characterisation by Xu *et al*. (2008).

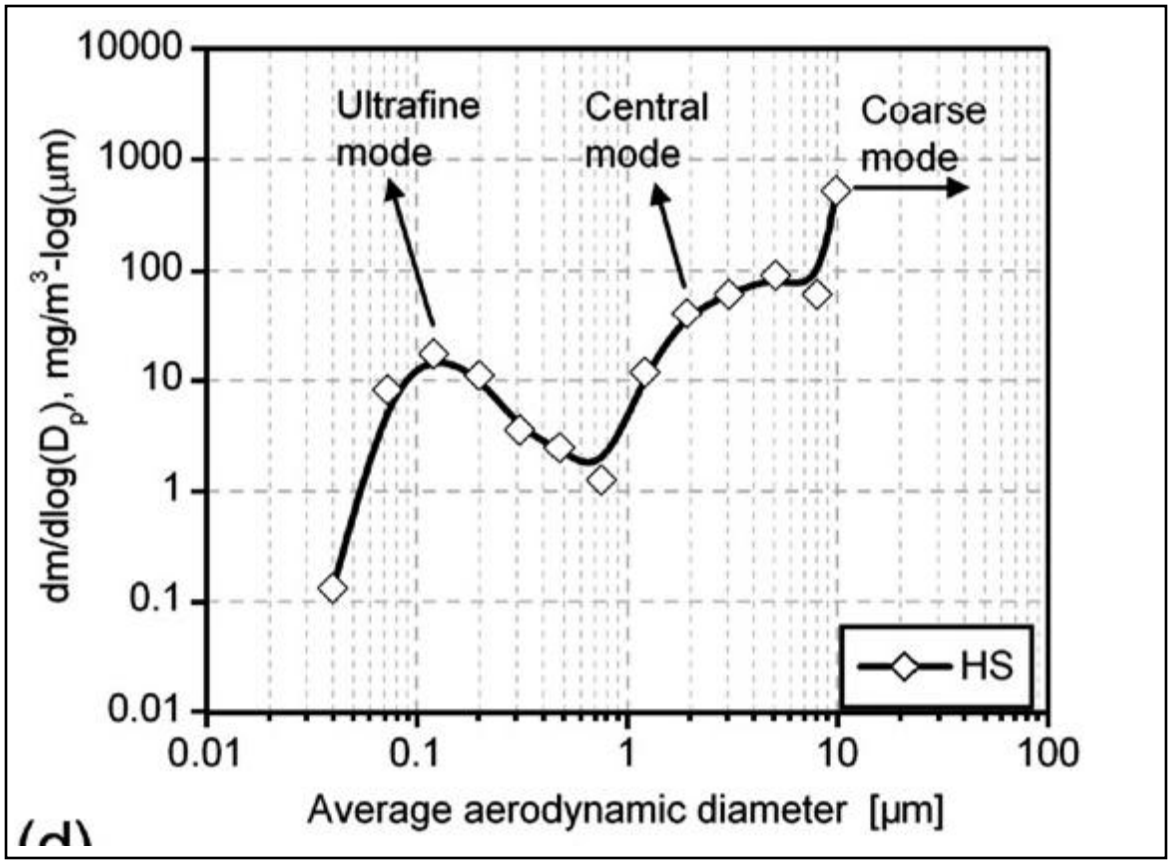

Figure 2.8(b): 1 Conventional fly ash PSD characterisation by Xu *et al* (2008).

Dunxi *et al.* (2007) developed a method of using elemental mass fraction PSD to characterize particulates. Dunxi *et al.* (2008) found particulates produced from pulverised coal combustion to be trimodal using elemental mass fraction characterisation. The short-coming of elemental mass fraction characterisation is that not all elements are in abundance in coal. Not all elements can be used to produce elemental mass fraction PSD for coal fly ash.

A trimodal PSD has the submicron fume region described by particle aerodynamic diameter of about 0.08 microns. The central mode is fine fragmentation centered and is positioned around 2 microns. The third mode class is a coarse mode fragmentation region for particles of approximately 5 microns in aerodynamic diameter and greater. The range values for the three modes differ from author to author even though they are similar.

2.3 Silicon and Aluminum

As discussed, the particulates PSD modes have different mechanisms of formation and different general elemental composition. Silicon and aluminum exist mostly in an oxidized form in coal combustion particulates. They exist in the ultra fine mode of coal combustion particulates even though they are considered nonvolatile. Dunxi *et al.* (2007,2008) report that aluminum and silicon amounts do not increase with increasing particle size in the ultra fine region as shown in Figure 2.7 from combustion of about three different coals. Xu *et al.* (2008) also found that the aluminum mass fraction is constant with increasing ultra fine particle size as shown in Figure 2.8(a).

Zhang *et al.* (2006) found similar results thereby concluding that some silicon and aluminum material does devolatilise at the pyrolysis stage and that silicon and aluminum melt under high temperatures in the combustion zone. Zhang *et al* (2006) quantified the amounts of silicon and aluminum oxides in the ultra fine mode from two bituminous coals and an anthracite coal as a function of temperature. Quann and Sarofim (1982) proposed that vaporization of silicon and aluminum is enhanced by the reducing effects of metal oxides such as CaO and MgO. The composition of the aluminum and silicon does not increase with increasing particle size in ultra-fine particles size range as a result of vaporization and successive condensation in the high temperature combustion regions (Smith *et al.*, 1979).

The amount of silicon and aluminum increases with increasing particle size in the central mode, and it is found that there are in large amounts in coarse mode particles as shown by Figure 2.7, and 2.8(a). The amounts of silicon and aluminum start increasing with an increase in particle size from the beginning of the central mode particle size range, and increase insignificantly in the coarse mode particles range. Coarse mode particle composition of both aluminum and silicon starts exceeding 60% at the end of central mode and nearing +90% in coarse mode particles size.

2.4 Sulphur and Other Elements

Sulphur, phosphorus, sodium and other elements are mostly transformed during coal de-volatilisation (Zhang *et al.*, 2006). Despite a significant variation of elemental inorganic composition in coal and in ultrafine particle chemistry, the dominant elements in the ultrafine particulates are sulphur, silicon, phosphorus and sodium (Seams, 2003). Sulphur exists in high proportions in ultra fine particulates relative to sulphur amounts in central mode and coarse mode and as shown in Figure 2.9(a) and Figure 2.10. Results have not been found for ultrafine particulates produced from coal with insignificant amounts of sulphur.

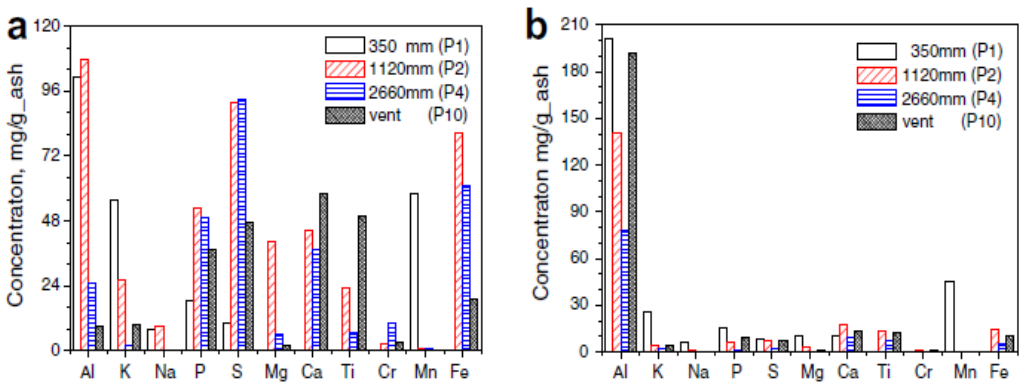

Figure 2.9: Elemental composition of two typical sizes in PM with aerodynamic diameter of 1 micron (PM_1):(a) for the size of 0.063 microns; (b) for the size of 0.655microns (Zhuo *et al.*, 2009).

(P is the distance from the start of the furnace to the vent).

Sulphur content decreases with increasing particle size in all particulates PSD modes in Figure 2.9(a) and (b), Figure 2.10 and Figure 2.11.

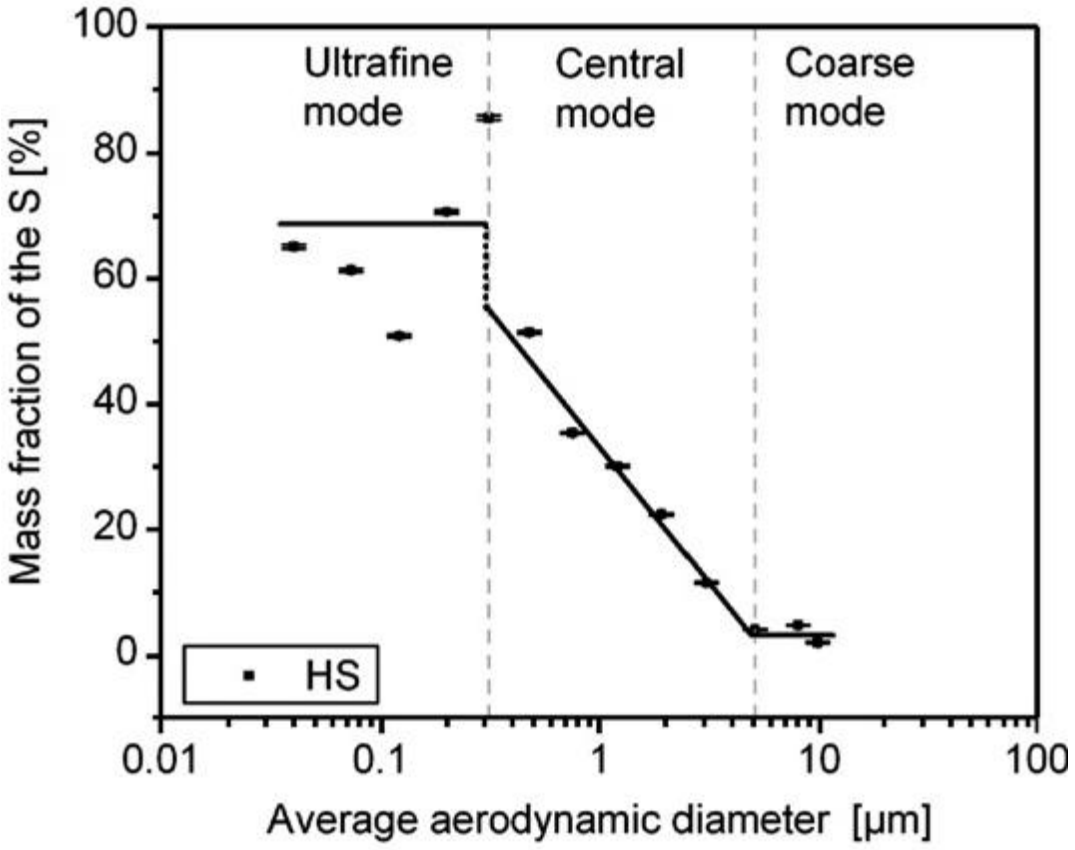

Figure 2.10: Sulphur mass fractions PSD for fly ash from pulverised coal combustion (Dunxi *et al.*, 2007).

Similarly, the concentrations of sodium and potassium decrease with increasing particle size in central mode and coarse mode particle size range as indicated in both Figure 2.9(a), (b) and Figure 2.11. All elements seem to exist in lower amounts as fly ash particle size increases, while aluminum and silicon increase with an increase in particle size.

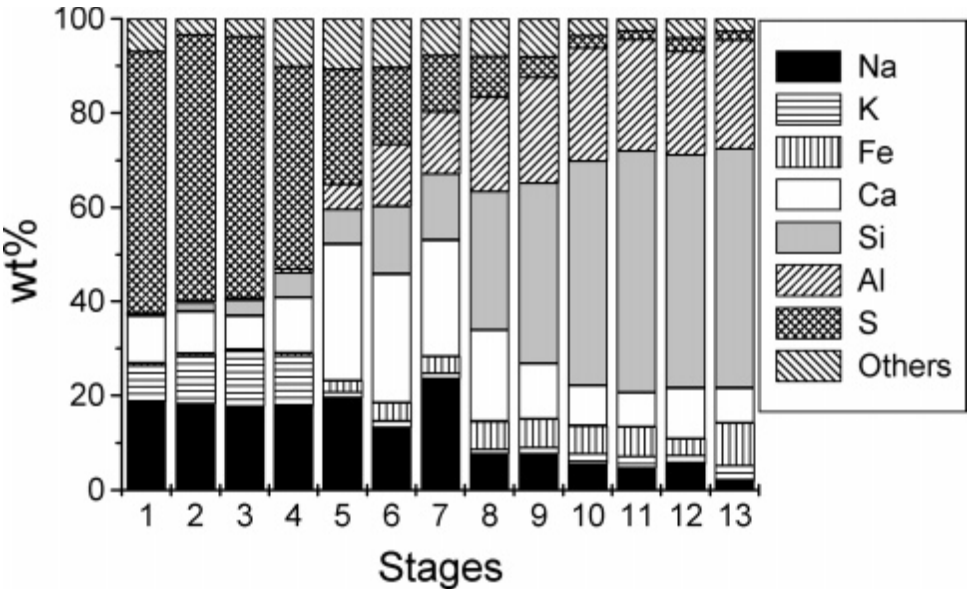

Figure 2.11: Elemental composition of each size class within PM class range collected on the 13 size-segregated Low Pressure Impactor, of 13 stages representing the aerodynamic cut-off diameter, 0.028, 0.057, 0.094, 0.15, 0.26, 0.38, 0.61, 0.94, 1.58, 2.36, 3.95, 6.60, and 9.80 µm, in increasing order (Xiaowei *et al.*, 2007).

2.5 Morphologies of fly ash particles

The three regions of the PSD have different morphologies. Combustion stage processes and process variables have a great influence on the morphologies of the particulates.

2.5.1 Ultra fine

The morphology of particles formed during pyrolysis and combustion differ because of different combustion stage temperatures and pressure. Some ultra fine particles morphology cannot be analysed fully due to the resolution limits of the SEM (Seams, 2003). However, particle morphologies examined by Seams (2003) and Zhang *et al.* (2006) appeared to be primarily spherical in shape as shown in Figures 2.12 (a) and (b). The unique agglomerations cluster as depicted in Figure 2.12(c) are said to arise when the temperature decreases thereby causing the particles to agglomerate into chain or cluster aggregates (Helble and Sarofim, 1989).

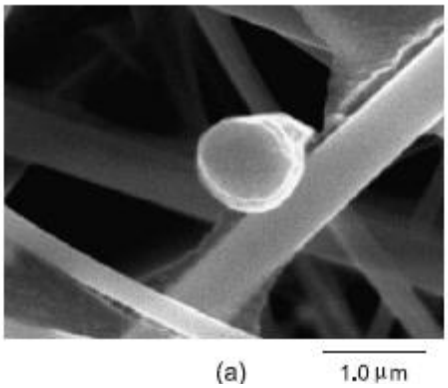

Figure 2.12 (a): Morphology of ultra fine particles as determined by SEM (Ninomiya *et al*, 2004).

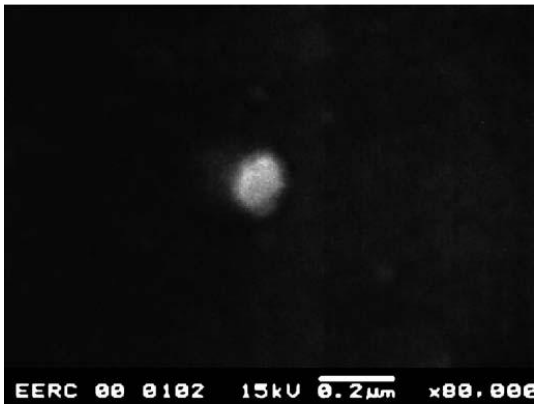

Figure 2.12 (b): Morphology of ultra fine particles as determined by SEM (Seams, 2003).

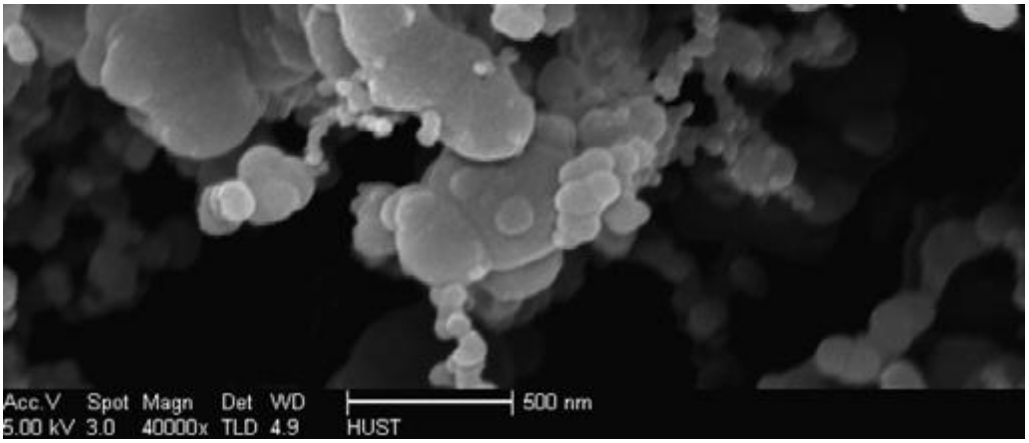

Figure 2.12 (c): Morphology of ultra fine particles as determined by SEM (Dunxi et al., 2007; Xu *et al*., 2008).

2.5.2 Central Mode

Morphologies of central mode particles are mostly spherical with some irregular shapes as shown in Figures 2.13 (a) and (b). The presence of irregular shapes in the central mode particles could be assigned to various fragmentation mechanisms that involve particle inflation, cracking and perimeter material shedding as the result of the expansion of gases within the coal particles (Seams, 2003). While Dunxi *et al*. (2005) attributed smooth spherical shapes to more oxygen and high temperatures, the irregularities in shape were assigned to low combustion temperature and poor oxygen concentrations.

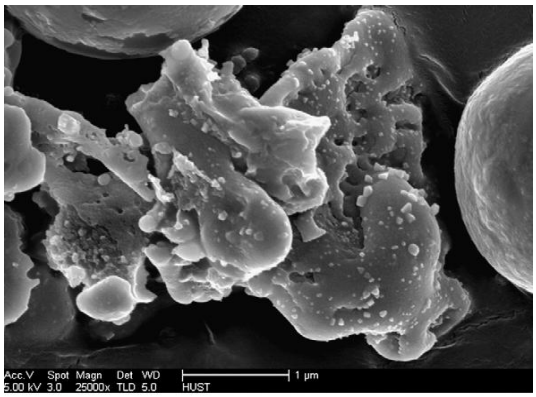

Figure 2.13(a): Morphology of central mode PM particle (Xu *et al.*, 2008).

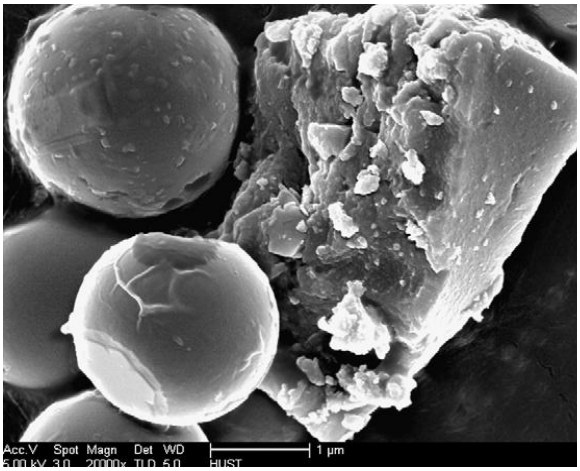

Figure 2.13(b): Morphology of central mode PM particle (Xu *et al.*, 2008).

2.5.3 Coarse Mode

Most minerals in coal have melting points below 2000K. Char surface temperatures are higher than temperatures in the combustion environment, i.e. up to 1750 to 1800K. As a result mineral grains are exposed to higher combustion temperatures. This causes mineral grains that are associated with organic matrices or on the surfaces of char particles to melt and occasionally form some spherical droplets, due to their high surface tensions (Ramsden, 1969). Some coarse mode particles also possess distinct ultra fine particles that have sintered and stuck onto the particle surface as shown in Figure 2.13(a) and (b) and Figure 2.14 (b).

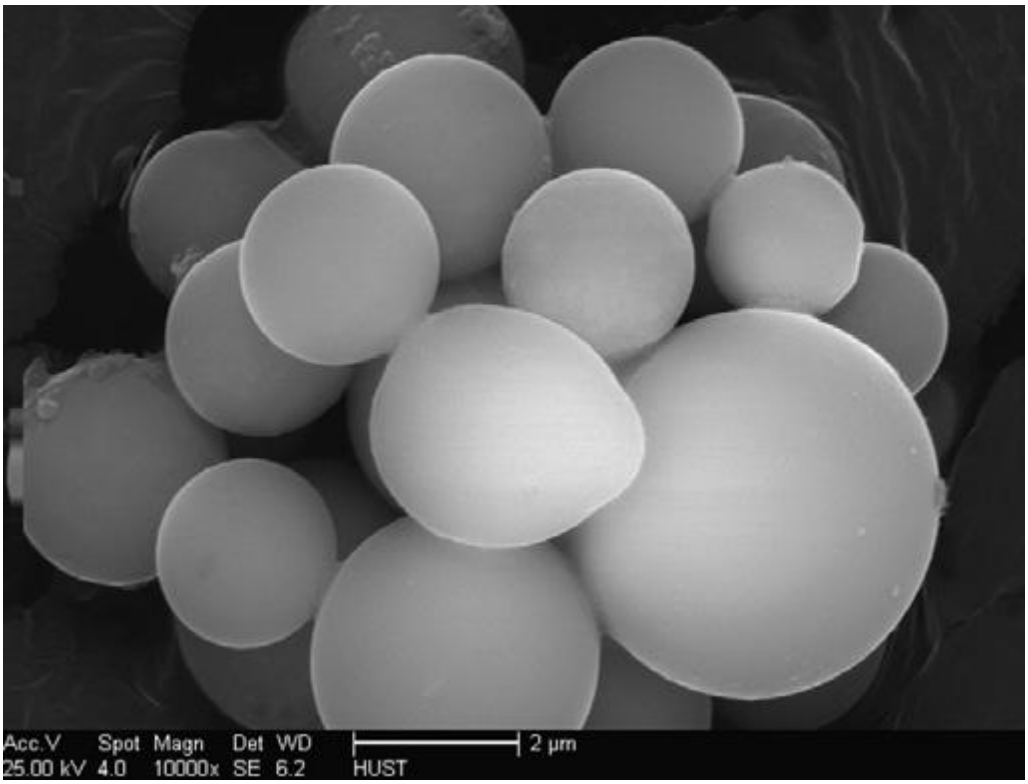

Figure 2.14(a): Typical Morphology of coarse particle (Dunxi *et al.*, 2007).

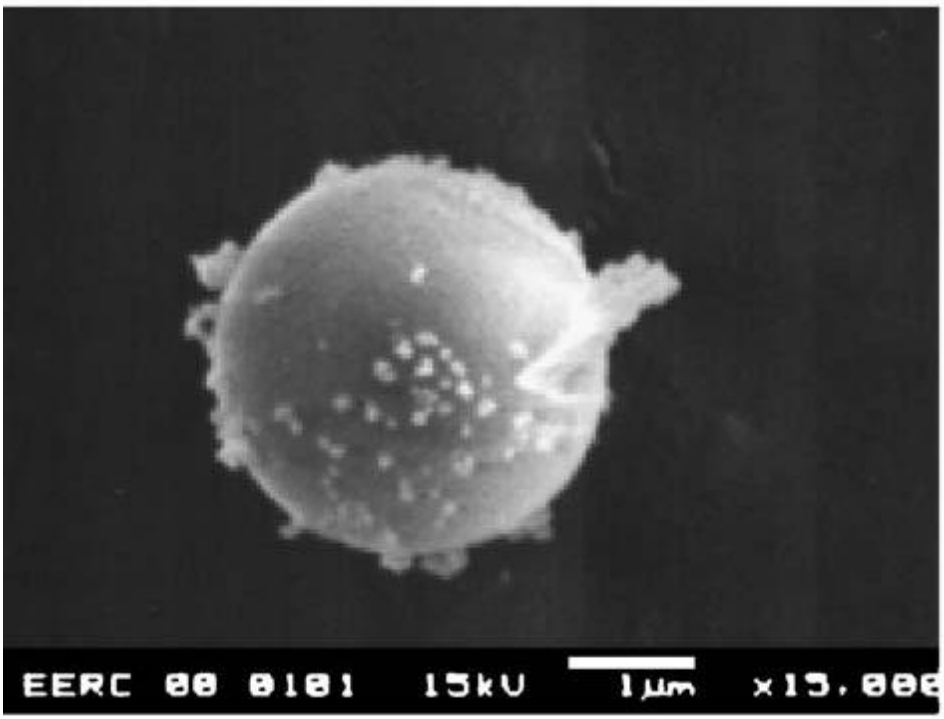

Figure 2.14(b): Typical morphology of coarse particles (Seams 2003).

2.6 Aluminum and Silicon Environmental Effects

Most PM_{10} particulates do not travel long atmospheric distance because they are denser than air and hence they settle out very quickly relative to $PM_{2.5}$ particulates. As discussed in section 2.3, aluminum tends to concentrate in the coarse mode relative to other PSD modes; the coarse particles are not that harmful to human life since they are readily exhalable. The increased deposition of coarse particles on the ground results in high aluminum concentration in the soil that causes the soil to be more acidic and hence this affects the plant life (Neal, 1991).

The continual inhalation and exposure to the silicon rich particulates that result from respirable crystalline silicon leads to silicosis or mucus hypersecretion (Brinckerhoff, 2009) because the silicon deposited on human lungs causes' irritation on lung air sacs reducing the capacity for oxygen inhalation. Some of the inhaled ultrafine particulates enter the human blood stream causing various diseases that could lead to heart disease (Amann *et al.*, 2006).

2.7 Summary and Conclusion

This chapter reviewed the literature concerned with the origin, formation, size distribution and nature of the ultra fine, central mode and coarse mode particulates produced from coal combustion.

The PSD of less than 10 microns particulates from coal combustion was recorded to be bimodal initially but more recent work characterizes it as trimodal. The ultra fine particles were found to have more sulphur, sodium, calcium and less silicon and aluminum while the central mode and coarse mode contained more aluminum and silicon, based on studies conducted predominantly at a laboratory scale.

The morphology of each particle size range differs as particle morphology is strongly influenced by combustion operating conditions, post combustion cooling rate and inter particle collisions, which is influenced by particle size and composition. The work reported above was conducted on coals in various international laboratories. The research in this investigation will concentrate on South African coal and fly ash particulates of PM_{10} and smaller.

South African coals do not have a lot of sulphur and as a result one would not expect sulphur to be dominant in the ultra-fines. The ultra-fines produced from local coals might have different chemical composition to the ultra-fines found in literature. The difference in chemical composition might result in different morphologies as well. The central mode and coarse mode chemical compositions should be the same to the one of international coals since aluminum and silicon are still the most common elements in the local coals minerals.

3.0 Introduction

This chapter outlines the methodology used in this research for the sampling and the analysis of the coal and fly ash products sampled from a Pf coal boiler and a chain grate stoker.

The coal was sampled from the coal fed to the chain grate stoker as well as fed to the pulverised coal fired boiler and these samples were subsequently analysed using XRF, SEM, SEM EDS and XRD. The parent coal sample from the Pf coal boiler was taken from the JV14 power station boiler only. There were no coal feed-stocks sampled from three other power stations, only fly ash samples were taken from in these installations.

The fly ash samples were sourced from four Pf boilers, namely from the power stations designated as: JV14, IA14, HY23 and JL10. There were two sets of fly ash samples taken from the JV14 boiler, one sample from the ESP and another from the stack. The fly ash samples from the three other power stations were sourced from the stacks only. The stack fly ash sampling methodology was similar for all four power stations. These stack fly ash samples were collected using filter thimbles while the ESP fly ash was collected using a cylindrical sample container.

The fly ash sample from the chain grate was sourced from the stack. The fly ash and coal samples were taken from one chain grate stoker only. All chain grate stoker fly ash and coal samples were analyzed using similar techniques to those applied in the analysis of the Pf boiler samples. The flow diagram that summarizes the whole experimental procedure is shown in Figure 3.1

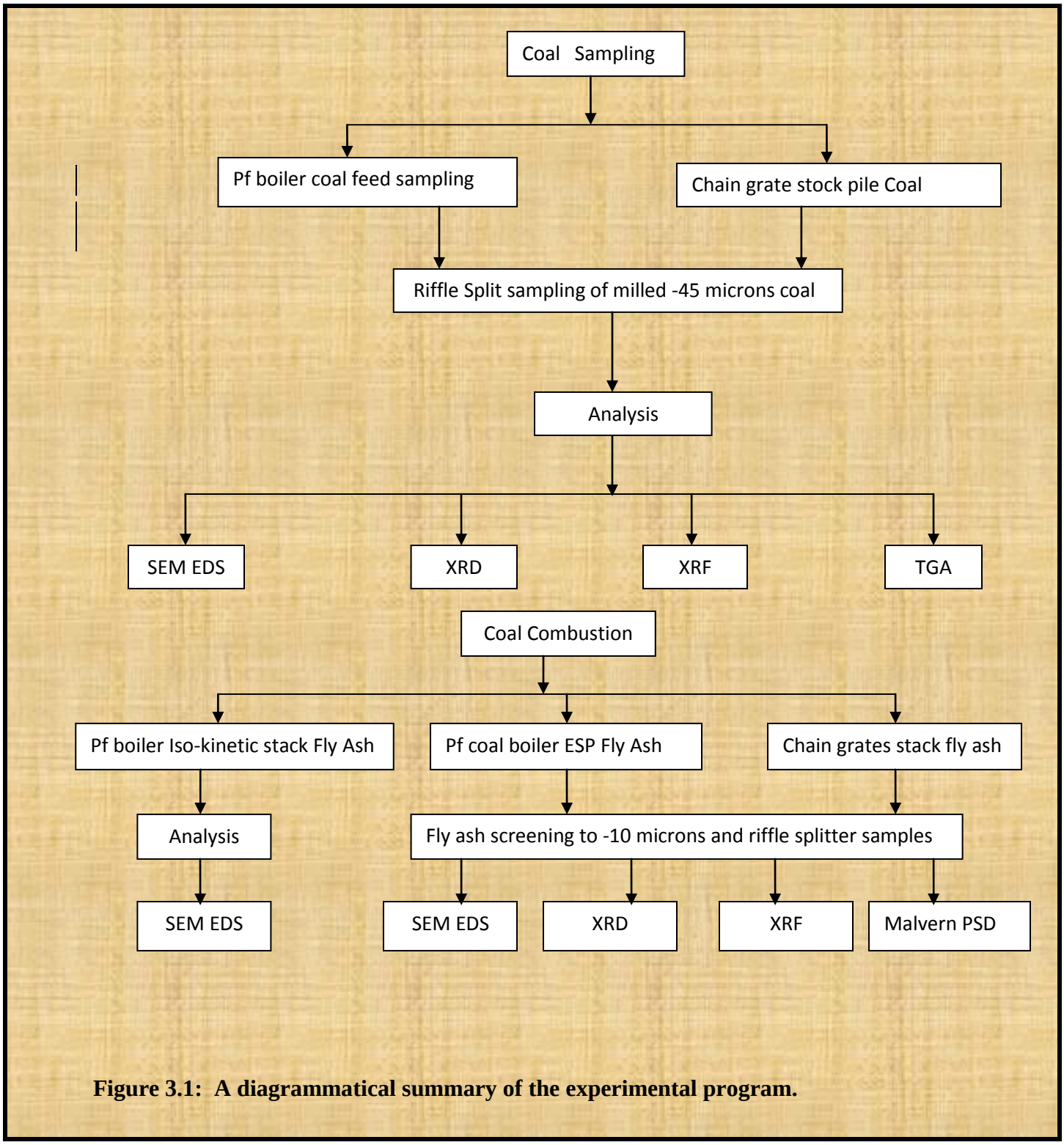

Figure 3.1: A diagrammatical summary of the experimental program.

3.1 Coal Sampling

Feed coal was sampled for both the Pf coal and the chain grate coal.

3.1.1 Pulverised Coal Sampling

The feedstock coal was sampled between the pulveriser and the JV14 power station boiler at the point SPC-01 as shown in Figure 3.1.

3.1.2 Chain Grate Coal Sampling

The chain grate coal was sampled from the coal feed stockpile. The opening dimensions of the sampling device employed were sufficient to permit the largest coal particle to pass into it freely without resistance. Several samples were taken from various positions on the stockpile. Samples were collected over the entire stockpile to account for any coal variance within the stockpile.

All individual sample batches were combined to form one sample consignment. The consignment was coned and quartered then milled. The milled coal sample was screened on a sieve stack mounted on an electric shaker and sampled further using at spinning riffle splitter. The riffled samples were sent for XRD, SEM and XRF analysis.

3.2 Fly Ash Sampling

This section describes the isokinetic sampling of the stack fly ash of the Pf coal fired boiler. The method utilized for collecting airborne particulates or fly ash was done on stack ports using sampling probes. The sampler is configured so that the flue gas stream entering the probe has a velocity equal to the velocity of the flue gas in the stack flue gas stream. The positioning of the sample probe inside the stack is a function of the stack diameter and stack ports and the number of traverse points (an end point position of the probe nozzle inside stack on stack diameter during iso-kinetic sampling)

3.2.2. ESP Fly Ash

The ESP fly ash was collected from power station JV14 from the ESP outlet using a cylindrical container. The iso-kinetic sampling could not be employed prior to the ESP inlet due to the fact that at the ESP inlet there are still particles much bigger than 10 microns that could lead to the blockage of the probe nozzle, since the probe is designed for ±10 micron particles.

3.2.1. Iso-kinetic Stack Sampling on the Pf Boiler

The in stack iso-kinetic sampling of particulates was done at corresponding times with coal sampling at point SST-01 also shown in Figure 3.2. This section does not include ESP fly ash sampling. The stack sampling was done in manner described above for power stations.

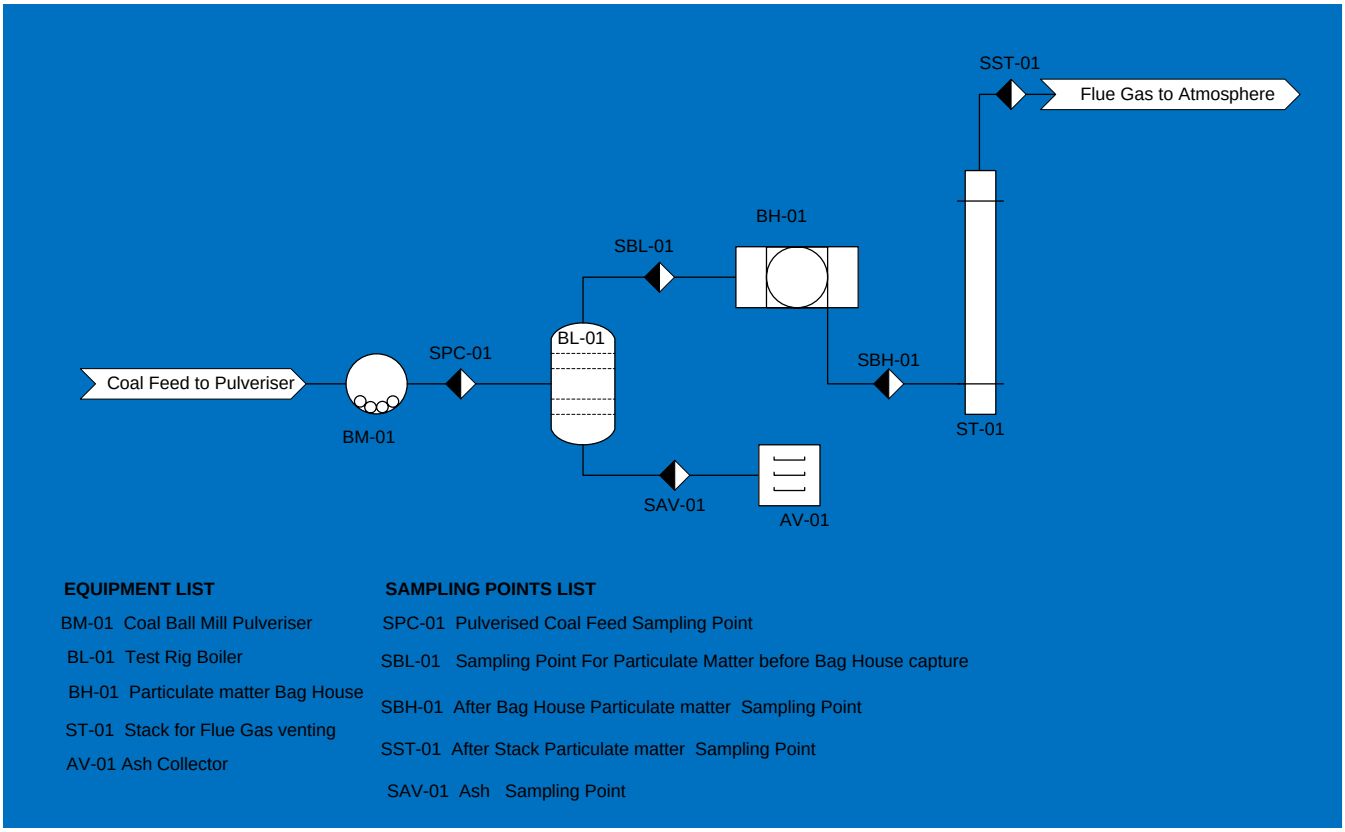

Figure 3.2: Flow diagram showing sampling points.

A long-stack sampling probe was fitted with a borosilicate thimble assembly from the sampling train similar to the type depicted in Figure 3.3. This probe was then inserted into the stack. The stack ports that were used for iso-kinetic particulates sampling, are positioned parallel and perpendicular to the longitudinal axis of the stack. The inner stack sampling positions and the traverse points of the circular stacks were determined according to the percentage of stack inner diameter as shown in Table 3.1.

Table 3.1: Location of Traverse Points in Circular Stacks (EPA, Method 101, 1989).

Traverse Point Number on a Diameter	Number of traverse points on a diameter											
	2	4	6	8	10	12	14	16	18	20	22	24
1	14.6	6.7	4.4	3.2	2.6	2.1	1.8	1.6	1.4	1.3	1.1	1.1
2	85.4	25.0	14.6	10.5	8.2	6.7	5.7	4.9	4.4	3.9	3.5	3.2
3		75.0	29.6	19.4	14.6	11.8	9.9	8.5	7.5	6.7	6.0	5.5
4		93.3	70.4	32.3	22.6	17.7	14.6	12.5	10.9	9.7	8.7	7.9

(Percent of stack diameter from inside wall to traverse point)

The nozzle of the probe was positioned at the first traverse point with the probe aperture inclined into the gas stream in order to measure the characteristics of the flue gas stream prior to the iso-kinetic sampling, namely; gas velocity, stack temperature, moisture and molecular weight of the stack flue gas. This was done in order to find the proper operating conditions for the sampling train assembly and for the iso-kinetic sampling.

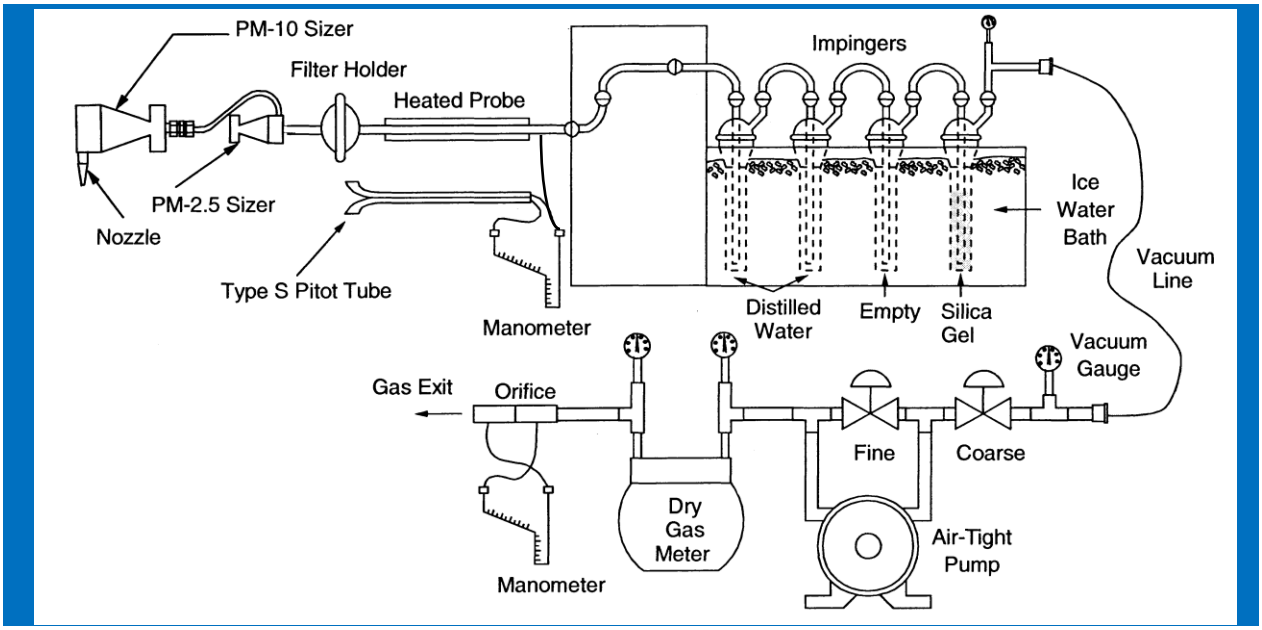

Figure 3.3: Typical Sampling train for stack sampling (Environmental Protection Agency, 2009).

A dry gas meter was used to measure the volumetric flow rates at the beginning of the test. A vacuum pump was used to regulate the flow of the iso-kinetic sampling conditions. Since there is no single complete standard sampling method for in-stack PM sampling, guidelines and standard procedures from various sampling methods were used to develop a complete sampling method. The procedures and guidelines were borrowed from various EPA methods, namely: Method 5, Method 3 and Method 2 have been extensively used to provide the appropriate guidelines for isokinetic sampling of the $PM_{2.5}$ material. Most of guidelines were however derived from EPA Method 5. These guidelines are general and therefore do not have specific details. The sampling trains defined by Method 5 are of different designs depending on which other EPA Methods were used to complete the gaps and short comings left by EPA method 5. The typical sampling train is shown Figure 3.3. The typical sampling train contains silicon gel that absorbs the moisture from flue gas to avoid the vacuum pump from becoming damaged by the moisture. The function of the vacuum pump is to transport the flue gas through the gas meter analyser. A valve is employed to control the flue gas flow rate while an orifice meter measures the flow rate to within ±2% of the isokinetic sampling flow rate.

Figure 3.4(a): Picture of filter thimble employed for PM collection in sampling train shown in Figure 3.3.

Figure 3.4 (b): The inner view of filter thimble.

A typical filter is shown in Figure 3.4 and is of the type inserted into the sampling train filter housing shown in Figure 3.3 for the collection of particulates. The fly ash collected in the filter is a bulk collection of ultra fine, central mode and coarse mode particles. The filter has a micro porosity of 0.3 microns. Ultra fine particles lower than 0.3 microns cannot be captured by the filter. The flue gasses contain some moisture that gets absorbed into the filter surface and results in a changed structure due to the moist surface.

Sampling positions were chosen using the traverse points that are determined according to Table 3.1. The numbers of traverse points were averaged using the stack diameter. The traverse points were picked from all the stack ports so that homogeneous representative samples could be collected. The top view of the stack showing stack ports and traverse points is shown in Figure 3.5

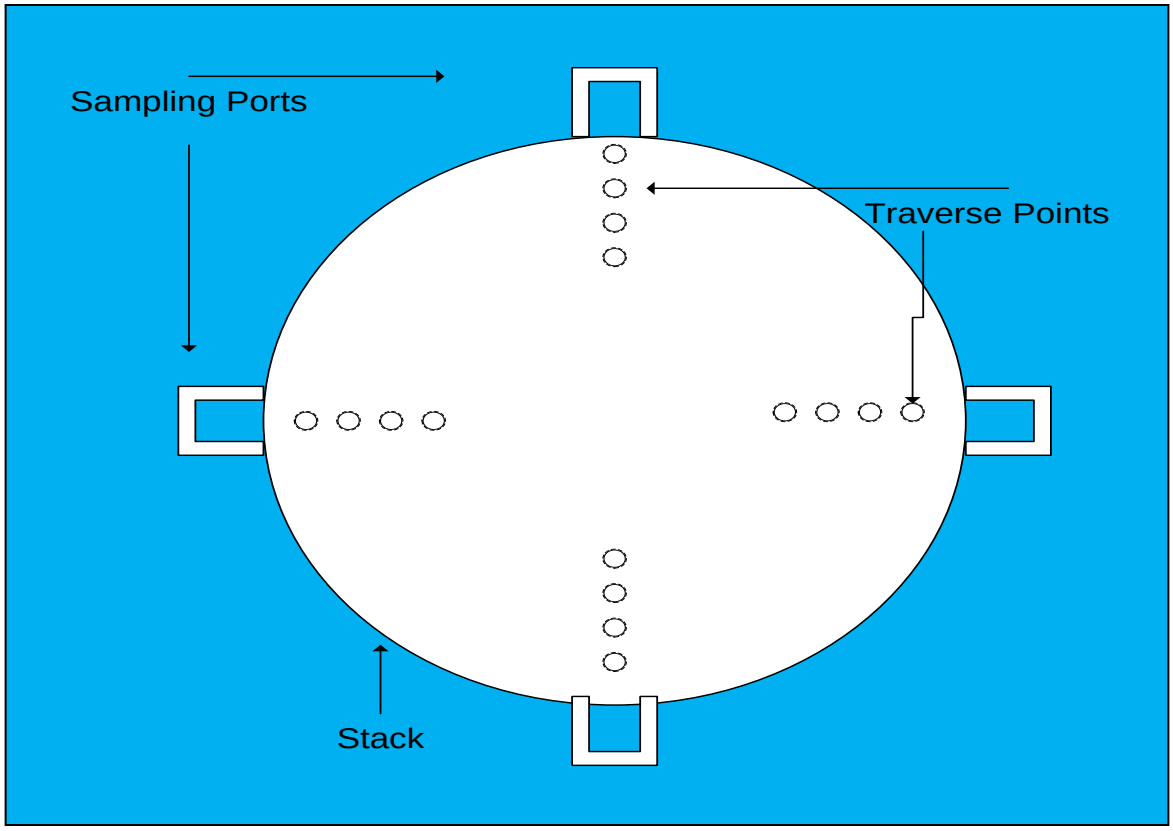

Figure 3.5: Top view of typical circular stack in showing the positions of traverse points (Sampling points).

3.2.3 Chain Grate Stack Fly Ash

The details of the stack fly ash sampling were not given by the company that provided the fly ash**.** It is assumed that a suitable cyclonic device was used to capture the fly ash particles in this case.

3.3 Fly Ash Screening

The fly ash particles were screened in order to determine the PSD and to obtain specific modes particles for analysis. The fly ash screening was done using a sieve screen stack mounted on an electric sieve shaker.

The fly ash that was screened was from JV14 power station ESP and the chain grate stoker stack. The fly ash particles were screened due to the fact that there were particles bigger than desired size of -10 microns present. The iso-kinetically sampled stack fly ash particles were not screened because the particles were smaller than 10 microns, small in quantity and since they were also found to be trapped within filter thimble fibres.

3.3.1 Dry Fly Ash Screening

A conventional laboratory screen stack mounted on an electric sieve shaker was employed to size segregate the fly ash into the three desired size classes. For this purpose, the screens were sequenced in the order of 20 microns, 15 microns and 10 microns. The recovery of -10 microns particles in each run was very small; and as a result repetitive runs were carried out so that sufficient amounts of <10 microns particles could be attained for analyses.

The poor collection efficiency was due to sieve screen mesh blinding as sieve blinding increased with decreasing screen mesh aperture. Severe sieve blinding begins at 100 microns aperture (Liu, 2009) and at 10 microns aperture the sieve bed became stagnant and immobile after an hour of sieving.

3.3.2. Wet Fly Ash Screening

A typical wet fly ash screening device as depicted in Figure 3.6 was used to increase the recovery of -10 micron fly ash material and to separate the particles into different size classes below 10 micron, 5 micron and 1 micron respectively. The +10 micron and -10 micron fly ash particles from the dry screen sieving were placed on 15 micron nylon mesh to recapture particles greater than 10 microns that had penetrated the 10 microns sieve mesh due to their irregular shapes. Some of the dry sieve screens mesh apertures were found to be bigger than the nominal diameter of 10 microns which allowed larger particles through.

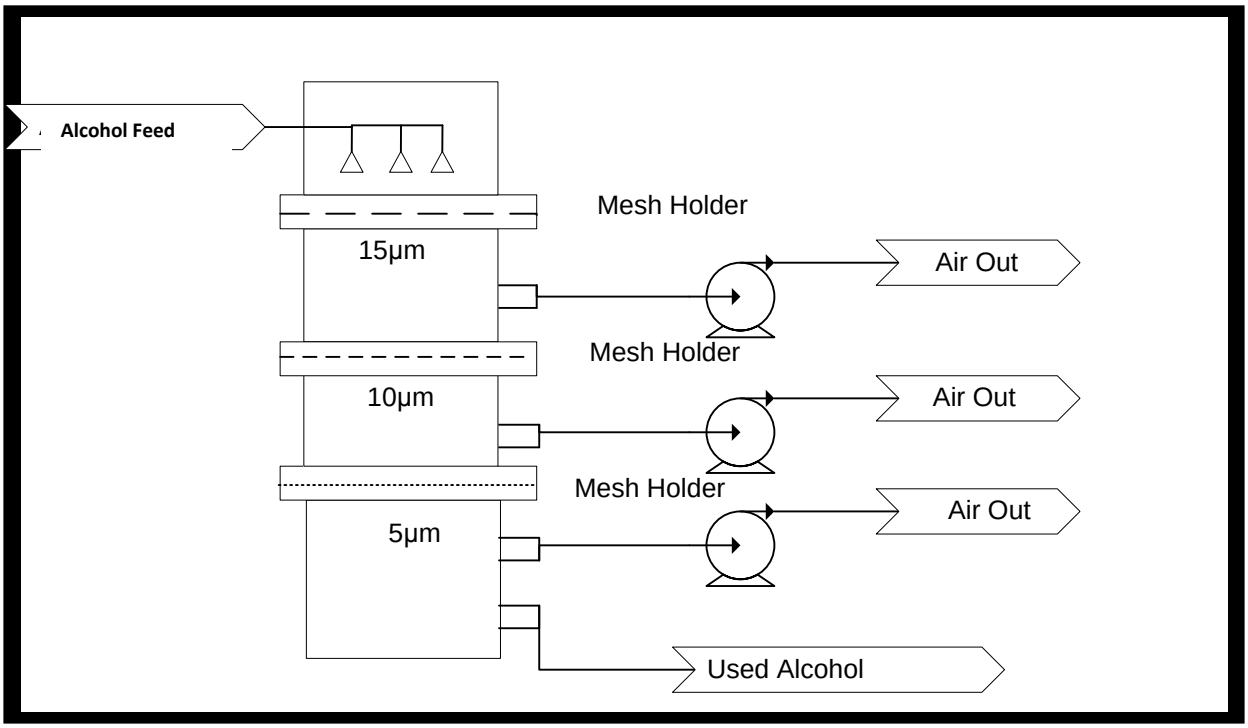

Figure 3.6: The wet fly ash sampling device.

The mesh sizes used in the wet fly ash screening device were 15 microns, 10 microns and 5 microns respectively and were made of nylon. Nylon meshes were positioned in the decreasing nominal aperture order of 15, 10 and 5 microns on the wet separation device as indicated in Figure 3.6. The 15 microns nylon mesh separation efficiency was poor so it was replaced with a 15 microns steel mesh which was found to have better separation efficiency.

The efficiency of the -10 microns and 5 microns nylon meshes were also found to be very poor. The quantity of fly ash samples collected on the nylon meshes was not sufficient to effectively determine the three size classes (ultra fine, central mode and coarse mode) and for SEM EDS, XRF and XRD analysis. The nylon meshes of 10 microns and 5 microns could not be replaced with the steel meshes or any metallic meshes because most of the local suppliers that were consulted only sold metallic meshes with a minimum size of 15 microns. The failure to secure metallic meshes with apertures smaller than 10 microns led to the failure of size segregating the fly ash into three size classes of ultrafine, central mode and coarse mode.

The <10 microns fly ash particles separated using stack mounted sieve screens on an electric shaker were taken for SEM, XRD and XRF analysis as they were. They were not subjected to any further separation of three size classes of ultra fine, central mode and coarse mode material.

The recovery of fly ash particles was very poor because the wet screening device lacked the ability to move both horizontally and vertically. The particle movement was only in a one dimensional downward vertical direction due to the vacuum pressure created by the vacuum pump. As a consequence of the lack of horizontal movement the particles were concentrated in the centre of the mesh, which resulted in the mesh developing a concave shape under the high vacuum pressure. The concave shaped mesh reduced the active surface area for screening and as a result, the particles became compact and hard to separate. The use of more alcohol was not attempted as this could have resulted in changes to the particle morphology and chemistry with the leaching of some fly ash constituents.

It should be noted that the separation efficiency of the 15 microns steel mesh was better than the 15 microns nylon mesh (as indicated above) due to the fact that the steel mesh had better mechanical strength and did not produce the pronounced concave shape as seen with the nylon mesh.

3.4 Coal Samples

The feed coals from the chain grate boiler and Pf fired boiler were weighed as received and left to dry overnight at room temperature. The residual moisture was determined for both coal samples. The dried samples were coned and quartered and stored in labeled plastic bags. Representative samples from both coal samples were milled further to below -75 microns and riffled. Riffled representative samples were sent for TGA XRD, XRF and SEM analyses.

3.5 Fly Ash Samples

The <10 micron fly ash samples from the JV14 ESP and the chain grate stack screened were riffled on a spinning riffle splitter in order to obtain representative samples. The representative samples were taken for XRF, SEM, XRD, SEM EDS and Malvern laser diffraction based particle size analysis.

The fly ash samples sourced from the stack using filter thimbles from the Pf coal boiler power stations were analyzed using SEM and SEM EDS only. The fly ash particles were still trapped within filter thimble fibers when they were analyzed.

3.6 Themo-gravimetric Analysis

Thermo-gravimetric analysis (TGA) was used to conduct the proximate analysis of the pulverised coal from the JV14 boiler as well as for coal from the chain grate boiler. The TGA equipment used was a PerhinElmer Simultaneous Thermo-gravimetric Analysis STA 6000 with pyn software. This instrument is located in the coal laboratory in School of chemical and metallurgical engineering in Richard Ward building at University of Witwatersrand. The proximate analysis of coal includes the composition of the following parameters:

- % Moisture,
- %Volatile Matter,
- %Ash Yield, and
- Fixed carbon (by difference).

The -45microns coal was riffle split and a representative sample was then taken for TGA analysis. An in-house technique was followed for this analysis and is described below. A water bath was fitted to the TGA and was run at an operating temperature of 10^{o}C. The sample mass of coal that was used in the TGA was 10.63mg; (the mass required by the TGA must be between 5 and 15 mg). The 10.63mg sample mass was determined in a crucible. After the sample was loaded the combustion reaction was started at a heating rate of $20^{o}Cmin^{-1}$. The oxygen flow rate was set at 20 ml/min. Nitrogen was supplied at inert conditions of 20 ml/min.

3.6.1 Determination of Moisture

The coal sample was heated to 110°C at a rate of 20°C min^{-1} in an inert atmosphere and the heating rate was kept uniform for about 5 minutes. The weight loss encountered during the first 5 minutes of heating was attributed to moisture loss.

3. 6.2. Determination of Volatile Matter

The coal sample was then heated further to 900°C at a rate of 50^{o}C/min in an inert atmosphere and at a constant heating rate. The resultant weight loss was attributed to the loss of the volatile matter component of the coal.

3.6.3. Determination of Ash Yield

The temperature of 900^{o}C was then maintained in an oxygen atmosphere and the resultant mass was taken to be the ash yield.

3.6.4 Determination of Fixed Carbon

Fixed carbon is determined from the following formula:
Fixed carbon =100% -(Moisture(%) + Volatile matter(%) +Ash yield(%))

3.7 Scanning Electron Microscope

The SEM was utilized to determine the morphology and chemical composition of both parent coals from the JV14 power station and the chain grate boiler. The screened and riffled representative -10 microns fly ash samples from the JV14 power station ESP, the chain grate stack fly ash and the filter thimble samples from other power stations were analysed in a similar way.

3.7.1 Coal and Screened Fly Ash Sample Preparation for SEM Analysis

The portions of homogeneous samples of coal below 45 microns were mounted on a sample holder and coated with a copper strip before being placed inside the SEM. This was done to improve sample electron conductivity, and to avoid charging during sample analysis. The -10 microns fly ash sample for SEM EDS analysis was prepared in a similar fashion to the coal sample.

3.7.2 Preparation of Stack Filter Samples for SEM Analysis

Due to poor emission rates and high ESP efficiency from the power stations stacks of JV14, HY23, IA14 and JL 13, only very small quantities of particulates were collected in the filter thimbles. In each case the fly ash quantities were deposited on the filter surface and trapped within the filter fibres. As a result, the particulates had to be analysed on the filter paper because the filter and collected particulates had become inseparable.

The filters were observed under a ZEISS semi DV4 optical microscope in order to identify areas of the filter loaded with particles. The particles were scattered all over the bottom part of the filter thimble and the concentration was found to be inhomogeneous. The areas of the filter thimble that were found to be particle loaded were labeled and cut out in 30 x 30mm pieces. The cut pieces were mounted on sample holders and carbon coated. The filter pieces mounted on sample holders were placed inside a carbon cylinder block coated with copper which was used as an indicator for coating thickness so that the filter samples could be coated to the required coating thickness.

The Auto Carbon Coater was used for filter sample coating since the filter samples were non-electron conductive before SEM X-ray analysis. High purity graphite carbon rods were held in position by springs and a rod holder assembly. The vacuum of the carbon coater was operated at a vacuum pressure exceeding 8 mbar and an operating voltage of 4.7 volts. The start button on the carbon coater was depressed for about 15 seconds which allowed the rods to heat up and for multiple evaporations to take place. This led to about 15nm thickness of coating on the filter samples.

3.7.3 SEM EDS Analysis

The carbon coated filter samples, copper coated samples of fly ash, and coal powder samples were placed on sample holders which were then inserted into a high pressure vacuum chamber that was linked to the SEM unit. The equipment that was used in this instance was a FEI Quanta 200 SEM which had an energy dispersive analyser of the Oxford INCA 400 EDS type fitted with a tungsten filament laser that could produce 1500K electrons per second.

The equipment was employed to quantify both coal and fly ash mineral constituents. Morphological characterisation of both fly ash and coal was also undertaken. Point analysis was employed in analysing filter samples because both the filter and the fly ash contained quantifiable silicon. The automated analysis would have quantified the silicon from both the filter material and fly ash. Point analysis avoided including the filter material. The automated analysis was applied to all fly ash and coal samples.

3.8 XRF Analysis

The low temperature coal XRF analysis method undertaken for this study by Witlab is not discussed in this research report due to the fact that the details of the method were not supplied by Witlab. Only fly ash XRF analysis is discussed.

3.8.1 Coal XRF

It is assumed that Witlab used an ISO standard method to quantify coal chemical composition.

3.8.2 Fly Ash XRF Analysis

XRF analysis was undertaken to determine the composition of the major elements. The XRF analysis was conducted by the Geology Department of University of Witwatersrand. The fly ash samples were subjected to a temperature of 110^{o}C for about 40 minutes to dry them. Representative samples of the fly ash were then mixed with lithium tetra-borate powder in a mass ratio of 5(flux) to 1(sample). The mixture was placed in a platinum gold crucible that was heated at 1000^{o}C for 40 minutes in a Mugfile furnace. The sample was dried so that the percentage of mass loss could be determined upon ignition of the sample, as calculated using Equation 1. The ignited fused product from the furnace was pressed into a homogeneous glass bead on an aluminum scientific hotplate and then weighed, so as to determine the starting mass that is required when calculating the percentage loss on ignition (LOI). The pressed sample was left for 24 hours before elemental analysis was undertaken.

%LOI is percentage loss on ignition

%LOL= **(**(W_1-W_2) / (W_1- W_c)**)***100%.....Equation 1

Where: W_1 is weight 1 at 110^{o}C,

W_2 is the weight 2 at 1000^{o}C,

W_c is weight of the crucible

L_{OL} is the percentage loss on ignition

The portion of the ignited sample and flux was fused into a homogeneous glass bead in order to eradicate any inconsistency, which effects could be due to particle size variation within the sample and mineralogical effects. The samples were then analyzed using Philips PW 2404 WDXRF equipment using SuperQ® software. The calibration standards used for the XRF machine are from MINTEK, formally National Institutes of Metallurgy (NIM) namely NIM-P NIM-D, NIM-S, NIM-N and NIM-G.

3.9 XRD

Same method and equipment was used to analyze both fly ash and coal.

3.9.1 XRD Analyses of Coal and Screened fly Ash

XRD analysis was conducted to determine the mineral matter constituents of coal and fly ash samples. Silicon compound metal powder of 99.9% purity supplied by Aldrich was added to each sample for quantitative determination of amorphous compounds. This material was micronized in a McCrone micronizing mill. The representative screened samples of both fly ash and coal were prepared for XRD analysis using a back loading preparation method. The samples were analysed with a PANalytical X'Pert Pro powder diffractometer with X'Celerator detector, variable divergence, fixed receiving slits and Fe filtered Co-Kα radiation. The machine is located at Mintek in Pretoria. The phases were identified using X'Pert Highscore plus software. The relative phase amounts (mass %) were estimated using the Rietveld method (Autoquan Program). The equipment used to do the analysis is not known since the samples were analysed at an external laboratory, namely, XRD Analytical and Consulting cc and the result report did not include the equipment utilized.

3.10 Malvern Particle Size Analyzer

The particle size analysis was undertaken in order to determine the PSD and the amounts of the three modes. The Malvern particle size analyser was located at University of Witwatersrand in Richard Ward building in material science laboratory.

The Malvern Particle Size Analyzer model is a MS2000. The sieved material from both the wet screening and the screen shaker were riffle split to create suitable representative samples. The sample batches were taken to the Malvern particle size analyser to determine the overall PSD. The sample gates of the sample tray were set to 10mm so as to allow all the sample material to be analysed by the Malvern. The compressor pressure was set at 4 bars since the material with particle size below 10 microns is cohesive and high pressure is necessary to reduce the cohesion of material so that agglomeration and aggregation of particles may be minimised or eliminated where possible.

The standard operating procedure of the Malvern was set as follows:

- Measurement Tab
- Background time was set to 12 seconds
- Measurement time of the sample 12 seconds
- Measurement obstruction limit was set to default range of 0.5 to 6.
- Time out period to 0.01seconds
- Malvern operating pressure was set to 3bar as recommend for more cohesive material.
- The feed rate was set to 50%

3.11 Summary and Conclusion

This chapter covered the sampling and analysis of the pulverised coal and the chain grate boiler coal samples as well as the corresponding fly ash samples. The details of the chain grate stack fly ash sampling program have not been included as this information was not provided by the company that supplied the fly ash. The stack fly ashes from the power stations were contained in filter thimbles and were not screened as there was insufficient sample material as well as the fact that the particles were already smaller than the desired size of 10 microns. The fly ash from the JV14 power station ESP and chain grate boiler stack were screened as discussed above.

The samples that were analysed were deemed to be sufficient to be able to address the aim and research questions posed on this research report.

The low temperature coal XRF analysis method conducted by Witlab was not discussed because the details of the method were not disclosed by Witlab.

The wet screening device used in separating the fly ash samples was found to be ineffective due to the lack of the horizontal movement and because of the poor mechanical strength of nylon meshes that resulted in the inability of this wet screening device to separate fly ash particles into three PSD size ranges of (ultra-fine, central mode and coarse mode particles). For these reasons only the -10 micron fly ash samples could be analyzed effectively.

4.0 Introduction

This chapter contains the results of the experimental program embodied in this research. It relates the chemical composition and mineral matter composition of the respective chain grate boiler and JV14 power station Pf boiler coals to the chemical composition and mineral matter composition of the -10 microns fly ash sourced from the JV14 boiler ESP, the JV14 stack and the chain grate boiler stack. The -10 microns fly ash morphology and PSDs from both combustion processes are discussed and compared. The PSD results of the JV14 power station boiler ESP and the chain grate stack screened fly ash samples were determined by a Malvern laser diffraction based particle size analyzer are also included.

In the last section of the results, the morphology, particle size range and SEM EDS results of the fly ash particles sourced from the stacks of IA4, JV14 and HY23 power stations Pf boilers, which were captured using filter thimbles are discussed. These fly ash samples did not have their parent coal samples characterised except the JV14 power station sample.

The only direct comparison of results made is between morphologies of chain grate stack particles and Pf boiler stack particles since the common analysis between the two processes was SEM EDS analysis of stack fly ash particles only.

4.1 Coal Characterisation

This section presents and discusses all coal analysis including TGA, SEM, XRD and XRF.

4.1.1 Themo-gravimetric Analysis

The results of proximate analysis for both coals are presented in Table 4.1. The chain grate coal has lower ash content than the pulverised coal. The fixed carbon of chain grate coal has higher carbon content than pulverised coal, with a difference of 20%, while the difference in moisture content between the two coals was found to be insignificant. The volatile matter accounts for 19.4% of the pulverised coal and 25.2% of the coal fed to the chain grate boiler.

Table 4.1: Proximate Analysis.

Sample Identity	Moisture	Ash	Volatile Matter	Fixed Carbon	Total
Chain Grate Coal (%)	4.0	15.8	25.2	55.6	100.6
Pulverised Coal (JV14) (%)	5.3	40.1	19.4	35.2	100.0

4.1.2 Morphology and Chemical Composition by SEM EDS

The automated elemental quantification results of the chain grate boiler coal and the Pf boiler coal are recorded in Table 4.2 (i) and (ii) as determined by SEM EDS. The amount of carbon material quantified by SEM is equivalent to carbon material recorded by XRD for both coals. The pulverised coal contained more inorganic oxides than chain grate coal as detected using SEM. It is found to contain 40.1% incombustible materials (See Table 4.1), while chain grate coal was found to contain only 15% incombustible material, using TGA analysis. The inorganic oxides that could not be detected in chain grate coal by SEM EDS were detected in the low temperature coal ash by XRF, these results are recorded in Table 4.3. The morphologies of the coals are shown in Figures 4.19(a) and 9 (b) respectively.

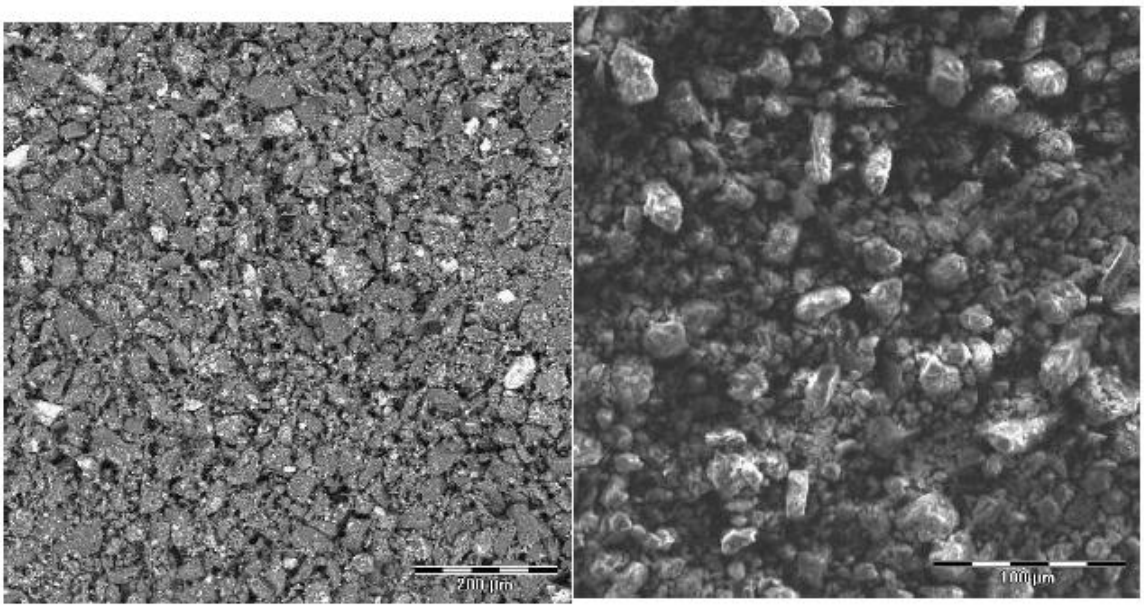

(a) **(b)**

Figure 4.1: (a) Chain grate boiler coal morphology. (b) Pulverised coal boiler morphology.

Table 4.2: Chemical compositions by SEM (i) of Chain grate coals, and (ii) pulverised coal fired boiler samples.

(i) Chain grate coal		(ii) Pulverised fired boiler coal from JV14		
Element	Atomic%	Element	Weight%	Atomic%
C	79.11	C	42.54	53.35
O	17.94	O	40.00	37.66
Al	1.08	Mg	0.22	0.14
Si	1.42	Al	5.87	3.28
S	0.28	Si	8.57	4.59
Ca	0.04	S	0.37	0.17
Ti	0.04	K	0.38	0.15
Fe	0.09	Ca	0.96	0.36
		Ti	0.31	0.10
Totals	100	Fe	0.76	0.20
		Totals	100.00	100

4.1.3 XRF Chemical Composition

It is found that in these samples aluminum and silicon are the most dominant minerals followed by iron, titanium and sulphur as shown in Table 4.3**.** The amounts of elements that could not be identified by the SEM have been quantified using a low temperature coal ash technique and XRF. The 40.1% of incombustible material in the Pf boiler coal recorded in Table 4.1 is consequently assumed to be mostly silicates, since Table 4.3 records 52% of incombustible material to be silica in the pulverised coal. Silicates accounts for 50% in chain grate coal with aluminum accounting for 34.3% of the material. This is found to be higher than Pf coal aluminum content of 28.1%.

Table 4.3: Metal oxides compositions for both coals from low temperature coal ash as determined by XRF.

Compound name	Pulverised coal (%)	Chain grates coal (%)
SiO_2	52.00	49.70
Al_2O_3	28.10	34.30
Fe_2O_3	3.55	3.94
TiO_2	2.34	3.21
P_2O_5	0.33	0.94
CaO	4.78	2.58
MgO	0.98	0.89
SO_3	4.15	1.73
Na_2O	0.59	0.21
K_2O	0.71	0.96
MnO	0.01	0.01
Cr_2O_3	0.01	0.02
Total	100	100

4.1.4 XRD Composition

The XRD SIROQUANT technique was used to determine the mineral matter composition of both sets of coal. The mineral matter compositions are recorded in Table 4.4. The chain grate coal XRD results indicate a high proportion of carbon at 72.26% with few mineral matter constituents detected as compared to the pulverised coal that contained 48% carbon. The other mineral matter constituents that have been identified by XRD are diopside, pyrite, kaolinite and quartz. Not all mineral matter constituents were identified by XRD, for instance, sodium, phosphorus and other inorganic oxides have been identified by the XRF analysis in the fly ash and in low temperature coal ash by XRF. The oxides that were identified by XRF are recorded in Table 4.5 for low temperature coal ash. No mineral matter constituents that are known to contain sodium and phosphorus were identified by XRD.

Table 4.4: The coal mineral matter composition for both chain grate boiler and pulverzed coal fired boiler as identified by the XRD.

Mineral Constituent	Chain Grate Boiler Coal Composition (%)	Pulverised coal fired boiler coal composition (%)
Carbon *(C)*	72.26 ± 1.56	48.50±3.6
Kaolinite *($Al_2Si_2O_5(OH)_4$)*	21.01 ± 1.17	26.67±1.98
Diopside *($MgCaSi_2O_6$)*	0.79 ± 0.36	0.00±0.00
Pyrite *(FeS_2)*	1.82 ± 0.16	0.00±0.00
Quartz *(SiO_2)*	3.47 ± 0.47	12.35 ± 1.57
Magnetite *($FeFe_2O_4$)*	0.46±0.2	0.46±0.20
Calcite (*$CaCO_3$)*	0.00±0.0	2.00±0.33
Muscovite *($KAl_2AlSi_3O_{10}(OH)_2$)*	0.00±0.0	6.37±0.81
Rutile *(TiO_2)*	0.00±0.0	0.56±0.16
Gypsum *($CaSO_4{\cdot}2H_2O$)*	0.00±0.0	3.06±0.81
Total	100	100

The XRF results presented in Table 4.3 records a silicon content of 52% for the Pf coal. Some of this silicon might have originated from quartz and muscovite, since Pf boiler coal contains more quartz and muscovite than chain grate coal. The second silicate mineral matter constituent is kaolinte which accounts for +20% in both coals. The carbon material that forms the chain grate coal is found to be 72% using XRD analysis and 71.77% from the SEM analysis. For the Pf boiler coal the carbon found to be 42.54% from the SEM analysis and 43% as determined by the XRD analysis. TGA results recorded a carbon content of 35.2% for the chain grate coal and 55.6% for the Pf boiler coal. The difference may be due to carbonates that could have released CO_2 during TGA analysis.

4.2 Fly Ash Characterisation

The coal mineral matter thermal transformation process comprises of melting, dehydration, degassing of CO_2 within carbonate minerals, coalescence and fragmentation of mineral constituents (Srinivasachar *et al*, 1990). The temperature of the combustion and the combustion environment itself determines the mineral matter transformation process. Fly ash is one of the end products of these processes.

4.2.1 The Thermal Transformation Chain Grate Coal

The second most dominant constituent in the chain grate coal is found to be kaolinite (21%). Kaolinite is known to exist in coal in both a perfectly crystallized and a poorly crystallized form in coal (Nankervis and Furlong, 1980). It is also known that mineral thermal transformation depends on the degree of crystallization of the kaolinite (Nankervis and Furlong, 1980). Crystallized kaolinite transforms into metakaolinite while poorly crystallized kaolinite transforms into amorphous aluminum and silicon.

Kaolinite starts breaking down when the hydroxyl group (OH) gradually begins to leave the chemical structure under heating. By 400^{o}C the kaolinite decomposes thermally into amorphous material and metakaolin (Nankervis and Furlong 1980, Mayoral *et al.,* 2001) and the complete transformation is attained at 550^{o}C (Nankervis and Furlong, 1980). Mayoral *et al.* (2001) found that the amorphous material and metakaoline produced from kaolinite remained unchanged up to

a temperature of 950^{o}C while the metakaoline transformed into crystallized mullite and crystobalite above 1000^{o}C.

Whilst Kaolinite accounted for (21%) of the crystallized mineral matter in chain grate boiler coal, the resulting fly ash had no kaolinite reported in it. It can consequently be concluded that the chain grate boiler combustion temperature must have been above 1000^{o}C, all the kaolinite was thermally transformed to amorphous material and into mullite in the stack fly ash in the size range below -10 microns. The high amounts of mullite in fly ash recorded in Table 4.5 would therefore have originated from the kaolinite transformation, due to the fact that it is the second most modal mineral matter constituent in the chain grate boiler fly ash after amorphous material. Mullite makes up 24.67% of -10 microns fly ash while the amorphous material fraction makes up 50.16%. The loss on ignition of chain grate stack fly ash is found to be 21% as determined by XRF. The ignition occurred at 1000^{o}C temperature. The loss on ignition comprised of CO_2 from carbonate minerals, combustion of some unburnt carbon and possibly SO_2 produced from the combustion of sulphur. Most of the amorphous material must have been produced from unburnt carbon, as well as from the non-combustible material lifted off the chain grate by heterogeneous air supply (Green and Waite, 2004). Some of the amorphous material may also have been produced from poorly crystallized kaolinite.

The chain grate coal had a pyrite content of 1.8% but none of this material was reported in the fly ash. It is therefore assumed that pyrite decomposed thermally into iron alpha and magnetite in the fly ash. Pyrite decomposes into iron and sulphur at a temperature of ±423^{o}C (Tomeczeck and Palugynik, 2002). The iron formed from pyrite was also oxidized to form magnetite. Most of the iron has formed magnetite while some iron remained unoxidized probably due to insufficient oxygen and localized oxygen concentrations and low combustion chamber temperature. This may be concluded from the fact that the oxidation of magnetite is low below the 823^{o}C combustion temperature (Tomeczeck and Palugynik, 2002). The fly ash of -10 microns particles does not show any traces of haematite in the crystallized mineralogy. According to Nankervis and Furlong (1980) the decomposition of pyrite is governed by the combustion atmosphere as well as temperature. For instance Nankervis and Furlong (1980) found pyrite to decompose completely to haematite and sulphur dioxide at a combustion temperature of 500^{o}C in an

oxidizing environment. The XRD results show formation of iron alpha in the fly ash which would suggest that some portion of pyrite did decompose to pure crystallized iron. Magnetite must have been produced from oxidation of both pyrite and alpha iron.

Table 4.5: Chain grate boiler stack fly ash mineral matter composition as determined by XRD.

Mineral Constituent	Fly ash Composition
Quartz (SiO_2)	5.08 ± 0.57
Amorphous	50.16 ±1.95
Calcite ($CaCO_3$)	3.23 ±0.48
Bassanite ($CaSO_4{\cdot}0.5H_2O$)	14.37 ±0.87
Iron Alpha(ά-Fe)	0.340 ±0.10
Mullite (Al_6Si_2O)	24.67 ± 1.62
Magnetite ($FeFe_2O_4$)	1.34 ± 0.22
Total	100.00

The fraction of quartz in the chain grate parent coal is 3.47±0.47% and the fraction in the product fly ash accounts for 5% of the total fly ash. The quartz appears to have remained unchanged since the melting temperature of quartz is 1500^{o}C which is not attainable in the chain grate boiler.

The only source of magnesium and calcium identified in chain grate feed coal by XRD is diopside as shown in Table 4.4. The calcium bearing minerals found in the chain grate coal stack fly ash were calcite, bassanite and anhydrite. The composition of diopside in the parent coal is 0.79% with an error of 45.5% which might be an indicator that the amounts of diopside might be lower than 0.79%. The calcium in the chain grate -10 microns fly ash is in the form of bassanite comprising 14.37%, followed by calcite with 3.23% and anhydride accounting for 0.75%. The total amount of calcium bearing products in the fly ash is 18.35%. The two products that comprise both calcium and sulphur are bassanite and anhydrite, amounting to a total of 15.12%. The calcium oxide detected in the XRF coal ash was found to be 2.58% which comprises only a

small fraction relative to the total amounts of calcium-bearing mineral matter constituents in the stack fly ash. It may however also be the case that some calcium in the low temperature coal ash existed in the form of sulphates.

Calcite was not detected in parent coal of chain grate boiler, as recorded in Table 4.4. However, calcite was found in the -10 microns fly ash particles with a composition of 3.23%. It is possible that calcite was not detected in the parent coal as XRD is a semi-quantitative analytical method and also because of the high carbon content of 72% in the parent coal, a factor which may have masked the presence of the calcite in the material. The calcite amounts might have been below the detection limits of the XRD equipment, and some portion of it might have existed in non crystallized form. Calcite thermal break-down takes places at around 900°C, during combustion thermal shock and as gas discharges change the crystalline structure (Yinghui *et al.*, 2007).

Ten Brink *et al.* (1996) found calcite to fragment during the degassing of carbon dioxide and ultrafine particles of CaO and calcite were produced. Some fragmented calcite in the fly ash might be the reason for the detection of the calcite in the fly ash by XRD because of increased surface area, since the particle size was below 10 microns with increased surface area unlike in coal where the particle size was below 45 microns. The fly ash fused beads were heated to 1000^{o}C before the major elements XRF composition analysis was done and the loss on ignition of 20% was recorded that resulted in high concentration of the CaO as degassing of CO_2, H_2O and combustion of unburnt carbon took place.

Bassanite represents 14.37% of the chain grate fly ash as determined by XRD. This mineral is normally produced from the dehydration of gypsum, but in the chain grate boiler coal no gypsum was detected by the XRD. Nor was gypsum detected in the fly ash of the chain grate coal. Bassanite could therefore have formed from calcium provided by both diopside and calcite while the source of sulphate could have been from the decomposition of pyrite. Nankervis and Furlong (1980) found that calcium (produced from calcite decomposition), and water (produced from oxidation) reacted with organically bound sulphur to produce bassanite at a temperature below 190^{o}C. In the current case, the hydroxyl groups might have originated from the transformation of kaolinite to metakaolin, but the bassanite thereby produced would have decomposed to anhydrite around 200^{o}C. In the chain grate boiler fly ash bassanite is present in higher proportion than

anhydrite. Some of the anhydrite might have decomposed to calcium oxide and formed some part of the amorphous material. It is therefore likely to have more anhydrite than the bassanite since the decomposition of the bassanite to anhydrite happens at around 200^{o}C (Nankervis and Furlong, 1980), while the chain grate boiler combustion temperature is above 500^{o}C. It should be noted that no anhydride was recorded in Table 4.4.

4.2.2 Pulverised Coal Thermal Transformation.

The pulverised coal fly ash contains very small amounts of anhydrite and bassanite, which are found to be below 0.52%, while the materials in the chain grate boiler fly ash contained 14% bassanite as explained above. Bassanite decomposes to water and anhydrite above 200^{o}C while anhydrite melts at 1200^{o}C and reacts with available calcium sulphide to produce sulphur dioxide and calcium oxide above 1200^{o}C (Nankervis and Furlong, 1980).

Table 4.6: Pulverised coal fly ash mineral matter composition as determined by XRD.

Mineral matter constituents	Fly Ash Composition (%)
Amorphous	58.05±1.41
Quartz *(SiO_2)*	9.07±0.72
Calcite *($CaCO_3$)*	0.46±0.27
Iron alpha (ά-Fe)	0.62±0.09
Magnetite (*$FeFe_2O_4$*)	1.01±0.18
Mullite32 (*Al_6Si_2O*)	30.01±1.14
Lime *(CaO)*	0.03±0.06
Bassanite *($CaSO_4{\cdot}0.5H_2O$)*	0.25±0.21
Anhydrite *($CaSO_4$)*	0.51±0.28
Total	100.01

Since the pulverised coal fired boiler combustion temperature is above 1200^{o}C most of the bassanite and anhydrite would have decomposed hence these low values present. On the other hand, the fact that the chain grate fly ash had considerably higher proportions of bassanite (14.3%) could be explained by the fact that it is possible for coal particle to have passed through the combustion chamber without attaining the combustion flame temperature of the chain grate boiler. The morphologies of the particles show that some of the particles have not been fully altered by the flame.

4.2.3 XRF and SEM EDS Fly Ash Chemical Composition

The fly ash XRF analyses as presented in Table 4.7 indicate that the pulverised coal fly ash had a very low loss on ignition, whereas the chain grate fly ash had a very high value of (21.5%). This was largely due to the mass loss when burning off the high percentage of unburnt carbon. In the chain grate fly ash, the transformation of bassanite and the evolution of CO_2 from calcite, water of crystallinity from kaolinite and SO_2 from pyrite.

In general, the inorganic oxides in the pulverised coal fly ash possess very high proportions of SiO_2 and Al_2O_3 similar in proportion to the chain grate fly ash, and low proportions of all other oxides.

The low temperature coal ash of pulverised coal as presented in Table 4.4 shows that it contained more calcium than chain grate coal low temperature ash. This was found to be 2% while the chain grate stack fly ash contained more calcium than the pulverised coal ESP fly ash by an amount of 6%.

Table 4.7: Fly ash chemical composition as determined by XRF.

Compounds	Chain grate coal composition (%)	Pulverised fired boiler coal composition (%)
SiO_2	**47.03**	**55.35**
Al_2O_3	**31.18**	**31.72**
Fe_2O_3	**0.57**	**0.37**
FeO	**4.6**	**2.98**
MnO	**0.08**	**0.03**
MgO	**1.09**	**1.04**
CaO	**8.51**	**3.47**
Na_2O	**0.06**	**0.22**
K_2O	**1.07**	**0.74**
TiO_2	**2.34**	**1.54**
Cr_2O_3	**0.09**	**0.169**
P_2O_5	**2.89**	**0.50**
NiO	**0.016**	**0.01**
Total	**100**	**100**
LOI	**21.64**	**0.25**

The SEM EDS chemical composition results for the pulverised coal fly ash are very similar to those obtained from the XRF analysis, with silicon and aluminum oxides were found to be the most dominant metal oxides in both fly ashes. The SEM EDS results in Table 4.8 records silicon amounting to 57.08% and the XRF chemical composition analysis results of the ESP fly ash silicon records silicon at 55.35%. The 2% difference is probably due to the fact that SEM EDS is a semi quantitative technique.

Table 4.8: Fly ash chemical composition as determined by SEM.

(a) Pulverised coal fly ash		**(b) Chain grate coal fly ash**	
Element	Weight%	Element	Weight%
C	0.00	C	12.31
Na	0.36	Na	0.03
Mg	0.73	Mg	0.97
Al	31.94	Al	30.02
Si	57.08	Si	41.32
P	0.00	P	1.27
S	0.00	S	1.71
K	0.78	K	1.07
Ca	3.30	Ca	6.13
Ti	1.68	Ti	1.96
Fe	3.07	Fe	3.21
Mo	1.07	Mo	0.00
Totals	**100.00**	**Totals**	100.00

The concentration of silicon and aluminum has been found to be lower in particles smaller than 1 micron in literature studies (Dunxi *et al.*, 2008, Xiaowei *et al.*, 2007) as discussed in chapter 2. In this research the study of -0.2 micron coal fly ash particles was not undertaken. The results on the +0.2 microns to +10 microns fractions are presented in this research are similar to literature records (Dunxi *et al.*, 2008, Xiaowei *et al.*, 2007). The smallest particle size is read from Figure 4.2. Particles bigger than 1 micron contain high amounts of silicon and aluminum. The silicon and aluminum content determined by the temperature coal ash technique is similar to those determined in the fly ash samples for both the chain grate stack and Pf boiler ESP fly ash.

4.3 PSD of -10 microns Fly Ash Particles.

The fly ash sourced from the chain grate coal boiler stack and the Pf boiler ESP were screened below -10 microns. The fly ash samples were submitted to size analysis in a Malvern particle size analyzer. The PSD results from Malvern particle size analyser are shown in Figure 4.2 and Figure 4.3. Figure 4.2 presents the frequency curves for the PSD, while Figure 4.3 shows the cumulative PSD curves in volume (%) versus specific particle diameter. Although the sieve tests were designed for -10 micron particles, some larger particles passed through the 10 microns screen sieve mesh as illustrated in Figure 4.2 and 4.3.

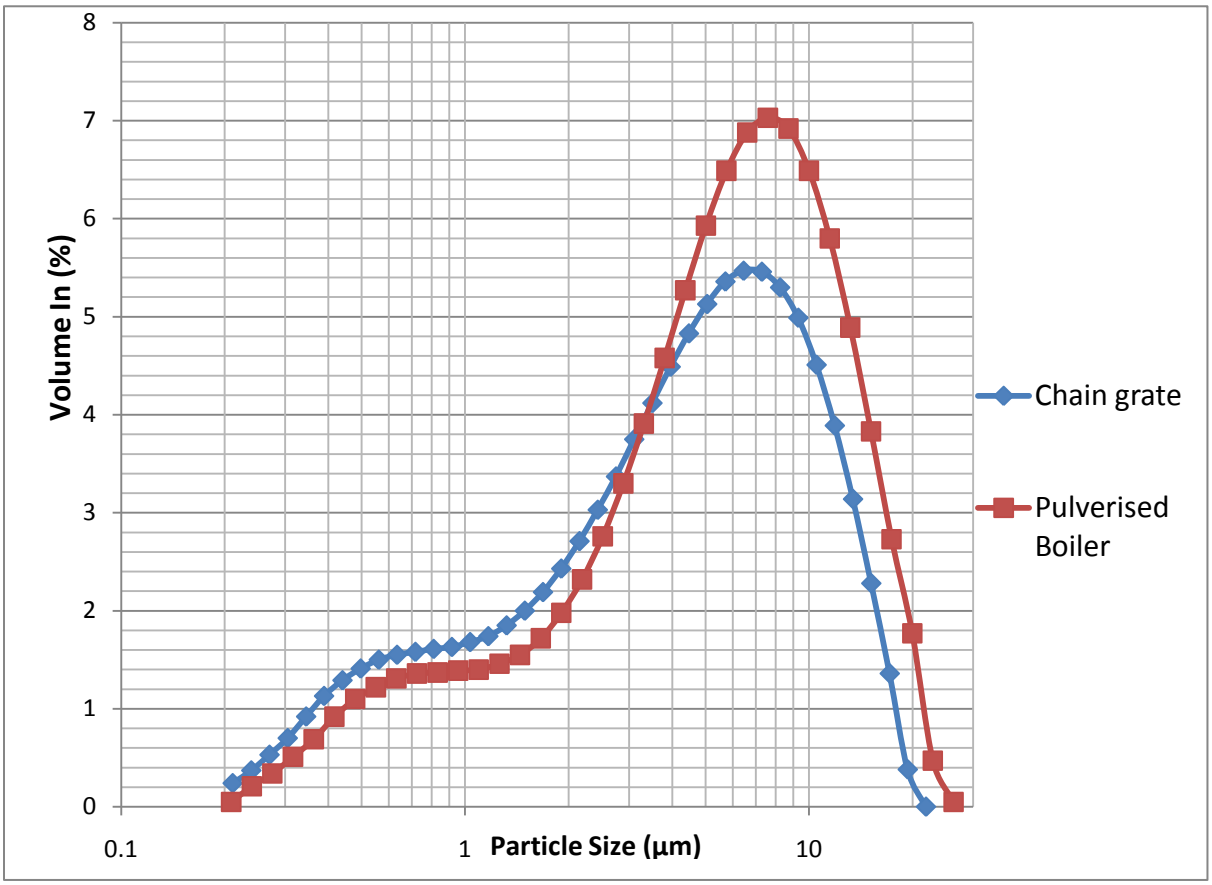

Figure 4.2 Frequency curves for the chain grate fly ash and Pulverised coal fly ash.

Figures 4.2 and 4.3 illustrate that the chain grate fly ash has a significantly higher proportion of ultra fine particles than the pulverised coal fly ash. Conversely the pulverised coal fly ash contains a higher proportion of coarse particles than the chain grate fly ash. This is possibly due to the fact that the chain grate fly ash was sourced from the stack while pulverised coal fly ash was sourced from the ESP. The modal size class range in both the chain grate and pulverised fly ash is 6 to 9 microns which belongs to the coarse fraction of fly ash particles.

Both PSD frequency curves (Figure 4.2) show a similar trend, with a low frequency in the -2 microns which makes up a family of ultra fine particles and central mode particles.

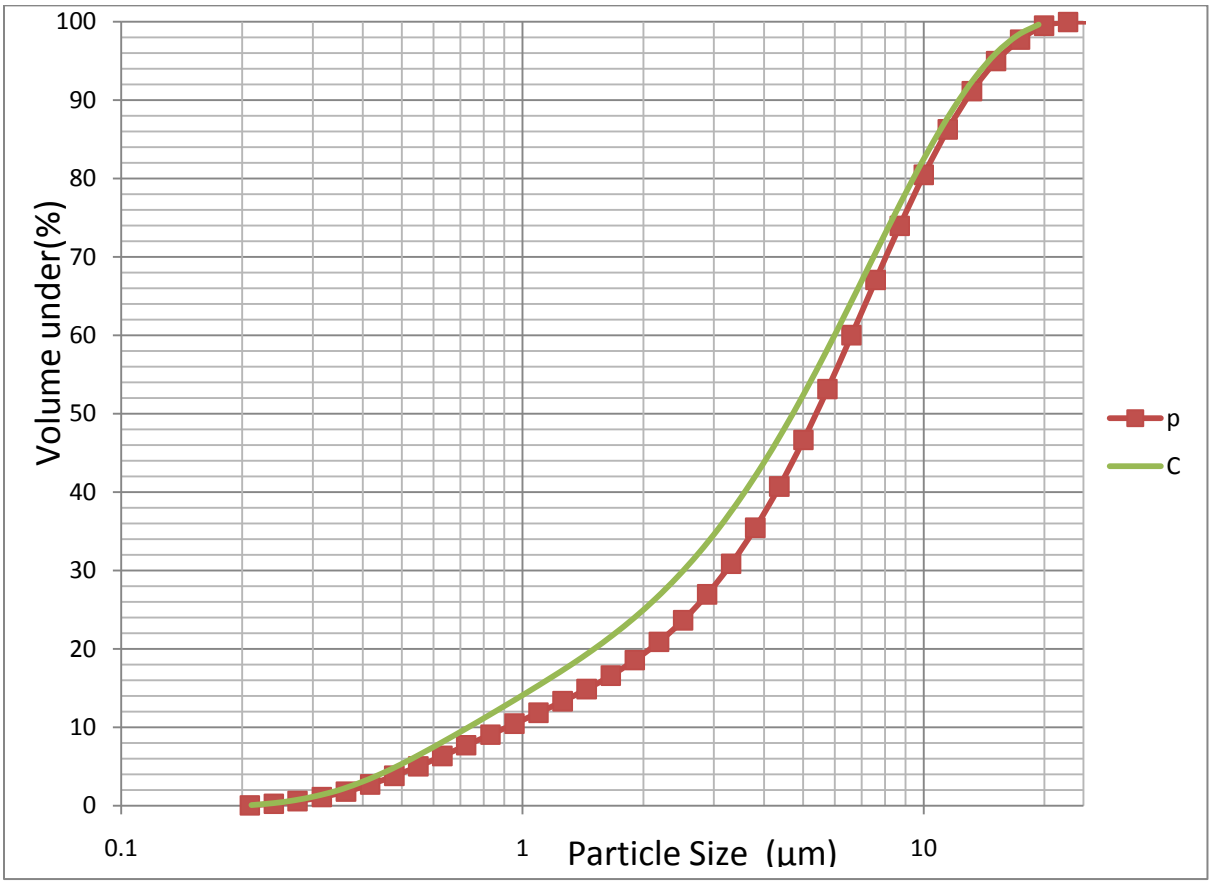

Figure 4.3: Chain grate stack fly ash (C) and Pulverised coal boiler ESP fly ash (P) PSDs as determined by Malvern Particle size analyser.

Figure 4.3 illustrates that 50% of the pulverised coal fly ash particles are about ±5 microns while ±10% are within the ultra fine particles size range (-1 micron). The chain grate fly ash has 50% of particles less than 4.5 microns, and 14% less than 1 micron.

4.4 Proportions of PSD Modes

The amounts of ultrafine particles, central mode particles and coarse mode particles were determined using the frequency curves in Figure 4.2. The size ranges assigned to each PSD region are recorded in Table 4.9. The size range boundaries were determined from the literature values recorded in Table 2.1.

Table 4.9: The particle size ranges used to defined ultrafine, central mode and coarse mode particles.

PSD Region	Size range (µm)
Ultra Fine	0.211-0.95µm
Central Mode	1.0-3.91µm
Coarse Mode	4µm<X

4.4.1 Possible Causes for Small Amounts of Ultrafine Particles

The fly ash PSDs in Figure 4.2 and 4.3 show very small amounts of particles in the +0.1 micron fraction and no particles in the size range less than 0.1 microns were determined. The smallest particle size found was 0.211 microns. The particles sized within 0.1 microns range agglomerate and aggregate readily because of the electrostatic forces and some of these agglomerate during cooling of the fly ash. This material also attaches itself onto the screen frame walls and on sieve mesh wires during separation.

When the PSD of ultrafine material was determined in the Malvern particle size analyzer some of the ultra fine particles were found to have attached to the Malvern tube surface and some remain on the Malvern sample tray walls. The ESP sourced fly ash possesses 9% ultra fine fly ash, which is also a low value due to the fact most of the ultra fine fly ash escapes the ESP.

Some ultrafine particles attach to bigger particles or agglomerate, resulting in high proportions of large composite particles rather than genuinely large particles as shown in Figure 4.5. The Malvern dry cell unit is normally operated at high pressure to minimize particle agglomeration and aggregation when analyzing very fine powders because particles are generally very cohesive.

In terms of the mode distributions, most of the particles fall into the coarse mode for both the chain grate fly ash and the pulverised boiler fly ash as quantified in Figure 4.4(a) and (b). Here more than 50% of the particles are shown to fall into the coarse mode for both the chain grate fly ash and pulversied fly ash, with the pulverised coal boiler fly ash possessing 70% in that category.

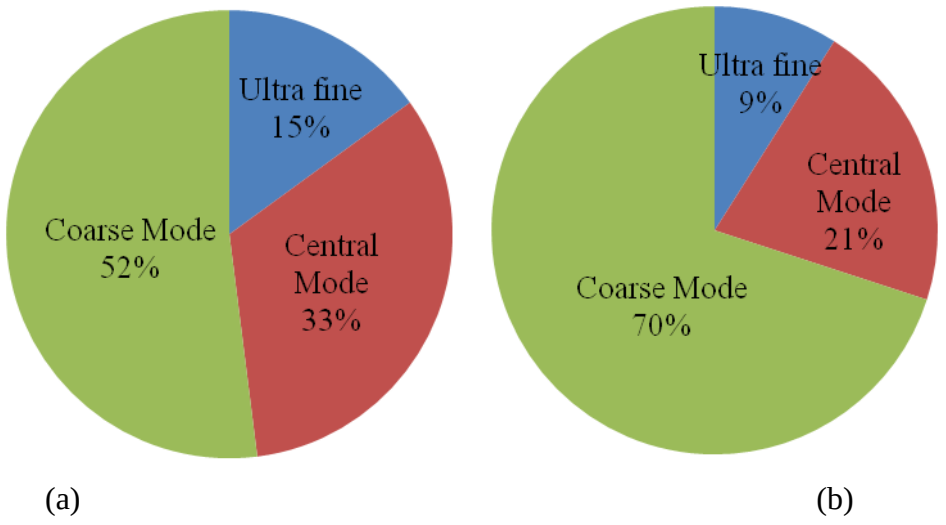

Figure 4.4: PSD Volume percentages: (a) Chain grate boiler fly ash, and (b) Pulverised boiler fly ash.

The ultra fine particles account for the lowest portion of the screened fly ash, primarily because most of it had been lost during separation, as discussed above.

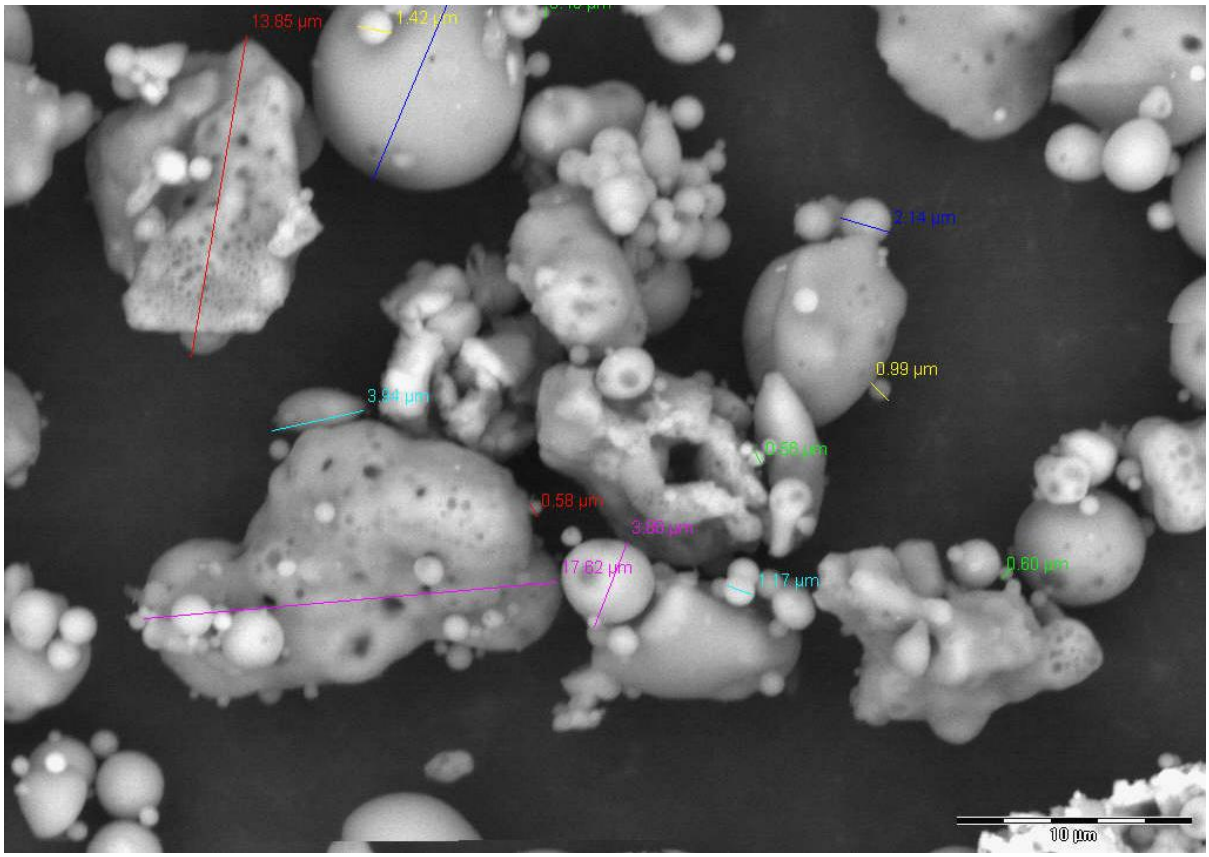

Figure 4.5: Agglomerations and aggregations of ultra fine particles.

4.4.2 Possible Causes of High Proportions of Coarse Particles

The typical ESP collection efficiency is 99.5% on fly ash particles size of ±10 microns and hence the particles bigger than 10 microns were not anticipated in the chain grate stack fly ash as in Figure 4.11. The chain grate boiler had only one ESP with poor efficiency that permitted particles bigger than 10 microns to escape. The efficiency of ESP was poor because of high amounts of unburnt carbon in the fly ash, as shown in Table 4.6, with the SEM atomic amount of carbon being 15%. The high proportions of unburned carbon in the fly ash generally decreases the resistivity of the fly ash which in turn changes the fly ash charging properties by reducing fly ash resistivity, this consequently results in reduced collection efficiency of the ESP (Air Pollutants and Control Techniques, EPA) even though the fly ash collection efficiency of the ESP is also a function of flue gas temperature, flue gas velocity, fly ash resistivity and fly ash PSD.

Poor coal combustion efficiency in the chain grate boiler led to more irregular fly ash particles in the product fly ash. For irregular particles the sieve screen aperture permits the particle to pass through depending on the particle cross-sectional orientation to the aperture. If the particle dimension oriented perpendicular to the aperture is smaller than the aperture the particle will pass through. On the other hand if the particle dimension orientated perpendicular to the aperture is bigger than the aperture then the access to the particle is not granted. An irregular particle inside the sieve screen mesh has a high probability of passing through due to the fact that the orientation of the particle dimension to the screen aperture keeps changing as the sieve mesh or sieve screen continuously vibrates. Screening for a longer period of time increases the probability of more irregular particles gaining a passage through the screen apertures. This resulted in some irregular particles with width less than 10 microns and lengths longer than 10 microns gaining access through 10 microns sieve apertures. As a result, the Malvern particle size analyzer recorded some particles that were bigger than 10 microns.

The nominal diameter of the screen sieve aperture size distribution is normally not uniform and mono size classed (Test Sieving: Principles and Procedures). The error permitted for aperture opening relative to nominal diameter ranges from ±2.9% for 125mm sieve screen up to ±15% for 10 microns according to ASTM E 11 standard method for sieve testing and calibration standards (Test Sieving: Principles and Procedures). The method allows the upper limit individual aperture to vary from 1.0472 times for nominal diameter of 125mm mesh to 1.75 or more for nominal aperture of 20 microns mesh. The amount of apertures bigger than 1.04 times the nominal diameter should be less than 5% for nominal aperture of 120mm mesh and 1.45 times for nominal aperture of 20 microns (Test Sieving: Principles and Procedures). This accounts for some particles that are bigger than the 10 microns on the fly ash PSDs characterised by the Malvern particle sizer. For 10 microns nominal diameter mesh, the biggest particle aperture would be ±17.5 microns.

The fly ash PSD characterised by the Malvern particle size analyzer reaches approximately 99% to 100% as it approaches the 17 microns particle size. Apart from irregular particles the spherical particles bigger than 10 microns also gained access through oversized apertures. Both PSDs do

not show a portion of ultrafine particles less than 0.1 microns. As mentioned above, the smallest particles characterised by the PSD are of +0.211 microns and they account for 0.08% of total particles.

4.5 Morphology of Fly Ash Particles

The Pf boiler ESP fly ash particles morphologies are shown in Figure 4.6(a). The random image particle size analysis was undertaken and irregular particles with lengths of up to 18.28 microns and widths of up to 9.84 microns were identified. This confirms the PSD results shown in Figures 4.2 and 4.3. Spherical particles are also present and they out-number the irregular particles. There are found to be no significant particle agglomerations, although there are a few notable particle aggregates. Some spherical particles surfaces have flat planes that could have formed from hot particles collisions or when a hot particle collided with the collection surface of a collection device. Some fractured particles surface might have developed during screen sieving.

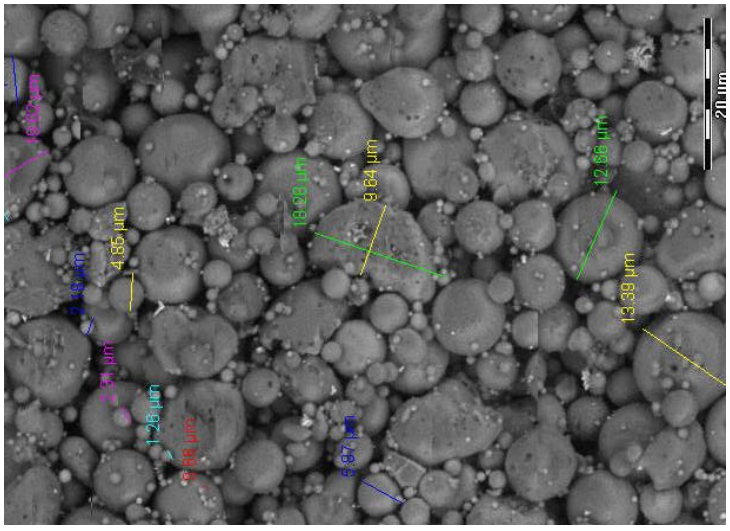

Figure 4.6(a): Pf ESP fly ash morphology.

Most of the particles depicted in Figure 4.6(b) from the chain grate fly ash are found not to be spherical due to the poor combustion conditions of the coal chain grate boiler. There are a few spherical particles as seen in Figure 4.6(b) but most of the particles are irregular and smaller than 10 microns as illustrated in Figure 4.6(b). The Pf boiler stack fly ash particles as shown in Figure

4.6(c) and are found to be mostly spherical in nature with very few or no irregular particles present. All of the particles are found to be smaller than 5 microns.

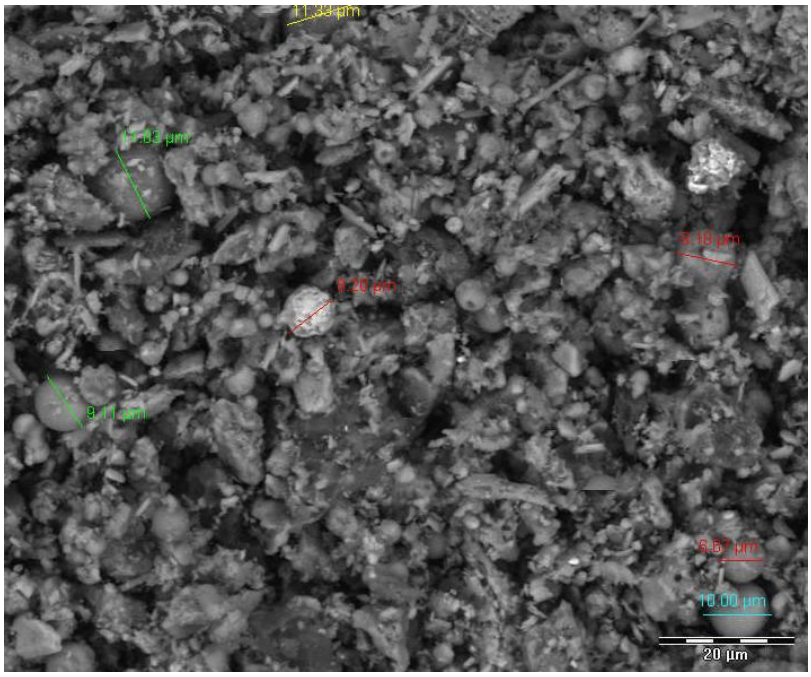

Figure 4.6(b): Chain grate boiler stack fly ash morphology.

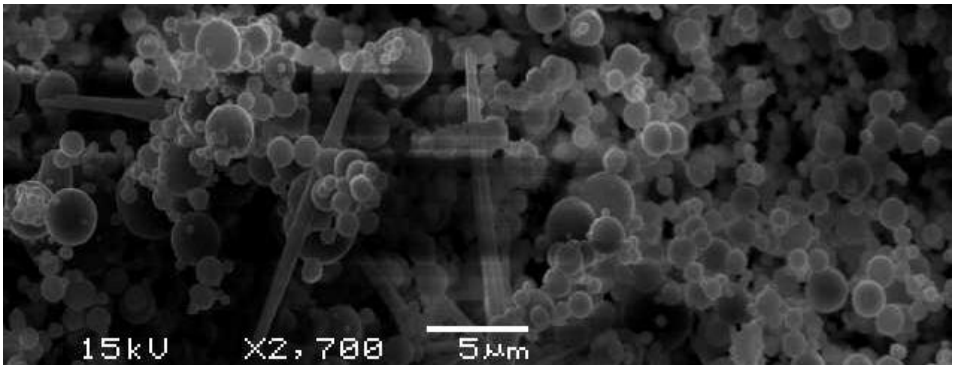

Figure 4.6(c): Pf boiler stack fly ash morphology.

The Pf boiler stack particles are smaller than both Pf ESP and chain grate stack fly ash particles. The mineral matter of Pf boiler stack particles are formed from melted mineral matter while chain grate stack particles formed from both melted and non-melted mineral matter. The melted material produced spherical particles, material that did not melt produced irregular particles. Some of the particles from the chain grate stack fly ash particles were formed from carbon

material that was not combusted due to the fact that the chemical composition of the stack particles contained 12.31% of unburnt carbon. The Pf boiler stack and ESP fly ash particles contained no carbon material.

4.6 Characterisation Filter Thimbles Stack Fly Ash Particles

The stack fly ash consists of ultra fine particles since most of the bigger particles are captured by the ESPs. Samples were taken from stacks of various power stations boilers and were captured on the filter thimbles. Only SEM EDS analysis was undertaken due to fact that only a limited amount of sample was available. These results are consequently discussed separately.

4.6.1 ESP Collection Efficiency

The ranges of particle sizes in the fly ash depicted in Figure 4.6 (c) are those that escape the ESP and any other particulates emission control equipment.

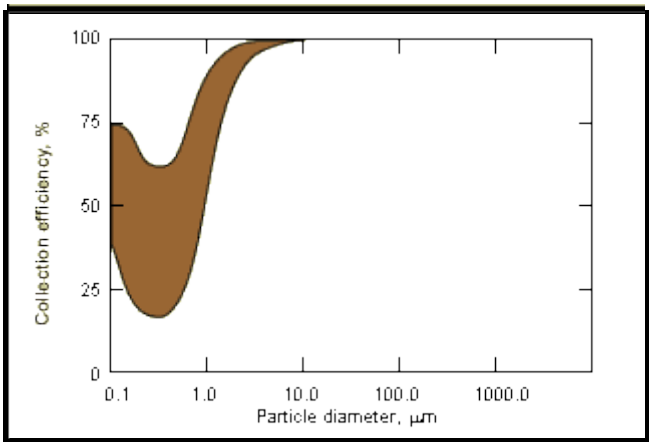

Figure 4.7: The collection efficiency of ESP as a function of particle size (Air Pollutants and Control Techniques, EPA).

Most of the particles that escape the ESP are below 10 microns, falling mainly in the ultra fine and central mode regions of the PSD, as shown in Figure 4.7 and Figure 4.8. Previous workers have shown that the efficiency of the ESP falls from 100% to nearly 25% for particles between 10 microns and 0.1 microns as shown in Figure 4.7. The ESP captures mainly particulates in the coarse mode region with an efficiency of 99.9% on ±10 microns fly ash particles (Zukeran *et al*., 1999, Air Pollutants and Control Techniques, EPA). On the other hand, ESP particulates

removal efficiency in terms of the numbers of fly ash particles in the ultra fine and central mode sized regions is below 50% (Ito *et al.*, 1995, Riehle and Loffler 1992, Zukeran *et al.*, 1997). This is due to poor particle charging and flow instabilities (Zukeran *et al.*, 1999).

High proportions of unburned carbon in the fly ash generally decrease the resistivity of fly ash which in turn changes the fly ash charging properties by reducing fly ash resistivity. This results in reduced collection efficiency of the ESP (Zukeran *et al.*, 1999), even though the fly ash collection efficiency of the ESP is also a function of flue gas temperature, flue gas velocity, fly ash resistivity and fly ash PSD.

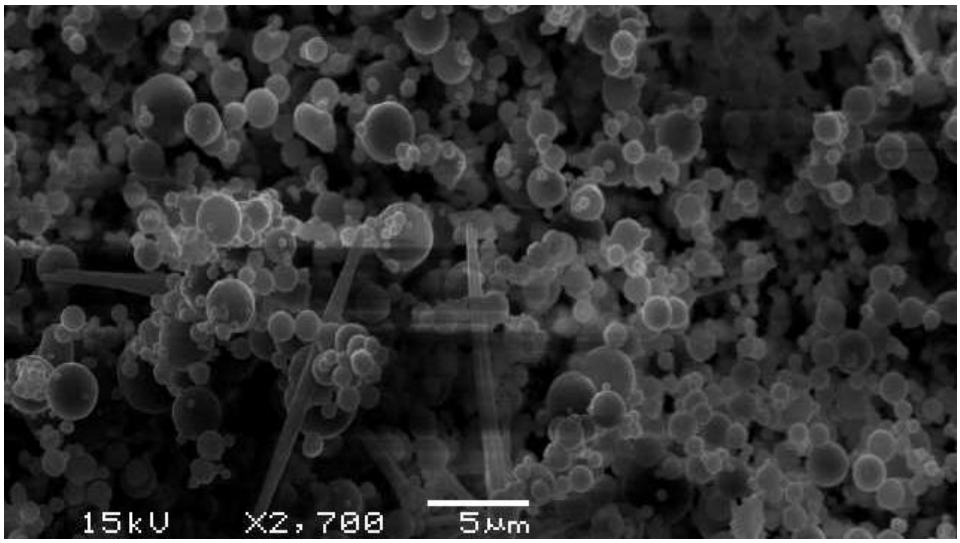

Figure 4.8: The pulverised coal boiler stack fly ash size range that escapes the stack.

The chain grate boiler fly ash comprises all the PSD modal regions as shown in Figure 4.5(a) while the pulverised coal stack sampled fly ash is more bimodal, since the coarse mode region particles are captured by the ESPs. The high collection efficiency of the coarse mode PSD region fly ash particles in the pulverised coal fired boiler may be due to the negligible amounts of unburnt carbon in the fly ash and the utilization of sets of ESPs at the back end of the pulverised coal fired boilers, unlike chain grate coal boiler that employed a single ESP. This consequently led to collection of few ultra fine and central mode particles by the filter thimble. Another factor that might also have contributed could be poor emission rates. The collected particles emitted are

both ultra fine and central mode particles that fit easily within filter fiber voids, as shown in Figure 4.12 and Figure 4.13. There are also some coarse particles present.

4.6.2 The Filter Thimble Properties

This section discusses the chemical composition and microporosity of filter thimbles using SEM and SEM EDS characterisation.

4.6.2.1 Filter Surface Morphologies and Chemical Composition

The inner and outer morphologies of an unutilized filter thimble are shown in Figure 4.9(a), (b) and Figure 4.10. These SEM photographs show the micro-porosity of the filter at different magnifications and on both the inner and outer surfaces of the filter thimble.

The micro-porosity of the filter thimble given by the manufacturer is 0.3 microns. However, some of the distances between the filter fibers are shown to be bigger than 5 microns thereby indicating that the filter thimble micro porosity does not appear to be uniform. The micro-porosity of the filter surface is not consistent horizontally and vertically as seen in Figures 4.9 (a), (b) and Figure 4.10. The inner surface appears to have porosity that is bigger than that specified by the manufacturer. The absorption of water by filter surface from flue gas moisture will probably have changed the porosity of the filter to some extent since absorbed water causes the filter fibers to expand and reduce distance between the fibers and consequently improves the filtration efficiency.

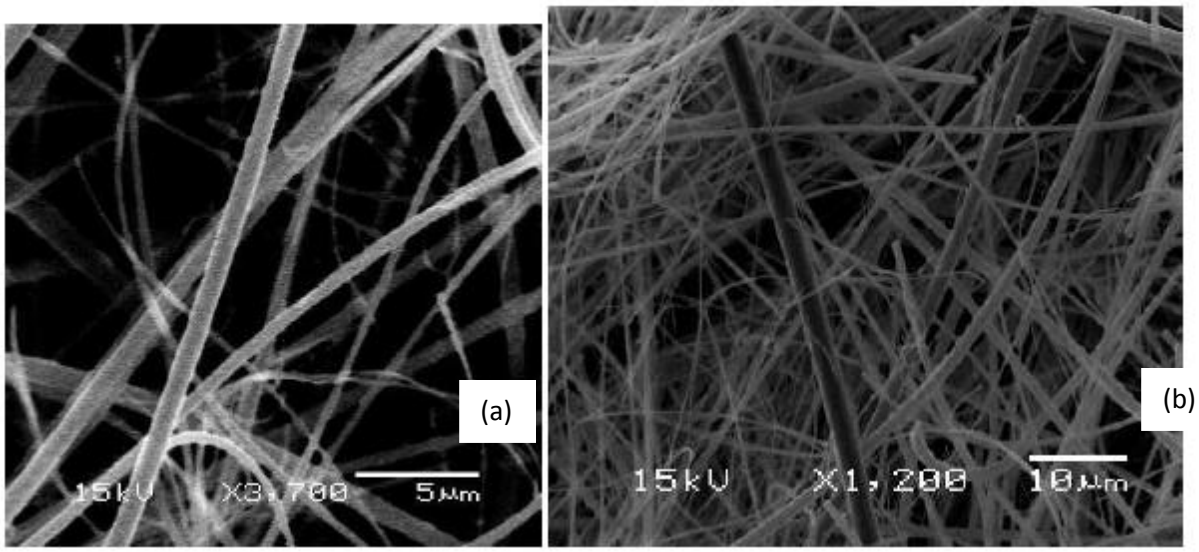

Figure 4.9: (a) Inner surface morphology of unused filter thimble under SEM at X3 700, (b) the material at X1,200.

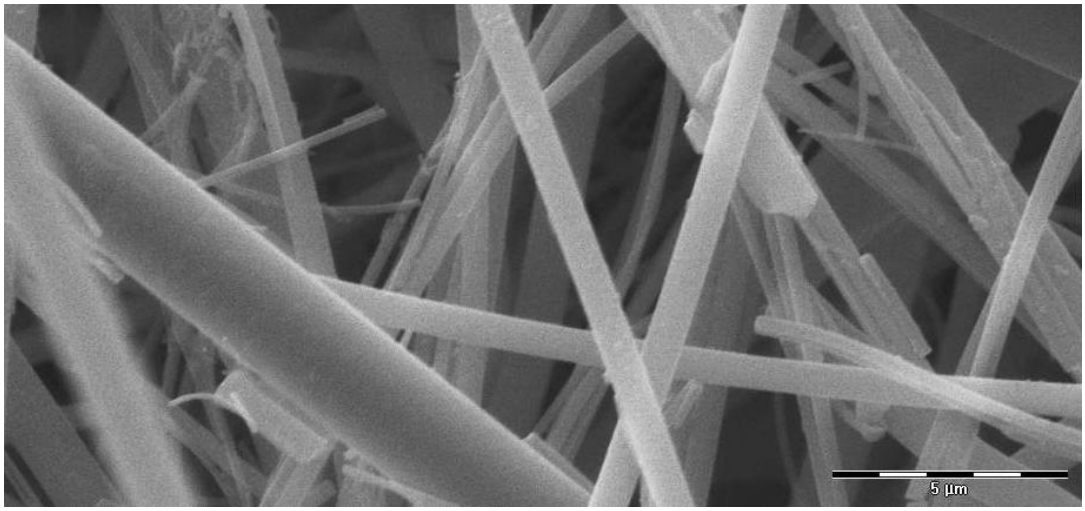

Figure 4.10: The morphology of the filter thimble bottom outer surface determined by SEM.

The automated elemental analysis of an unused filter was undertaken using SEM EDS and the elemental composition is presented in Table 4.10. The composition of the fibers is dominated by the Si and O_2. This suggests that the filter consists of SiO_2 glass wool.

Table 4.10: Filter elemental composition as quantified by SEM EDS.

Element	Weight (%)	Atomic (%)
C	4.22	7.02
O	44.88	56.00
F	1.51	1.58
Na	8.43	7.32
Mg	1.42	1.17
Al	1.19	0.88
Si	32.29	22.95
Cl	0.88	0.49
K	0.60	0.31
Ca	4.57	2.28
Totals	100.00	100.00

Following the iso-kinetic sampling, the surfaces of the filter thimbles used to capture fly ash from the pulverised coal power station stacks were found to be partially covered with abundant fine particles although, due to the enormous micro-porosity of the filters, some particles may have escaped. The captured particles were mostly smaller than the void distance between the filter fibers and it was a challenge for ultra fine particles and central mode particles to fill the filter thimble voids completely.

The fly ash particles collected by the filters were analyzed using individual particle point analysis rather than automated analysis, so that the filter fibers would not be analyzed simultaneously with the fly ash particle elements.

4.6.3 Fly Ash Particles Morphologies

Most of the fly ash particles from the stack of the Pf coal boilers are spherical, unlike the irregular particles of the chain grate boiler fly ash particles. Xu *et al.* (2007) attributed the spherical particles to high oxygen concentration and temperature. The results of Xu *et al.* (2007) results were obtained from laboratory experiments at a temperature of 1473^{o}C which is close to the combustion chamber temperature of power station boilers. The effect of oxygen concentration cannot be commented upon in this report because it is beyond the scope of this research project.

Normally the stack temperature would be lower than the particle temperature, so those particles that still exist in a semi-liquid state solidify and agglomerate as the particles cool down on the collection surface of the filter thimble. Some agglomerates and aggregates of ultra fine particles might also arise during the combustion process. The literature (Kutchko and Kim, 2006, Wang *et al.,* 2007) has attributed some morphological features to both cooling and the rate of cooling. The laboratory experimental set-up used in studies described in the literature to study the formation of coal combustion particulates only had one cooling stage, namely the water cooled probe collecting the fly ash. In the case of stack emissions there are two post flame zone cooling stages, namely, (1) the probe collecting the fly ash is water cooled, and (2) the post combustion zone of a power station boiler is cooled as well. The sampling probe is water cooled and the cooling from the probe, before particles settle inside the filter, could cause further solidification of particles that might have still existed in the liquid state. Figure 4.12 shows some melted mineral matter with various granules adsorbed on the surface of the filter fibers while the big spherical particle of ≥10 micron has smaller particles trapped within its surface. Some of the bigger particulates depicted in Figures 4.12 and 4.13 have distinct coatings on their surfaces that Kutchko and Kim (2006) attributed to some volatile elements that entered the combustion chamber in the vapor phase.

The proportions of unburnt carbon in the filter thimble particulates were insignificant. This implies that irregular shaped particles could not be attributed to un-burnt carbon. The irregular shaped particles with amorphous surfaces have been attributed to both rapid cooling and inter particle collisions by Kutchko and Kim (2006) in cases where un-burnt carbon proportions are insignificant.

In some of the literature (Dunxi *et al.,* 2008, Xiaowei *et al.,* 2007) particulates were collected in a narrow range of size classes; as a result the detailed studies of particle morphologies were therefore made possible. The current study on filter trapped fly ash particles has been conducted on a wide range of particle size classes, due to the fact that the detailed study of each PSD region was not possible. Most of the ultra fine particle sizes and particle sizes below 2 microns were trapped within the filter fibers. Most particles in the size range 1 micron to less than 5 microns were spherical, as reported by Xu *et al* (2007).

4.6.4 Filter Thimble Fly Ash SEM EDS Results

Point analysis of particles smaller than 1 micron was not undertaken due to the fact that these particles were mostly attached to the filter or to bigger particles. As a result, the chemical composition of these ultra-fine particles would also include components from adjacent filter fibers or from the coarse or central mode particles that are within close range of the ultrafine particles. The five labeled particles in Figure 4.11 are those that have been analysed by SEM EDS point analysis, and the results are tabulated in Table 4.11.

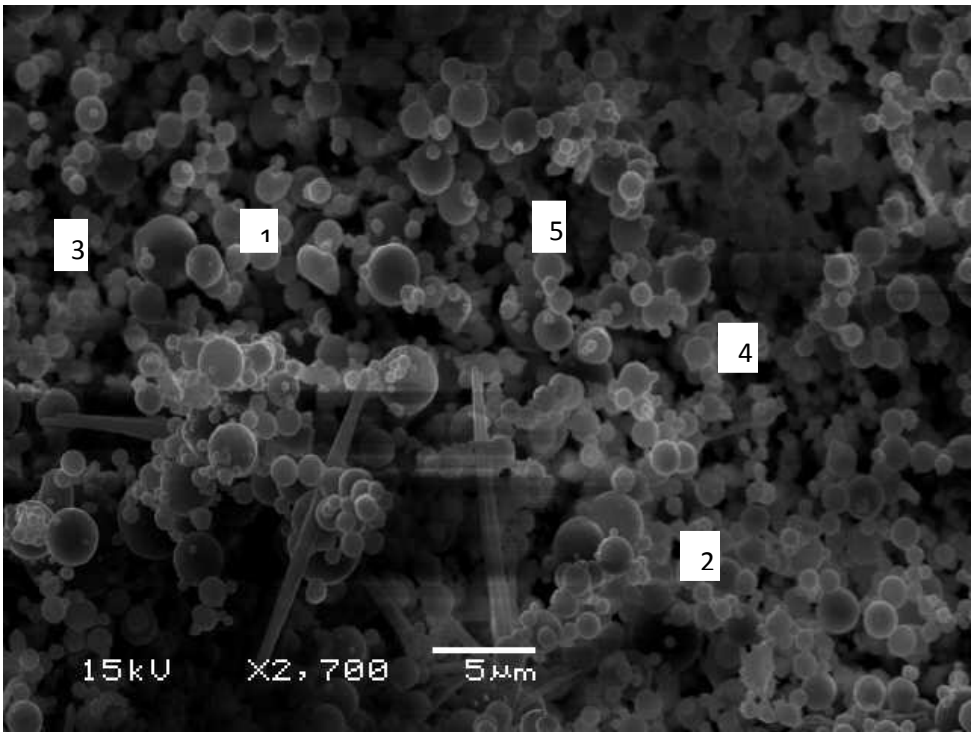

Figure 4.11: Morphology of stack captured fly ash particles from IA14 determined by SEM.

Table 4.11: Chemical composition of fly ash particles in Figure 4.11 as determined by SEM EDS.

Composition	Point 1	Point 2	Point 3	Point 4	Point 5
TiO_2	2.6	0.0	0.4	1.8	2.3
SiO_2	50.4	42.0	53.9	51.1	51.2
SO_3	0.8	1.3	0.1	0.3	0.9
P_2O_5	0.6	2.3	0.0	0.4	0.2
Na_2O	1.8	2.9	1.5	2.0	1.8
MgO	1.3	0.4	2.3	1.1	1.0
K_2O	1.9	5.5	1.9	2.1	2.6
FeO	1.7	2.9	0.5	0.6	2.4
CaO	5.5	8.2	7.7	2.6	5.0
Al_2O_3	33.4	34.6	31.7	38.1	32.6
Total	100.0	100.1	100.0	100.1	100.0

All five particles contained more than 40% silicon oxide and 30% aluminum oxide, as recorded in Table 4.11. Other metal oxides make up the remaining 30%, of which calcium was the next most abundant compound. These results indicate that silicon and aluminum melted and formed solid spheres during post combustion cooling. Several authors record that +2 microns coal fly ash particles are composed mostly of silicon and aluminum (Wang *et al.*, 2007, Xiaowei *et al.*, 2007, Dunxi *et al.*, 2008). The quantity of particles analyzed is not statistically sufficient for one to conclude the same, but it is however evident that silica and alumina did thermally decompose to form central mode fly ash particles as the composition of the particles in the current stack sampled filter thimble.

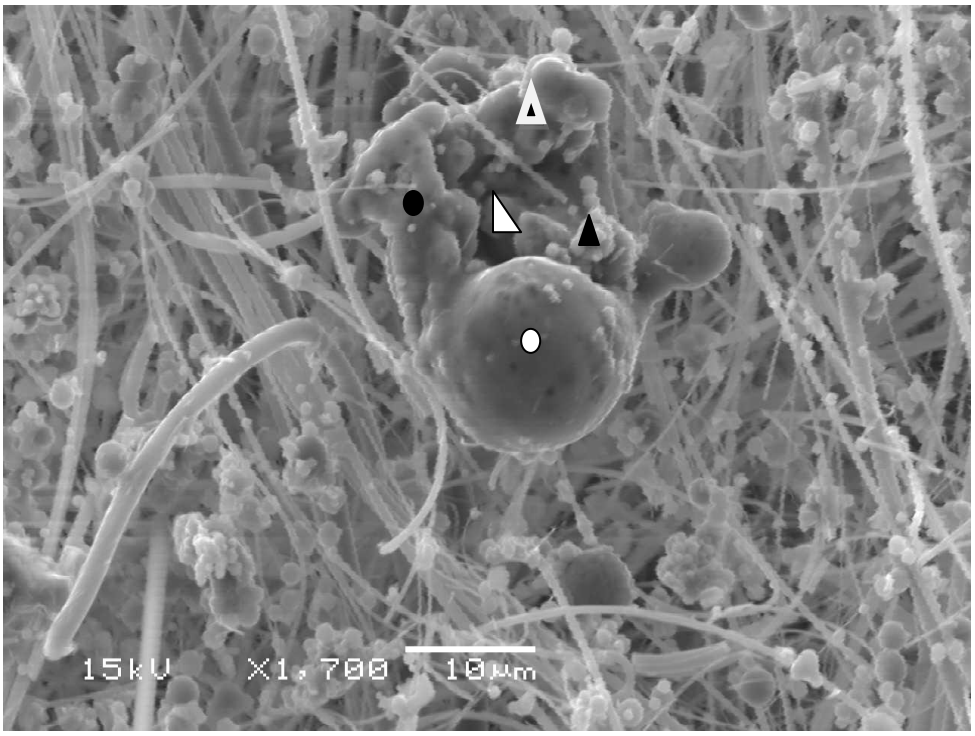

Figure 4.12: Fly ash particles from JV14 stack characterised by SEM (Symbols indicate SEM EDS reading location).

A further example of fly ash particles (> 10 microns) trapped in the filter is presented in Figure 4.12. The chemical composition of 5 points indicated Figure 4.12 is reported in Table 4.12. The amount of silicon oxide in the fly ash particles shown in Figure 4.12 is slightly higher than that of the fly ash shown in Figure 4.11. All fly ash particles analyzed and shown in Figure 4.11 and Figure 4.12 possess silicon contents of more than 45% and aluminum contents of more than 19%. The remaining 30% is made up mostly by the other oxides with phosphorus pent-oxide and sulphur oxides existing in very small amounts.

Table 4.12: Chemical composition for fly ash particles shown in Figure 4.12 determined by SEM EDS.

Composition	Point ●	Point ▲	Point △	Point ◺	Point ○
TiO_2	2.4	4.0	2.0	5.3	5.6
SiO_2	52.1	49.3	59.6	48.4	67.3
SO_3	0.1	0.3	1.9	4.5	1.5
P_2O_5	0.4	0.3	0.4	0.2	0.6
Na_2O	0.4	0.5	2.1	5.0	1.5
MgO	0.3	0.3	0.6	1.0	0.9
K_2O	0.7	0.7	0.6	0.7	0.7
FeO	1.2	1.3	0.7	2.7	1.3
CaO	0.5	0.6	1.2	2.7	1.1
Al_2O_3	42.0	42.7	31.0	29.5	19.5
Total	100.1	100.0	100.1	100.0	100.0

A third example of a fly ash particle (2 microns in size) trapped in the filter is shown in Figure 4.13. Here silicon and aluminum oxides still exist in high amounts as recorded in Table 4.13. The composition of the ultrafine particle on the centre of the 2 microns particle has the same chemical composition as the 2 micron particle. This is likely to be due to the fact that the electron beam aimed at the ultra fine particle must also have covered the surface of the 2 microns particle, because the particle is smaller than 1 micron. This particle has more sodium than most of other particles analyzed from previous samples in this section.

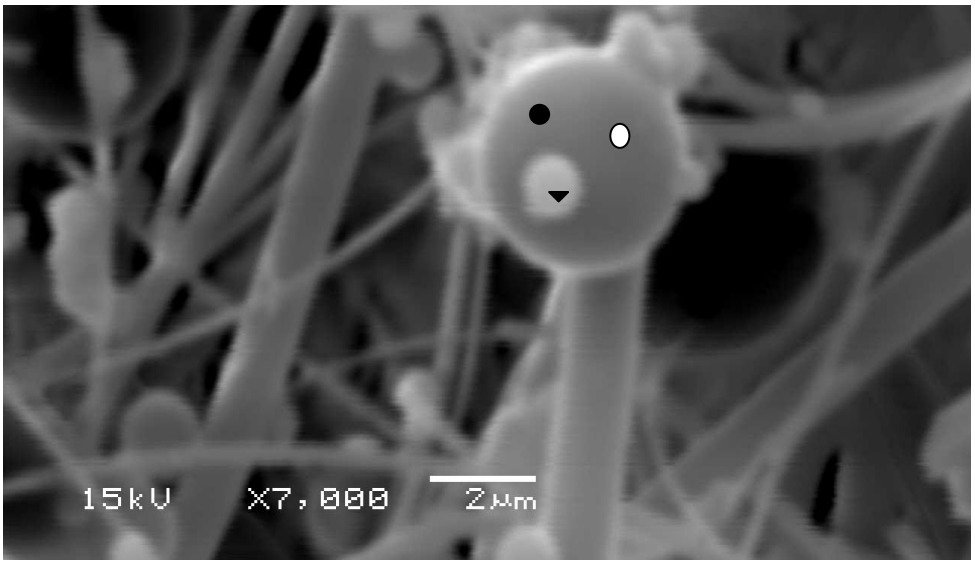

Figure 4.13: Fly ash particle of 2 micron sampled from JV14 stack analyzed using SEM.

Table 4.13: Chemical composition of fly ash particles shown in Figure 4.13 as determined by SEM EDS.

Compounds	Point ○	Point ●	Point▼
TiO_2	0.2	0.2	0.3
SiO_2	54.1	53.1	54.1
SO_3	2.9	2.0	3.2
P_2O_5	0.3	0.4	0.4
Na_2O	5.8	5.7	5.4
MgO	1.0	0.7	0.9
K_2O	0.7	0.7	0.7
FeO	1.5	1.5	1.1
CaO	2.2	1.2	1.6
Al_2O_3	31.3	34.6	32.4
Total	100.0	100.0	100.0

The chemical composition of the fly ash particle in Figure 4.14 is similar to the chemical composition of the other fly ash particles analyzed. This shows that particles from 2 microns up to 10 microns have a consistent chemical composition of silicon and aluminum oxides with the composition of other metal oxides being nominal and slightly variable.

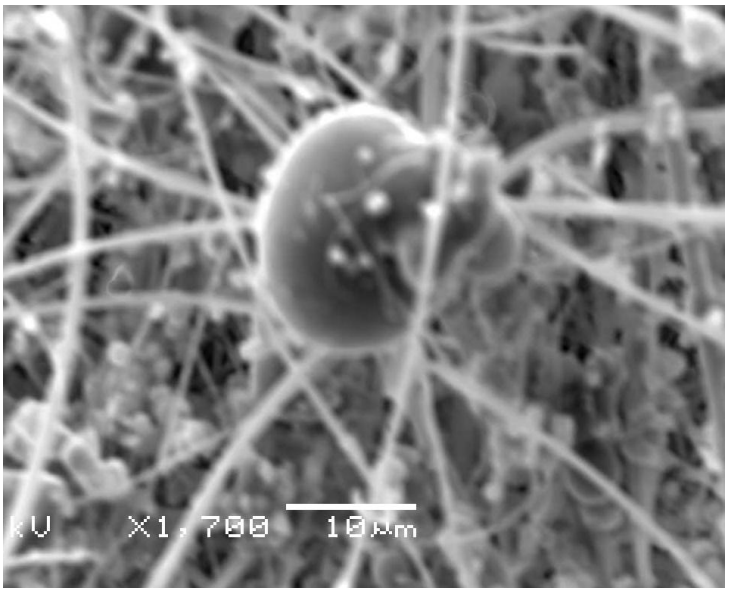

Figure 4.14: Single 10 micron stack fly ash particle from JV 14 ESP outlet analyzed using SEM EDS.

Table 4.14: Chemical composition for fly ash particle shown in Figure 4.14 as determined by SEM EDS.

Compounds	Composition(%)
TiO2	1.6
SiO2	55.7
SO3	1.6
P2O5	0.4
Na2O	2.1
MgO	1.1
K2O	1.3
FeO	3.0
CaO	3.6
Al2O3	29.9
Total	100.0

The chemical composition of fly ash particles shown in Figure 4.15 and tabulated in Table 4.15 contains more silicon than the rest of fly ash samples recorded in this research report. This could be due to the coal source containing higher amounts of silicon bearing minerals than most local coals. The coal source in this instance is unknown. The amount of aluminum is lower than all reported amounts of aluminum in the other fly ash samples. In all the samples analysed the amount of silicon has not exceeded 60%, while the amount of aluminum has not been lower than 15%.

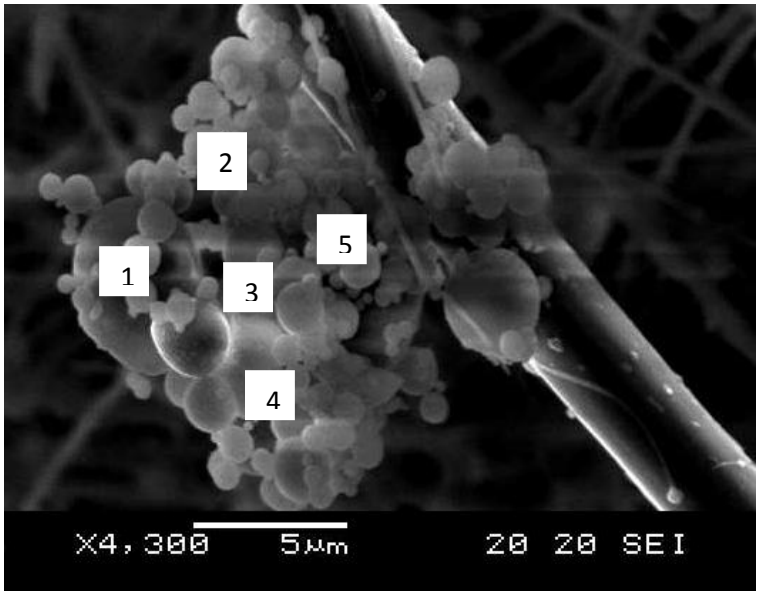

Figure 4.15: The stack fly ash below 5 microns from HY23 as determined by SEM.

Table 4.15: Chemical composition of fly ash particles shown in Figure 4.14 as determined by SEM EDS.

Compounds	Point 1	Point 2	Point 3	Point 4	Point 5
TiO_2	0.0	1.3	1.0	0.3	0.0
SiO_2	66.5	64.1	66.0	72.6	68.9
SO_3	3.2	1.6	1.9	1.1	2.9
P_2O_5	0.5	0.0	0.5	0.7	0.0
Na_2O	3.5	4.4	4.3	5.4	5.5
MgO	0.6	0.8	1.1	1.4	1.4
K_2O	1.3	1.3	1.4	1.5	2.2
FeO	0.5	2.3	2.4	0.0	0.0
CaO	3.0	8.3	11.5	14.1	15.5
Al_2O_3	20.8	16.0	10.0	3.0	3.6
Total	100.0	100.0	100.0	100.0	100.0

4.7 Summary and Conclusions

The chain grate boiler had poor combustion efficiency which consequently resulted in irregular fly ash particles and few spherical particles. This indicates that only a small portion of the mineral matter melted changing the particle morphology. The chain grate stack fly ash particles also contained more ±10 microns sized particles than the stack sample particulates from the pulverised coal combustion process.

The identification of primary carbonates and other elements in the fly ash that were not indentified in parent coal could be because the fly ash particle size analyzed was -10 microns while the coal analyzed was -45 microns. The finer fly ash particles produced more surface area than the coarse coal particles and hence more surface area could have exposed more mineral chemical composition.

The sieve stack screening method for determining the size of fly ash particles is not a reliable screening method since some mesh apertures are bigger than the specified nominal diameter. The larger irregular shaped particles can also pass through the screen apertures.

The ESP appears to have poor collection efficiency of ultra-fine and central mode particles as determined by analyzing the thimble samples using the SEM, while the collection efficiency of coarse mode particles is 99.9%. This indicates that the legislation should consider stringent emission control for $PM_{2.5}$ rather than PM_{10} due to fact that even though emission control equipment can handle PM_{10} very well, it does not appear to be able to handle the dangerous ultra fine and central mode particulates ($PM_{2.5}$).

The fly ash particles analyzed in the filter thimbles presented in this chapter all range from ±2 micron up to 10 microns and all particles size have high silicon and aluminum contents.

The fly ash particles from the chain grate stack and the JV14 ESP had, unsurprisingly, a chemical composition similar to the parent feed coal chemical composition. The individual particles analyzed by SEM EDS from stack thimble samples contained higher proportions of silicon and aluminum than the chain grate stack and the JV 14 ESP samples, even though the results are not directly comparable since point analysis was applied on stack thimble samples while automated analysis was employed on chain grate stack samples and the JV14 ESP samples.

5.0 Summary

The research aims set out in this research project was to examine feed coals as well as -10 microns fly ash particles produced from both chain grate boiler and Pf coal fired boilers. The fly ash particles from the chain grate boiler were sourced from the stack of the boiler, while the fly ashes from the Pf coal fired boiler were sourced from both the ESP and the stack. The coals and fly ashes were analysed using XRD, SEM EDS and XRF. The Pf boiler ESP and chain grate boiler stack fly ash particle size distributions (PSDs) were established using a sieve screen stack as well as Malvern laser diffraction based particle size analyzer. The Pf coal fired boiler stack fly ashes were captured in thimbles and were not analysed for PSDs due to the fact that the fly ash particles were trapped within the filter fibres and the quantities were found to be insufficient for effective analysis by either XRD, Malvern particle size analyzer and XRF. Only SEM EDS analysis and observations were conducted on those sample materials.

5.1 Conclusions

Based on the research questions posed and the findings in this research, the following conclusions may be drawn:-

1. In terms of size distributions, the Pf fired boiler ESP fly ash contained 70% coarse mode particles, 9% ultra fines and 21% central mode particles. The Pf coal fired boiler stack fly ash samples contained particles mostly from central to ultra fine modes i.e. 4 microns to 0.1 microns. The particles collected from the Pf coal boiler ESP and the chain grate stack had particles size ranges from 0.2 micron to +10 microns. The chain grate boiler stack fly ash particles were coarser than Pf fired coal boiler stack fly ash. The chain grate boiler stack coarse fly ash particles accounted for 53% of the -10 microns particles while Pf coal fired boiler stack fly ash had an insignificant quantity of coarse mode particles.

   From the above it may be concluded that 0-10 micron fly ash particles are produced during the combustion of typical South African coals. The coal combustion fly ash PSD is trimodal but the fly ash escaping the ESP is mostly bimodal because the ESP collection efficiency is very high for the coarse particle mode range. In the case of the chain grate boiler where the ESP collection efficiency was not high, 53% of coarse mode fly ash particles were emitted via the stack.

2. In terms of chemical compositions, the dominant elements in the fly ashes and coal mineral matter were found to be silicon and aluminum as determined by the XRF and SEM EDS. The fly ash particles between ± 2 microns to 10 microns contained aluminum and silicon in amounts that accounted for around 70% of the total composition. The amounts of other elements were not consistent; with it was found that the composition of each element varied from sample to sample. However, the fly ash chemistry did resemble the parental coal chemistry. In the literature study it was found that silicon and aluminum occur in higher concentrations in central mode and coarse mode particles but in lower concentrations in the ultra fine particles. The ultra fine particles were reported to contain mostly sulphur, calcium, sodium and phosphorus. Unfortunately this literature finding could not be validated in the current study due to the fact that chemical analysis was carried out on the bulk sample rather than on the individual size fractions referred to as PSD modes chemical analysis. This was due to difficulties in splitting the -10 microns samples.

3. In terms of mineral to fly ash transformation, the coal mineral matter constituents were thermally transformed mostly into amorphous material in the fly ash. Quartz was the only mineral matter constituent that was identified in both parent coals and relevant fly ashes for both combustion processes.

4. In terms of shape, the stack fly ash particles from the Pf coal boiler were mostly spherical with a few irregular particles. This indicates high temperature melting above 1000^{o}C to produce these “cenospheres” The irregular particles observed under the SEM were found to be caused mostly by inter particle collisions and due to the post combustion rate of cooling of fly ash particles. The chain grate stack fly ash particles were mostly irregular, this could be due to poor combustion, since most of the mineral matter did not reach melting point. A few spherical fly ash particles were present.

5. From this research it would appear that the particulates that are mostly emitted into the environment via the stacks are found to be in ultra fine and central modes ($PM_{2.5}$) rather than coarse mode (PM_{10}) due to the fact that the ESP and emission control equipment collection efficiencies capturing the PM_{10} are found to be high. It is also noted that the current South African legislation seeks to control the concentration of coarse particles (PM_{10}) in the atmosphere rather than the central and ultra fine mode particles ($PM_{2.5}$).

   It may consequently be concluded that the $PM_{2.5}$ material currently poses more threat to human health than PM_{10} due to its emission into the environment. This information needs to be verified further and a step taken to investigate the impacts on human health.

5.2 Recommendations

Thus the new aims and objectives of the research project to determine and characterize the quantity and quality of the fly ashes in bulk without separating them physically into three particulates size classes below 10 microns, and where possible to characterise the three different size modes using chemical and optical procedures were addressed.

The research questions as to whether Pf boilers and chain grate stokers combustion processes of South African coals produce particulates less than 10 microns and if so, how do the morphologies and chemical compositions of different particle size modes differ, and can they be related to their original coal feedstock were answered.

Based on the results obtained so far, a number of recommendations are as follows:-

1. Further research needs to be conducted on the three modes of fly ash particles determined for South Africa coals. In addition to major and minor elements, the distribution and mode of occurrences of trace elements within the three modes should be investigated. This would be particularly relevant for the ultrafine and central mode particles because they are not readily captured and collected by emission control equipment. They have been demonstrated to have significant environmental and health effects in the literature.

2. The scope of the current project included the study of only inorganic particulates. Further work should therefore consider study of organic particulates.

3. In terms of sample collection, the use of a stage numbered cascade impactor and a cyclone should be considered for sampling and characterising the PSD of fly ash emitted from boiler stacks or from laboratory combustion facilities since they can separate particles into numerous size fractions from small diameters of between -0.1 microns to -10 microns depending on the manufacturers design. The cyclone is normally used to collect bigger particles that can block the apertures of the cascade impactor stages. The cascade impactor separates the fly ash particles into three regions of ultra fine, central mode and coarse mode particles and thereby characterizes each particle size range independently. This would enable a more accurate determination of the composition of the ultra fine particles. This approach has been undertaken with most particulates studies in the literature.

4. The National Environmental Management Air Quality Act (the AQA) 2004 (No. 39 of 2004) should be revised so that it accounts for both $PM_{2.5}$ and organic particulates. It has been demonstrated that $PM_{2.5}$ is more of a human health hazard than PM_{10}, and this research has indicated that a significant amount of $PM_{2.5}$ is likely to be emitted from South Africa coal fired facilities. This would bring the South Africa air quality legislation in line with USA, EU and Australian legislation and could be of considerable benefit to the health of the nation in future.

6.0 References

Amann M, Derwent R, Forsberg B, Hurley F, Krzyzanowski M, Kuna-Dibbert B. World Health Organization 2006. European Centre for Environment and Health Bonn Office. Task Force on the Health Aspects of Air Pollution Health risks of particulate matter from long-range trans-boundary air pollution.

Barranco R, Gong M, Thompson A, Cloke M, Hanson S, Gibb W, Lester E. The impact of fly ash resistivity and carbon content on electrostatic precipitator performance. Fuel 86(2007)2521–2527.

Bar-Ziv E, Kantorovich I.I. Mutual effects of porosity and reactivity in char oxidation. Progress in Energy and Combustion Science. 27(2001)667–697.

Baxter L.L. Char Fragmentation and Fly Ash Formation during Pulverised-Coal Combustion. Combustion flame. 90(2)(1992)174-184.

Brinckerhoff P. Menangle Park West. Review of crystalline silicon health risks in response to community concerns. Landcom 24 September 2009.

Buhre B.J.P, Hinkely J.T, Gupta R.P, Nelson P.F, Wall T.F. Fine ash formation during combustion of pulverised coal-coal property impacts. Fuel 85(2006)185-193.

Desrosiers R.E, Riehl J.W, Ulrich G.D, Chiu A.S. Submicron fly-ash formation in coal-fired boilers. Seventeenth Symposium (International) on Combustion. 17(1)(1979)1395-1403.

Douglas W.D, Pope A.C, Xu X, Spengler Ware J.H. Association between air pollution and mortality in Six U.S. Cities. The New England Joumal of Medicine. (329)(24)(1993)1753-1759.

Dunbar C. Analysis of cascade impactor mass distributions inhalation technology. Focus Group Baltimore ALKERMES, 30 September 2005.

Dunxi Y, Xu M, Yu Y, Li X. Swelling behavior of a Chinese bituminous coal at different pyrolysis temperatures. Energy & Fuels. 19(2005)2488–2494.

Dunxi Y, Minghou X, Yao H, Jiancai S, Xiaowei L. Use of elemental distributions in identifying particle formation modes. Proceedings of the Combustion Institute. 31(2007)1921-1928.

Dunxi Y, MingHou X, Hong X.L, Xiao W, Zhou K. Effective identification of the three particle modes generated during pulverised coal combustion. Chinese Science Bulletin. 53(10) (2008)1593-1602.

Environmental Protection Agency, 40 CFR Part 51 Methods for Measurement of Filterable PM_{10} and $PM_{2.5}$ and Measurement of Condensable Particulate Matter Emissions from Stationary Sources Federal Register / Vol. 74, No. 56 / Wednesday, March 25, 2009.

Flagan R.C, Friedlander S.K. Physical transformation of the mineral matter in pulverised coal under simulated combustion conditions. Combustion Science Technology. 16(3-6)(1977)187-204.

Green A.S, Waite M.L. The redesign of chain grate stoker links to reduce pollutant emissions: aerodynamic design. Fuel. 83(2004)1391-1395.

Harrison R.M, Jianx Y. Particulate matter in the atmosphere: which particle properties are important for its effects on health? The Science of the Total Environment. 249(2000)85-101.

Helble J, Neville M, Sarofim A. F. Aggregate Formation from Vaporized Ash During Pulverised Coal Combustion. Proceedings of Combusion Institute. 21(1986)411-417.

Helble J, Sarofim A.F. Influence of char fragmentation on ash particle size distributions. Combustion and Flame 76(1989)183-196.

Hetland R.B, Schwarze P. E, Johansen B. V, Myrant T, Uthus N, Refsnes M. Silicon- induces cytokine release from A549 cells importance of surface area versus size. Human and experimental toxicology. 20(2001)46–55.

Holve D.J. In *Situ* Measurements of Fly ash Formation from Pulverised Coal. Combustion Science and Technology 44(5–6)(1986)269–288.

Ito T, Kubota T, Zukeran A, Takashi T, Shinkai K, Miyamoto M, Yoshimochi T. Collection characteristics of submicron particles on electrostatic precipitator. The Institute of Electrical Engineers of Japan. 15(2)(1995)113–120.

Kanf S.G, Helble J, Sarofim A.F, Beer J.M. Time-Resolved Evolution of Fly Ash during Pulverised Coal Combustion. Proceedings of combustion Institute. 22(1)(1989)231-238.

Kanf S.G, Sarofim A.F, Beer J.M. Effect of Char structure on residual ash formation during pulverised coal combustion. Proceedings of combustion Institute. 24(1)(1992)1153-1159.

Kok M.V, Ozbas E, Karacan O, Hicyilmaz C. Effect of particle size on coal pyrolysis. Journal of Analytical and Applied Pyrolysis. 45(1998)103-110.

Kramlich J.C, Newton G.H. Influence of coal rank and pre-treatment on residual ash particle size. Fuel Processing Technology. 37(2)(1994)143–161.

Kutchko B.G, Kim A.G. Fly ash characterisation by SEM–EDS. Fuel. 85(2006)2537–2544.

Lee W.S. Fine particulate matter measurement and international standardization for air quality and emissions from statutory sources. Fuel. 89(2010)874-882.

Linak W.P, Miller C.A, Wendt J.O.L. Comparison of Particle Size Distributions and Elemental Partitioning from the Combustion of Pulverised Coal and Residual Fuel oil. Air and Waste Management Association. 50(2000)1532.

Linak W.P, Miller C.A, Seams W.S. On trimodal particle size of distributions of fly ash from pulverised coal combustion. Proceedings of combustion Institute. 29(2002) 441-447.

Liu G, Wu H, Gupta R.P, Lucas J.A, Tate A.G, Wall T.F. Modeling the fragmentation of non-uniform porous char particles during pulverised coal combustion. Fuel 79(2000)627–633.

Liu K.S. Some factors affecting sieving performance and efficiency. Powder Technology. 193(2009)208-213.

Mayoral M.C, Izquierdo M.T, Andrés J.M, Rubio B. Alumino-silicates transformations in combustion followed by DSC. Thermochimica Acta. 373(2)(2001)173-180.

McElroy M.W, Carr R.C, Ensor D.S, Markowski G. R. Size Distribution of Fine Particles from Coal Combustion. Science 215(4528)(1982)13-19.

Module 6: Air Pollutants and Control Techniques - Particulate Matter - Control Techniques. Available from: http://www.epa.gov/apti/bces/module6/matter/control/control.htm#espefficiency Accessed 24 January 2010.

Myaliwiec M.J, Kleeman M.J. Source Apportionment of Secondary Airborne Particulate Matter in a Polluted Atmosphere. Environmental Science and Technology. 36(2002)5376-5384.

Nankervis J.C, Furlong B.R. Phase changes in mineral matter of North Dakota lignites caused by heating to 1200°C. Fuel 59(1980)425-430.

National Environment Protection Council (NEPC), ambient air quality, http://www.ephc.gov.au/nepms/air/air_nepm.html. National environment protection and heritage council; 2003. Accessed August 2009.

National Environment Protection Council (NEPC). Variation to the national environment protection (ambient air quality) measure. Adelaide, National Environment Protection Agency. 2003.

Neal C. Environmental chemistry and Toxicology of aluminum. Book Review Environmental Pollution. 69(1991)259-264.

Ninomiya Y, Zhang L, Sato A. Zhongbing D. Influence of coal particle size on particulate matter emission and its chemical specie Produced during coal combustion. Fuel Processing Technology. 85(2004)1065–1088.

Quann R.J, Sarofim A.F. Vaporization of Refractory Oxides During Pulverised Coal Combustion. Proceedings of Combusion Institute. 19(1982)1429–1440.

Ramsden A.R. A Microscopic Investigation into the Formation of Fly Ash during the Combustion of a Pulverised Bituminous Coal. Fuel 48(2)(1969)121–137.

Riehle C, Loffler F. The effective migration rate in electrostatic precipitator. Aerosol Science and Technology. 16(1992)11–14.

Sarofim A.F, Howard J.B, Padia A.S. The physical transformation of the mineral matter in pulverised coal under simulated combustion conditions. Combustion Science Technology. 16(1977)187-205.

Seams W.S. An initial study of the fine fragmentation fly ash particle mode generated during pulverised coal combustion. Fuel Processing Technology 81(2003)109-125.

Shao D, Hutchinson E.J, Heidbrink J, Pan W, Chou C. Behaviour of sulphur during coal pyrolysis. Journal of Analytical and Applied Pyrolysis. 30(1994)91-100.

Singleton T. Managing Climate Change – the pressures on coal utilisation, Perspective from the power generation sector. University of Witwatersrand. Graduate Diploma Engineering, Coal Management and Marketing 2008.

Smith, R.D, Campbell J.A, Nielson K.K. Characterisation and formation of submicron particles in coal-fired plants. Atmospheric Environment. 13(5)(1979)607–617.

Soukup J. M, Becker S. Human alveolar macrophage responses to air pollution are associated with insoluble components of course material, including particulate endotoxin. Toxicology and applied pharmacology. 171(2001)20–26.

South African No.31987 Government Gazette South Africa, Department of Environmental Affairs and Tourism, Government Notices 13 MARCH 2009.

South coast air quality management district. EPA, Method 1.1. Sample and velocity traverses for stationary sources. Office of operations. Technical services division, march 1989. http://www.aqmd.gov/tao/methods/stm/stm-001-1.pdf. Accessed 20 July 2009.

Srinivasachar S, Helble J.J, Boni A.A, Shah N, Huffmant P.G, Hugginst F.E. Mineral behavior during coal combustion 2. Illite Transformations. Progress in Energy and Combustion Science. 16(4)(1990)293-302.

Ten Brink H.M, Eenkhoorn S, Weeda M. The behaviour of coal mineral carbonates in a simulated flame. Fuel Processing Technology. 47(1996)233-243.

Test Sieving: Principles and Procedures: A Discussion of the Uses, Capabilities, and Limitations of Testing Sieves as Analytical Tools. Advantech Mfg, 2450 S Commerce Drive. The leader in sieving technology®.

Tomeczeck J, Palugynik H. Kinetics of mineral matter transformation during coal combustion. Fuel. 81(2002)1251-1258.

Wang Q, Zhang L, Sato A, Ninomiya Y, Yamashita T. Interactions among inherent minerals during coal combustion and their impacts on the emissions of PM_{10}. 1. Emission of micrometer sized particles. Energy and Fuels. 21(2007)756-765.

Wang Q, Zhang L, Ninomiya Y, Yamashita T. Effects of coal blending on the reduction of PM10 during high temperature combustion. 1. Mineral transformation. Fuel 87(2008)2997-3005.

World Health Organisation, Europe. Particulate matter air pollution: how it harms health. Fact sheet EURO/04/05 Berlin, Copenhagen, Rome, 14 April 2005.

Wu H, Wall T, Liu G, Bryant G. Ash liberation from included minerals during combustion of pulverised coal: the relationship with coal structure and burnout Energy. Fuels. 13(1999)1197–1202.

Xiaowei L, Minghou X, Hong Y, Dunxi Y, Xiangpeng G, Qian C, Youmin C. Effect of Combustion Parameters on the Emission and Chemical Composition of Particulate Matter During Coal Combustion. Energy & Fuels. 21(2007)157-162.

Xu M, Dunxi Y, Hong Y, Xiaowei L, Ke Z. A new method for identifying the modes of particulate matter from pulverised coal combustion. Powder Technology. 183(2008)105–114.

Xu M, Dunxi Y, Hong Y, Xiaowei L, Ke Zhou, Lin L, Chang W. Mechanisms of the central mode particle formation during pulverised coal combustion. Proceedings of the Combustion Institute. 32(2009)2075–2082.

Xu M, Yun Y, Hong Y, Dunxi Y, Yu Q, Jiancai S, Xiaowei L, Qian C. Char characteristics and particulate matter formation during Chinese bituminous coal combustion. Proceedings of the Combustion Institute. 31(2007)1947–1954.

Yinghui L, Gupta R, Wall T. Ash Formation from Excluded Minerals Including Consideration of Mineral-Mineral Associations. Energy & Fuel 21(2007)461-467.

Yinon L .Ultrafine particle emissions: Comparison of waste- to-energy with coal- and biomass-fired power plants. Thesis, Chemical Engineering Columbia University January 2010 http://www.seas.columbia.edu/earth/wtert/sofos/yinon_thesis.pdf. Accessed 30 February 2010.

Yuanzhi C, Naresh S, Frank E. Gerald P. Huffman, Linak W.P, Miller CA. Investigation of primary fine particulate matter from coal combustion by computer-controlled scanning electron microscopy. Fuel Processing Technology 85(2004)74.

Zhang L, Ninomiya Y, Yamashita T. Formation of submicron particulate matter during coal combustion and influence of reaction temperature. Fuel 85(2006)1446-1457.

Zhuo JK., Li SQ, Yao Q, Song Q. The progressive formation of submicron particulate matter in a quasi one-dimensional pulverised coal combustor. Proceedings of the Combustion Institute 32(2) (2009)2059–2066.

Zukeran A, Chang J.S, Berezin A.A, Ito T. Control of ultrafine particles from incense smoke by an air cleaning electrostatic precipitator. Journal of Aerosol Science 28(1)(1997)289–290.

Zukeran A, Looy P.C, Chakrabarti A, Cross J.D, Jayaram S. Collection efficiency of ultrafine particles by electrostatic precipitator under DC and pulse operating modes. IEEE Transactions on industrial applications. 35(5)(1999)1184-1191.

7.0 Appendix A

Table 7.1: PSD for chain grate boiler stack fly ash.

Size (µm)	Vol Under %	Size (µm)	Vol Under %	Size (µm)	Vol Under %	Size (µm)	Vol Under %	Size (µm)	Vol Under %	Size (µm)	Vol Under %
0.010	0.00	0.080	0.00	0.634	8.17	5.053	52.73	40.244	100.00	320.535	100.00
0.011	0.00	0.090	0.00	0.717	9.72	5.709	57.86	45.469	100.00	362.148	100.00
0.013	0.00	0.102	0.00	0.810	11.30	6.450	63.22	51.371	100.00	409.163	100.00
0.014	0.00	0.115	0.00	0.915	12.91	7.287	68.69	58.041	100.00	462.281	100.00
0.016	0.00	0.130	0.00	1.034	14.54	8.233	74.15	65.575	100.00	522.296	100.00
0.018	0.00	0.147	0.00	1.168	16.22	9.302	79.45	74.089	100.00	590.102	100.00
0.021	0.00	0.166	0.00	1.320	17.96	10.510	84.44	83.707	100.00	666.711	100.00
0.024	0.00	0.187	0.00	1.491	19.81	11.874	88.95	94.574	100.00	753.265	100.00
0.027	0.00	0.211	0.08	1.684	21.81	13.416	92.84	106.852	100.00	851.056	100.00
0.030	0.00	0.239	0.32	1.903	24.00	15.157	95.98	120.724	100.00	961.542	100.00
0.034	0.00	0.270	0.69	2.150	26.43	17.125	98.26	136.397	100.00	1086.372	100.00
0.038	0.00	0.305	1.22	2.429	29.14	19.348	99.62	154.104	100.00	1227.408	100.00
0.043	0.00	0.345	1.92	2.745	32.17	21.860	100.00	174.110	100.00	1386.753	100.00
0.049	0.00	0.389	2.84	3.101	35.54	24.698	100.00	196.714	100.00	1566.785	100.00
0.055	0.00	0.440	3.97	3.503	39.29	27.904	100.00	222.251	100.00	1770.189	100.00
0.062	0.00	0.497	5.26	3.958	43.41	31.527	100.00	251.105	100.00	2000.000	100.00
0.070	0.00	0.561	6.67	4.472	47.90	35.620	100.00	283.704	100.00		

Table 7.2: Amounts of particles in specified narrow range for chain grate boiler stack fly ash (Values used to produce frequency curves).

Size (µm)	Volume In %	Size (µm)	Volume In %	Size (µm)	Volume In %	Size (µm)	Volume In %	Size (µm)	Volume In %	Size (µm)	Volume In %
0.010	0.00	0.080	0.00	0.634	1.55	5.053	5.13	40.244	0.00	320.535	0.00
0.011	0.00	0.090	0.00	0.717	1.58	5.709	5.35	45.469	0.00	362.148	0.00
0.013	0.00	0.102	0.00	0.810	1.61	6.450	5.47	51.371	0.00	409.163	0.00
0.014	0.00	0.115	0.00	0.915	1.63	7.287	5.46	58.041	0.00	462.281	0.00
0.016	0.00	0.130	0.00	1.034	1.68	8.233	5.30	65.575	0.00	522.296	0.00
0.018	0.00	0.147	0.00	1.168	1.74	9.302	4.99	74.089	0.00	590.102	0.00
0.021	0.00	0.166	0.00	1.320	1.85	10.510	4.51	83.707	0.00	666.711	0.00
0.024	0.00	0.187	0.08	1.491	2.00	11.874	3.89	94.574	0.00	753.265	0.00
0.027	0.00	0.211	0.24	1.684	2.19	13.416	3.14	106.852	0.00	851.056	0.00
0.030	0.00	0.239	0.37	1.903	2.43	15.157	2.27	120.724	0.00	961.542	0.00
0.034	0.00	0.270	0.52	2.150	2.71	17.125	1.36	136.397	0.00	1086.372	0.00
0.038	0.00	0.305	0.70	2.429	3.03	19.348	0.38	154.104	0.00	1227.408	0.00
0.043	0.00	0.345	0.93	2.745	3.38	21.860	0.00	174.110	0.00	1386.753	0.00
0.049	0.00	0.389	1.13	3.101	3.74	24.698	0.00	196.714	0.00	1566.785	0.00
0.055	0.00	0.440	1.29	3.503	4.12	27.904	0.00	222.251	0.00	1770.189	0.00
0.062	0.00	0.497	1.41	3.958	4.49	31.527	0.00	251.105	0.00	2000.000	
0.070	0.00	0.561	1.50	4.472	4.83	35.620	0.00	283.704	0.00		
0.080		0.634		5.053		40.244		320.535			

Table 7.3: PSD for JV14 Pf ESP fly ash.

Size (µm)	Vol Under %	Size (µm)	Vol Under %	Size (µm)	Vol Under %	Size (µm)	Vol Under %	Size (µm)	Vol Under %	Size (µm)	Vol Under %
0.010	0.00	0.105	0.00	1.096	11.87	11.482	86.26	120.226	100.00	1258.925	100.00
0.011	0.00	0.120	0.00	1.259	13.33	13.183	91.15	138.038	100.00	1445.440	100.00
0.013	0.00	0.138	0.00	1.445	14.88	15.136	94.98	158.489	100.00	1659.587	100.00
0.015	0.00	0.158	0.00	1.660	16.60	17.378	97.71	181.970	100.00	1905.461	100.00
0.017	0.00	0.182	0.00	1.905	18.58	19.953	99.48	208.930	100.00	2187.762	100.00
0.020	0.00	0.209	0.05	2.188	20.90	22.909	99.95	239.883	100.00	2511.886	100.00
0.023	0.00	0.240	0.26	2.512	23.66	26.303	100.00	275.423	100.00	2884.032	100.00
0.026	0.00	0.275	0.60	2.884	26.96	30.200	100.00	316.228	100.00	3311.311	100.00
0.030	0.00	0.316	1.11	3.311	30.87	34.674	100.00	363.078	100.00	3801.894	100.00
0.035	0.00	0.363	1.80	3.802	35.45	39.811	100.00	416.869	100.00	4365.158	100.00
0.040	0.00	0.417	2.72	4.365	40.72	45.709	100.00	478.630	100.00	5011.872	100.00
0.046	0.00	0.479	3.82	5.012	46.65	52.481	100.00	549.541	100.00	5754.399	100.00
0.052	0.00	0.550	5.04	5.754	53.14	60.256	100.00	630.957	100.00	6606.934	100.00
0.060	0.00	0.631	6.35	6.607	60.02	69.183	100.00	724.436	100.00	7585.776	100.00
0.069	0.00	0.724	7.71	7.586	67.05	79.433	100.00	831.764	100.00	8709.636	100.00
0.079	0.00	0.832	9.08	8.710	73.97	91.201	100.00	954.993	100.00	10000.000	100.00
0.091	0.00	0.955	10.47	10.000	80.46	104.713	100.00	1096.478	100.00		

Table 7.4: Amounts of particles in specified narrow range for chain grate boiler stack fly ash (Values used to produce frequency curves).

Size (µm)	Volume In %	Size (µm)	Volume In %	Size (µm)	Volume In %	Size (µm)	Volume In %	Size (µm)	Volume In %	Size (µm)	Volume In %
0.010	0.00	0.105	0.00	1.096	1.45	11.482	4.89	120.226	0.00	1258.925	0.00
0.011	0.00	0.120	0.00	1.259	1.55	13.183	3.84	138.038	0.00	1445.440	0.00
0.013	0.00	0.138	0.00	1.445	1.72	15.136	2.73	158.489	0.00	1659.587	0.00
0.015	0.00	0.158	0.00	1.660	1.98	17.378	1.76	181.970	0.00	1905.461	0.00
0.017	0.00	0.182	0.05	1.905	2.32	19.953	0.48	208.930	0.00	2187.762	0.00
0.020	0.00	0.209	0.21	2.188	2.76	22.909	0.05	239.883	0.00	2511.886	0.00
0.023	0.00	0.240	0.34	2.512	3.30	26.303	0.00	275.423	0.00	2884.032	0.00
0.026	0.00	0.275	0.50	2.884	3.91	30.200	0.00	316.228	0.00	3311.311	0.00
0.030	0.00	0.316	0.70	3.311	4.58	34.674	0.00	363.078	0.00	3801.894	0.00
0.035	0.00	0.363	0.91	3.802	5.27	39.811	0.00	416.869	0.00	4365.158	0.00
0.040	0.00	0.417	1.10	4.365	5.93	45.709	0.00	478.630	0.00	5011.872	0.00
0.046	0.00	0.479	1.23	5.012	6.49	52.481	0.00	549.541	0.00	5754.399	0.00
0.052	0.00	0.550	1.31	5.754	6.88	60.256	0.00	630.957	0.00	6606.934	0.00
0.060	0.00	0.631	1.35	6.607	7.04	69.183	0.00	724.436	0.00	7585.776	0.00
0.069	0.00	0.724	1.37	7.586	6.91	79.433	0.00	831.764	0.00	8709.636	0.00
0.079	0.00	0.832	1.38	8.710	6.50	91.201	0.00	954.993	0.00	10000.000	0.00
0.091	0.00	0.955	1.40	10.000	5.79	104.713	0.00	1096.478	0.00		
0.105	0.00	1.096		11.482		120.226	0.00	1258.925	0.00		

Table 7.5: U.S.A. Standard Testing Sieves ASTM Specification E 11-04 (Test Sieving: Principles and Procedures)

Sieve Designation		Nominal Sieve Opening, in.	Permissible Variation of Average Opening from the Standard	Opening Dimension Exceeded by not more than 5%	Maximum Individual	Nominal Wire Diameter (mm)
Standard (b)	Alternative	(see c below)	Sieve Designation	of the Openings	Opening	(see a below)
(1)	(2)	(3)	(4)	(5)	(6)	(7)
125 mm	5"	5	±3.70 mm	130.0 mm	130.9 mm	8.00
106 mm	4.24"	4.24	±3.20 mm	110.2 mm	111.1 mm	6.30
100 mm d	4"	4	±3.00 mm	104.0 mm	104.8 mm	6.30
90 mm	3 ½"	3.50	±2.70 mm	93.6 mm	94.4 mm	6.30
75 mm	3"	3	±2.20 mm	78.1 mm	78.7 mm	6.30
63 mm	2 ½"	2.50	±1.90 mm	65.6 mm	66.2 mm	5.60
53 mm	2.12"	2.12	±1.60 mm	55.2 mm	55.7 mm	5.00
50 mm d	2"	2	±1.50 mm	52.1 mm	52.6 mm	5.00
45 mm	1 ¾"	1.75	±1.40 mm	46.9 mm	47.4 mm	4.50
37.5 mm	1 ½"	1.50	±1.10 mm	39.1 mm	39.5 mm	4.50
31.5 mm	1 ¼"	1.25	±1.00 mm	32.9 mm	33.2 mm	4.00
26.5 mm	1.06"	1.06	±.800 mm	27.7 mm	28.0 mm	3.55
25.0 mm d	1.00"	1	±.800 mm	26.1 mm	26.4 mm	3.55
22.4 mm	7/8"	0.875	±.700 mm	23.4 mm	23.7 mm	3.55
19.0 mm	¾"	0.750	±.600 mm	19.9 mm	20.1 mm	3.15
16.0 mm	5/8"	0.625	±.500 mm	16.7 mm	17.0 mm	3.15
13.2 mm	.530"	0.530	±.410 mm	13.83 mm	14.05 mm	2.80
12.5 mm d	½"	0.500	±.390 mm	13.10 mm	13.31 mm	2.50
11.2 mm	7/16"	0.438	±.350 mm	11.75 mm	11.94 mm	2.50
9.5 mm	3/8"	0.375	±.300 mm	9.97 mm	10.16 mm	2.24
8.0 mm	5/16"	0.312	±.250 mm	8.41 mm	8.58 mm	2.00
6.7 mm	.265"	0.265	±.210 mm	7.05 mm	7.20 mm	1.80
6.3 mm d	¼"	0.250	±.200 mm	6.64 mm	6.78 mm	1.80
5.6 mm	No. 3 ½	0.223	±.180 mm	5.90 mm	6.04 mm	1.60
4.75 mm	No. 4	0.187	±.150 mm	5.02 mm	5.14 mm	1.60
4.00 mm	No. 5	0.157	±.130 mm	4.23 mm	4.35 mm	1.40
3.35 mm	No. 6	0.132	±.110 mm	3.55 mm	3.66 mm	1.25
2.80 mm	No. 7	0.110	±.095 mm	2.975 mm	3.070 mm	1.12
2.36 mm	No. 8	0.0937	±.080 mm	2.515 mm	2.600 mm	1.00
2.00 mm	No. 10	0.0787	±.070 mm	2.135 mm	2.215 mm	0.900
1.70 mm	No. 12	0.0661	±.060 mm	1.820 mm	1.890 mm	0.800
1.40 mm	No. 14	0.0555	±.050 mm	1.505 mm	1.565 mm	0.710
1.18 mm	No. 16	0.0469	±.045 mm	1.270 mm	1.330 mm	0.630
1.00 mm	No. 18	0.0394	±.040 mm	1.080 mm	1.135 mm	0.560
850 µm	No. 20	0.0331	±35 µm	925 µm	970 µm	0.500
710 µm	No. 25	0.0278	±30 µm	775 µm	815 µm	0.450
600 µm	No. 30	0.0234	±25 µm	660 µm	695 µm	0.400
500 µm	No. 35	0.0197	±20 µm	550 µm	585 µm	0.315
425 µm	No. 40	0.0165	±19 µm	471 µm	502 µm	0.280
355 µm	No. 45	0.0139	±16 µm	396 µm	426 µm	0.224
300 µm	No. 50	0.0117	±14 µm	337 µm	363 µm	0.200
250 µm	No. 60	0.0098	±12 µm	283 µm	306 µm	0.160
212 µm	No. 70	0.0083	±10 µm	242 µm	263 µm	0.140
180 µm	No. 80	0.0070	±9 µm	207 µm	227 µm	0.125
150 µm	No. 100	0.0059	±8 µm	174 µm	192 µm	0.100
125 µm	No. 120	0.0049	±7 µm	147 µm	163 µm	0.090
106 µm	No. 140	0.0041	±6 µm	126 µm	141 µm	0.071
90 µm	No. 170	0.0035	±5 µm	108 µm	122 µm	0.063
75 µm	No. 200	0.0029	±5 µm	91 µm	103 µm	0.050
63 µm	No. 230	0.0025	±4 µm	77 µm	89 µm	0.045
53 µm	No. 270	0.0021	±4 µm	66 µm	76 µm	0.036
45 µm	No. 325	0.0017	±3 µm	57 µm	66 µm	0.032
38 µm	No. 400	0.0015	±3 µm	48 µm	57 µm	0.030
32 µm	No. 450	0.0012	±3 µm	42 µm	50 µm	0.028
25 µm d	No. 500	0.0010	±3 µm	34 µm	41 µm	0.025
20 µm d	No. 635	0.0008	±3 µm	29 µm	35 µm	0.020